Immunotherapeutic and Diagnostic Potential of Engineered Materials

by

Ravi M. Raghani

A dissertation submitted in partial fulfillment
of the requirements for the degree of
Doctor of Philosophy
(Biomedical Engineering)
in the University of Michigan
2022

Doctoral Committee:

Professor Lonnie Shea, Chair
Professor Jacqueline Jeruss
Professor David Kohn
Professor James Moon

Ravi M. Raghani

rraghani@umich.edu

ORCID iD: 0000-0003-0677-0789

Dedication

This thesis is dedicated to my family – my parents, my partner, and my friends. This thesis is also dedicated to the wonderful humans that have mentored me and the music that has provided a sonic landscape for my journey. Without all the amazing people I've been blessed to cross paths with during my life, I would not be who I am today.

Acknowledgements

I feel such intense gratitude for all the amazing people I've had the opportunity to meet during my quarter century on this planet. Without the abundant mentors whom I've received inspiration from, I would not be where I am today. While I will attempt to express my deep appreciation for the wonderful people who have helped shape me, these words will undoubtedly capture only a fraction of the immense love and respect I feel for everyone who has impacted my life.

I would like to start off by thanking my parents. My mother and father have had their own vast and tumultuous journeys, and have been exceptionally supportive of me during my journey through adolescence and young adulthood. I think the best way I can illustrate how compassionately my parents have encouraged me to be myself, is through their support of my obsession with music. As a youngster, my friends and I would jam in my parents' basement whenever we could get the chance. I had an obnoxiously vociferous tube amp, and both friends and neighbors commented that they could hear my guitar noodlings down the street. My parents not only abstained from complaining about our cacophonous noise making, but they generously supported us by giving us the freedom and space to creatively express ourselves. In all facets of my life, my parents have graciously met me with the same, unlimited levels of understanding and support, and for that I'm eternally thankful.

Growing up as an only child, the friends I've been blessed to know have become my inherited family, and I feel such intense gratitude for the incredible impact each friend has made on my life. My friends have inspired me and made me so appreciative of being alive on this

planet. I would like to thank Beza Bekele, Christopher Tossas, Dan Matera, Kevin Hanna, Laura Saunders, Marny Ehmann, and Sang Won Choi for their daily support during this joyful and tumultuous journey – I could not have done this without all of you. Thank you Marny for the loving support, cathartic phone conversations, long walks to explore Ann Arbor/Philadelphia/ Manhattan/Pittsburgh, constant eagerness for an adventure, and for being the best sous chef. Dan Matera, thank you for letting me be myself – our marathon walks throughout Ann Arbor, times in the Arb, late night jams, and long winded soapboxes have made this such a life changing experience. I would also like to thank Aaron Morris, Bobby Graham, Chris Mostek, Dan Clough, Grace Bushnell, Guillermo Escalona, Ian Schrack, Jakin Zhang, Jeffrey Ma, Kelly Wang, Liam Casey, Morgan Bolger, Nick Schott, Noah Meurs, Richard Youngblood, Scott Ensel, and Tim Baker for their deep friendships during my time in Michigan. And, I would especially like to thank Alek Nyberg, Alex Miller, Alex Todd, Elliot Sandfort, Erich Vogel, Freshta Baher Engel, Jeffrey McCabe, Kevin Jia, Luke Dance, Michael Gharzai, Peter Burnett, Robert Moore, Sarah Heindl, Skyler Simpson, and Zachary Bram for their continued friendship and support since my upbringing in Nebraska. Each one of these friends has made an endlessly profound impact on my life.

To the members of the Shea lab, thank you for your mentorship, friendship, and willingness to support my maturation as a scientist. The Shea lab has been an integral, supportive force during my graduate training. Thank you Dr. Lonnie Shea for your vast compassion and empathy during both the turbulent and successful moments - I am so appreciative that you've given me the freedom and tools to pave my own trajectory during my growth as a researcher. Thank you Drs. Jacqueline Jeruss, David Kohn, and James Moon for your mentorship, scientific feedback, and support. I am so appreciative of the Biomedical Engineering community at the

University of Michigan. Being a part of the BME Graduate Student Council has given me a great sense of community, and I am so thankful of the friendships and relationships we've cultivated together. Thank you Maria Steele for the massive impact you make on all BME students at the University of Michigan.

If you know me, you know that music has played an immeasurable role in my life. I'm not sure I can quite articulate in words how deeply emotional I feel about the music that has provided the score for my journey. I would like to thank the following artists for impacting my life: Anderson Paak, Frank Ocean, Herbie Hancock, Hiatus Kaiyote, Kamasi Washington, Kendrick Lamar, Khruangbin, Parliament Funkadelic, Pink Floyd, Radiohead, Red Hot Chili Peppers, Tame Impala, Al Green, Avenged Sevenfold, The Black Keys, Black Sabbath, Bob Marley, Cardi B, Chance the Rapper, D'Angelo, David Bowie, Fela Kuti, Frank Zappa, Green Day, James Brown, John Coltrane, King Gizzard and the Lizard Wizard, Nusrat Fateh Ali Khan, Prince, Queens of the Stone Age, Questlove, Rage Against the Machines, Steely Dan, Stevie Wonder, Talking Heads, Terrace Martin, The Beatles, The Bee Gees, The Doors, Thundercat, Tyler the Creator, and The White Stripes.

To everyone that I've crossed paths with who has changed the course of my trajectory, I am deeply and sincerely appreciative of having the opportunity to know you.

Table of Contents

List of Figures

Abstract

Globally breast cancer has the highest rates of incidence and mortality among women, and the progression of localized breast cancer to metastatic disease is associated with a stark decrease in survival. Although robust advances have been made in the treatment of localized disease, few effective therapies exist to treat metastasis. As such, distant spread marks the disease stage where treatment no longer has curative intent, and disease progression leads to mortality. Decreased survival, as a result of metastatic progression, emphasizes the necessity for developing diagnostic and therapeutic strategies to manage metastatic disease, and I hypothesize that the microenvironment of the metastatic niche can serve as a target for these strategies.

In **Chapter 2** and **Chapter 3** I present studies investigating the utility of cargo-free PLG nanoparticles (NPs) that, upon intravenous delivery, can be internalized by myeloid cells, altering their impact on an anti-tumor immune response at the metastatic niche. We demonstrated that NPs reduce metastatic colonization of the lungs in a murine model of metastatic triple negative breast cancer (mTNBC). The NPs were found to modulate the immune microenvironment of the lungs, skewing myeloid cells toward inflammatory, anti-tumor phenotypes through single cell RNA sequencing. We then found that the reduced metastatic spread was dependent on mature T-cells. Finally, NPs were administered in a primary tumor (PT) resection model and shown to clear established metastatic lesions when delivered as an adjuvant therapy, following surgical resection.

Immunomodulatory therapies have become an integral component of cancer management, along with surgery, chemotherapy, and radiation therapy. Furthermore, the treatment of TNBC with immune checkpoint blockade (ICB) therapy, a T-cell-targeting immunotherapy, has shown

robust improvements in patient outcomes. However, while ICB-sensitive patients experience durable responses to therapy, there are no effective biomarkers available to predict ICB-response or stratify ICB-sensitivity from resistance. Our lab has previously investigated the utility of a microporous PCL scaffold that integrates with the host upon surgical implantation, finding that the immune milieu of the implant recapitulates key features of the native metastatic niche. We have shown that gene expressions from the implant microenvironment can be longitudinally probed to monitor 1) progression of cancer and 2) response to a PT resection. As such, in **Chapter 4**, I investigate the hypothesis that the microporous implant can be longitudinally probed to glean insight into ICB-response. Divergent responses to therapy were observed when treating murine TNBC with anti-PD-1, and gene expressions at the implant were probed to monitor ICB-sensitivity versus resistance. Differential lymphocyte and myeloid cell responses were identified for the divergent therapy responses. Finally, implant-derived gene expressions were probed before ICB administration, illuminating predictive analytes for ICB-response prior to initiating therapy.

Overall this dissertation demonstrates the potential for applying engineered materials to 1) treat metastatic disease by modulating cancer-associated myeloid cells with the goal of enhancing anti-tumor T-cell surveillance and 2) stratify divergent ICB-responses and investigate mechanisms underlying therapy sensitivity versus resistance.

Chapter 1
Introduction

1.1 Background on Metastatic Breast Cancer

Cancer is the second leading cause of death in the United States, and breast cancer has the highest rates of incidence and mortality in women worldwide [1,2]. While there is a 99% five-year relative survival rate for localized breast cancer, survival drops to 29% for metastatic disease [1]. Although robust advances have been made in the treatment of localized breast cancer, few efficacious therapies exist to treat metastasis, or the spread of cancer from a primary tumor (PT) to distal sites [3,4]. Both the 1) scarcity of treatments to manage metastasis and 2) disparity in outcomes between primary and metastatic disease has sparked considerable interest in leveraging the immune system as a novel treatment [5]. In fact, as of 2020, there were 6,281 active clinical trials investigating immunotherapies, of which over 60% of these were for T-cell-targeted immunomodulators [6].

1.2 Background on Immuno-Oncology

1.2.1 Immune Dysregulation in Cancer

Dysregulated immune cells are integral to the initiation and progression of the metastatic niche [7]. Whereas the immune system of a healthy individual utilizes both innate and adaptive immune surveillance mechanisms to suppress neoplastic cells, cancer-induced immune dysregulation suppresses many of these mechanisms and drives the formation of aberrant, pro-tumor immune cells [7–10]. Tumor-secreted factors induce the formation of immature,

immunosuppressive myeloid cells, largely neutrophils and monocytes, which play a vital role in both the initiation and progression of a metastasis [11–13]. These immature myeloid cells have been shown to secrete arginase-1, IL-17, TGFβ, IL-10, and reactive oxygen species, such as nitric oxide and hydrogen peroxide, which can inhibit T-cell proliferation and function [14–17]. Monocyte-derived tumor-associated macrophages have additionally been shown to suppress T-cell-mediated immune surveillance through their secretion of IL-10, CCL22, and TGF-β; dysregulated MHC; and their surface expression of PD-L1, B7-H4 and HIF-1α [18–22]. Additionally, cancer-associated neutrophils and monocytes have also been shown to facilitate the formation of a pre-metastatic niche, arrival of disseminated tumor cells to the metastatic niche, and the suppression of adaptive immunity to promote the progression of metastatic disease [10,23–26].

1.2.2 Immunosuppression and T-cell Checkpoints

Cytotoxic CD8+ T-cells are some of the most powerful mediators of anti-cancer immune responses [27]. In a healthy individual, cytotoxic T-cells are able to detect and eliminate neoplastic, pre-cancerous cells [28]. CD4+T-cells aid in this process by helping to augment cytotoxic CD8+T-cell responses through multivariate effector function [29]. Despite T-cell-mediated immunosurveillance, some neoplastic cells evade surveillance and form cancerous lesions. At the tumor microenvironment, much of the immune landscape is polarized as a result of multifaceted interactions within the cancerous milieu [30]. Cytotoxic T-lymphocyte-associated antigen 4 (CTLA-4) and programmed death 1 (PD1) are two immune checkpoint receptors that function as negative regulators of T-cell function [31,32]. CTLA-4 regulates T-cell activity, primary in lymph nodes, and plays a vital role in establishing peripheral tolerance [33]. PD-1 is a protein upregulated on activated T-cells that regulates T-cell function following an inflammatory response, to prevent

T-cell hyperactivity in a healthy individual [34,35]. Ligation of PD-1 with programmed death ligand-1 (PD-L1) inhibits T-cell activity, and the exploitation of PD-1:PD-L1 ligation within the tumor microenvironment to suppress T-cell-mediated surveillance has made it a target of great clinical interest [36]. PD-1 activation on a CD8+ T-cell negatively regulates the signals downstream of the TCR receptor. Specifically, PD-1 ligation on T-cells impacts the T-cell receptor signaling cascade, targeting downstream effectors including the ZAP70, P13K-AKT, and RAS signaling pathways, inhibiting the activation of T-cell activation-associated transcription factors [37,38].

Inflammatory cytokines such as interferons (IFN) α, β and γ are potent drivers of PD-L1 expression [37], and can impact T-cell exhaustion within the context of cancer [39]. IFN-γ has been found to directly induce PD-L1 expression by both cancer cells and stromal cells at the tumor microenvironment [37,40]. Cancer cells can also carry mutations that cause them to express high levels of PD-L1, despite low levels of inflammation [37]. While T-cells have been the focus of investigations into PD-1/PD-L1 signaling, it is important to note that innate immune cells can have a profound impact on these pathways. For example, tumor associated macrophages (TAMs) can secrete cytokines that increase PD-1 and PD-L1 expression [41]. TAM-derived IFN-γ, IL-1β, TNF-α, TGF-β, IL-6 and IL-18 have all been shown to suppress T-cell function [41]. Counterintuitively, TAMs have also been found to express PD-1, which has shown negative correlation with macrophage-mediated cancer cell phagocytosis [42]. In general, a myriad of cells within the tumor microenvironment, including cancer cells, immature myeloid cells, and macrophages have been implicated in leveraging T-cell checkpoints to induce anergy among anti-tumor T-cells [43,44].

1.3 Targeting Myeloid Cell-Mediated Immunosuppression in Cancer

1.3.1 Overview of Targeting Myeloid Cells in Cancer

Recently, precision therapies that enable the directed treatment of metastatic disease have begun to be incorporated into clinical practice. These therapies aim to directly target metastatic tumor cells, as with PARP inhibitors, or to augment an adaptive immune response, as with immune checkpoint inhibitors and CAR T-cells [45,46]. Novel immunotherapies targeting pro-tumor myeloid cells in the metastatic niche have also begun to emerge recently. Cancer-associated myeloid cells have been directly associated with poor clinical outcomes, and thus serve as highly compelling therapeutic targets [47,48]. Approaches targeting myeloid cells include the depletion of pro-tumor populations and the inhibition of signaling molecules driving their recruitment to metastatic sites [49]. In murine models, depletion of pro-tumor myeloid cell populations has been shown to enhance anti-tumor immunity, impair angiogenesis, and inhibit the seeding of metastases [50–52]. Likewise, targeted inhibition of CCL2 signaling has been shown to block the recruitment of pro-tumor monocytes to the lung and inhibit metastasis [25]. While these immunotherapy strategies have shown early promise, non-specific cell depletion or systemic inhibition of a signaling pathway has demonstrated mixed results in clinical trials due to the heterogeneity among myeloid cell populations [53]. Some inflammatory subsets of neutrophils and macrophages have been found to possess immune-stimulating and anti-tumor behavior, motivating the development of therapies to skew myeloid cell progenitors towards anti-tumor phenotypes [17,54–57].

1.3.2 Nanoparticle-Mediated Immunomodulation

Nanoparticles (NPs) are an emerging technology for targeting pathological inflammation in cancer and other diseases. Traditionally, nanoparticles have been investigated as vehicles for

the targeted delivery of chemotherapies and other pharmaceuticals to tumors [58]. Nanoparticles are believed to home to tumors as a result of increased vascular permeability and poor lymphatic drainage in a phenomenon termed the enhanced permeability and retention (EPR) effect [59]. In addition, NPs can be targeted towards tumor cells with surface modifications such as transferrin or folate [60]. Recently, cargo-free polymer NPs have been found to modulate immune cell behavior in a manner dependent on their physical and chemical properties [61–63]. Upon intravenous delivery, nanoparticles are largely phagocytosed by myeloid cells, such as macrophages, neutrophils, and dendritic cells, and predominantly home to the liver, spleen, and lymph nodes [64]. NP administration has been shown to alter myeloid cell phenotype and redirect myeloid cell trafficking away from sites of inflammation toward the spleen [65]. Our lab has previously shown the efficacy of drug-free nanoparticles to mitigate pathological inflammation by modulating myeloid cells in models of traumatic injury and autoimmune disease [66,67]. Notably, we have also shown that cargo-free poly(lactide-co-glycolide) (PLG) NPs modulate myeloid cells and inhibit primary tumor growth in a murine model of breast cancer [68]. Our nanoparticle platform was recently found to be well-tolerated in a Phase 2a clinical trial, demonstrating the translational potential of nanoparticles [69].

The engineering properties of nanoparticles, including their size, charge, and polymer composition, play an integral role the internalization and function of NPs [70]. In a study of cargo-free nanoparticles, with the goal of eliciting anti-inflammatory action against innate immune cells challenged by TLR agonists, our lab found that NP-mediated immunomodulation was dependent on their physicochemical properties [61]. Several formulations of PLG and poly(lactic acid) (PLA) NPs were investigated to this end. The authors first found that PLG and PLA particles prepared with PEMA as a surfactant possessed a more negative surface charge and were associated with

more rapid uptake by cells in vitro, as compared to NPs prepared with PVA as a surfactant, which were less negatively charged. In addition to cellular uptake, researchers in the study also found that particle formulation significantly impacted the immunomodulatory effect of nanoparticle administration on cytokine secretion by innate immune cells. Finally, this study investigated cargo-free NPs in vivo, finding that the charge and formulation of the particles played a significant role in the quantity and breadth of association with innate immune cells, as well as murine survival in response to inflammatory challenge. Our lab followed this investigation by studying the role of tunable material properties on NP-mediated immunomodulation in a murine model of breast cancer [68]. Surfactant type and PLG molecular weight were tested in an in vitro assay for internalization by innate immune cells. This study found that altering the charge and molecular weight of NPs significantly impacted internalization, specifically that PEMA-High NPs exhibited the maximal internalization by innate immune cells. Notably, the ability to tune the properties of NPs for the desired internalization and biodistribution makes them a highly modular therapy candidate for targeting the immune system.

1.4 Immune Checkpoint Blockade in Cancer

1.4.1 Clinical Trials for Checkpoint Inhibition in Breast Cancer

Immune checkpoint blockade (ICB), or the inhibition of T-cell checkpoints, has become the most successful immunotherapy in a variety of tumors and was awarded the 2018 Nobel Prize in Physiology or Medicine. Specifically, the treatment of triple negative breast cancer (TNBC) with ICB has shown improvements in outcomes [71]. TNBC is a more immunogenic BC subtype and has thus been a focus of ICB clinical efforts [72–74]. Pembrolizumab, a monoclonal antibody (Ab) against PD-1 (aPD-1), was the first ICB studied in advanced, PD-L1+ TNBC [75]. This phase 1b clinical trial (KEYNOTE-012) of pembrolizumab showed an 18.5% overall response rate

(ORR) for PD-L1+ advanced TNBC patients receiving aPD-1. In the follow-up phase II study (KEYNOTE-086), investigators evaluated first-line pembrolizumab in patients with PD-L1+ mTNBC [76]. Whereas the previous phase 1 trial was conducted in a heavily pretreated population, the phase II study found a 21.4% objective response rate (ORR), 10.4 month median duration of response, 2.1 month progression free survival (PFS), and 18.0 month overall survival (OS) among the first-line ICB-receiving patients. Interestingly, among the heavily pretreated arm of this phase II study, investigators found a 5.3% ORR, 2.0 month PFS, and 9.0 month OS, indicating that aPD-1 monotherapy was less effective as a second- or third-line treatment [77]. The randomized, open-label, phase 3 trial of pembrolizumab found that the ICB performed similarly as effective, and had reduced grade 3-4 adverse events, as compared to the gold standard chemotherapy in mTNBC patients [78].

While the majority of ICB trials have been focused on the safety and clinical activity of aPD-1 in breast cancer, studies have been investigated into targeting PD-L1 [74]. Atezolizumab and avelumab are both anti-PD-L1 (aPD-L1) ICB monoclonal Abs with the goal of inhibiting PD-1:PD-L1 ligation. In the first phase 1 study of atezolizumab in mTNBC patients, a higher ORR was seen in the first-line (24%), as compared to the second-line setting (6%), and also for patients with PD-L1 expression of at least 1% on tumor-infiltrating immune cells (12% ORR), in contrast to < 1% PD-L1+ immune cells (0% ORR) [79]. The Phase 1b JAVELIN study of avelumab investigated its activity in heavily pretreated metastatic breast cancer patients [80]. Investigators found a 3.0% ORR in overall breast cancer patients, and a 5.2% ORR in patients with TNBC. A higher ORR was also observed in breast cancer patients with PD-L1+ tumor-infiltrating immune cells (16.7%) versus the PD-L1- cohort (1.6%).

Recently, ICB has been investigated as a neoadjuvant therapy, prior to surgical resection, in stage 2 or stage 3 TNBC, with the goal of improving pathological complete response and decreasing disease progression following surgery. The phase 3 KEYNOTE-522 trial studied the efficacy of neoadjuvant pembrolizumab in previously untreated stage 2 or stage 3 TNBC patients [81]. Randomized patients were assigned to receive pembrolizumab plus chemotherapy or placebo plus chemotherapy as their neoadjuvant therapy. After surgery, patients received either adjuvant pembrolizumab or placebo. Investigators observed that early TNBC patients receiving ICB had higher pathological complete responses (64.8%), versus the placebo cohort (51.2%), and reduced disease progression (7.4% versus 11.8% of patients).

The summary of current clinical evidence has shown that the most effective contexts for treating breast cancer with ICB is either in the early TNBC setting to augment surgical resection, or as a first-line therapy in treating metastatic TNBC. Additionally, the clinical trials-to-date have shown the greatest efficacy of ICB monotherapy 1) in TNBC versus other BC subtypes, 2) as an early-line therapy (neoadjuvant for early TNBC or first-line for mTNBC), and 3) in PD-L1+ tumors [82]. While breast cancer patients that are sensitive to ICB therapy have incredible responses, only about 10-20% of PD-L1+ mTNBC patients benefit from ICB. As such, there is a great need for biomarkers to stratify patients based on response.

1.4.2 Biomarkers for Checkpoint Inhibition

One of the greatest limitations of PD-1/PD-L1 blockade is the lack of biomarkers to accurately predict response to therapy. While many biomarkers have been investigated in pre-clinical studies as predictors for aPD-1/aPD-L1 response, very few are used clinically [83]. The most widely used biomarker for aPD-1/aPD-L1 is PD-L1 expression, which can be measured though immunohistochemistry (IHC) [83]. Many TNBC trials, including the Impassion130 and

Keynote520 trials, have used PD-L1 expression as a biomarker to stratify between ICB-sensitive and ICB-resistant patient populations [84,85]. The Impassion130 trial investigated PD-L1-expression on tumor infiltrating lymphocytes, while the Keynote520 trial studied the PD-L1 combined positive score (CPS), which was calculated by dividing the total number of PD-L1+ cells by the total number of tumor cells. A score of more than 1% was defined as the cut off for positivity, in both cases. While both trials found that PD-L1+ patients had a significantly higher ORR, as compared to PD-L1- patients, the majority of PD-L1+ patients were resistant to ICB (74.6% for the Impassion130 trial and 51.6% for the Keynote520 trials), showing that PD-L1 expression is not the only factor driving ICB-response. Furthermore, some PD-L1- patients showed ICB-sensitivity. Although PD-L1 expression is currently the most utilized ICB-response-associated biomarker, it is greatly limited in its ability to predict response.

High tumor mutational burden (TMB) is another ICB biomarker utilized in solid tumors, which acquired its FDA approval based on the results of the Keynote-158 trial [86]. This trial tested the efficacy of pembrolizumab in patients with high microsatellite instability and mismatch repair-deficiency in non-colorectal cancers. As T-cells survey self- and non-self-antigens, it is hypothesized that higher TMB increases the T-cell-recognition of tumor cell, and thus provides biological insight as an ICB biomarker [87]. However, while some studies have shown that higher TMB is associated with improved ICB response in TNBC, as with PD-L1 expression, TMB alone cannot accurately stratify between ICB-sensitivity and resistance [88]. There is also limited information about its efficacy in TNBC. Although additional biomarkers, such as tumor infiltrating leukocytes (TIL), have been pursued, they have shown limited clinical efficacy in predicting response [87]. Tumor-derived gene signatures have also been pursued for predicting ICB-response. Genomic assays like Oncotype DX are currently emerging as powerful tools to help clinicians

make treatment decisions [89]. However, most genomic assays have failed to provide predictive insight into ICB-response in TNBC [90]. There are some tumor-derived gene panels, like FoundationOne, that are used in the clinic to predict ICB-response, however they mainly test for biomarkers like TMB, and as such, suffer from the same limitations as directly measuring TMB, while often being less sensitive [91]. In addition to the lack of effective ICB biomarkers, there are limitations associated with relying on primary tumor (PT) biopsies for identifying biomarkers predictive of ICB. While a PT biopsy can offer insight into the local tumor microenvironment, it offers little information about systemic changes that influence treatment efficacy. Examples of this include dynamic changes in the immune cell millieu at lymphoid tissues or metastatic lesions.

1.4.3 Liquid Biopsy for Immunotherapy Biomarkers

IHC analysis of the PT for biomarkers has typically been used to determine patient eligibility when treating metastatic disease, as biopsying a metastatic lesion within the lungs or brain, for example, is anatomically challenging and the spatial heterogeneity of biomarker expression makes this technique additionally impractical. As a result of recent technological advancements in cellular- and molecular-capture methods, as well as the emergence of highly sensitive sequencing modalities, liquid biopsies have been pursued to replace conventional IHC [92]. Liquid biopsy has garnered much interest as it is minimally invasive, cost-effective, and can be used for repeat measurements throughout the evaluation and treatment of a patient [92–95]. Liquid biopsy-derived circulating tumor cells (CTCs), circulating cell-free DNA (cfDNA), and circulating tumor DNA (ctDNA) have all been pursued as biomarker candidates [92].

Quantification of cfDNA levels has been investigated, as high levels of cfDNA in circulation have been correlated with tumor burden [96]. Moreover, mutation profiling of cfDNA has been studied as inclusion criteria for immunotherapies, with variable results. One study found

that copy number variations in cfDNA were predictive for clinical outcomes for PD-1 inhibition in cervical cancer [97]. Conversely, another report showed that copy number variations provided no value in predicting ICB-response in several cancer types [98]. While these contradictory results may be resolved with improved cfDNA-isolation and detection, they fail to consider that ICB targets cell-surface receptors, and thus ignore key mechanistic insight into ICB function and efficacy [99].

CTCs, in contrast to cell-free DNA, are intact cells that have potentially detectable extra- and intra-cellular biomarkers. PD-L1 positivity on CTCs has been investigated for various cancers, including non-small cell lung cancer, melanoma, and breast cancer [92]. Unfortunately, these studies have had conflicting results, with some reports demonstrating a correlation between clinical response to aPD-L1 for patients with PD-L1+ CTCs, while others show no predictive value for PD-L1 expression on CTCs [100–103]. Because aPD-1/aPD-L1 administration also abrogates PD-1 ligation with PD-L1 expressed on non-tumor cells (e.g., T cells, B cells, DCs, macrophages) at the tumor microenvironment, probing for PD-L1 on tumor cells in the peripheral blood may explain the lack of efficacy in gleaning ICB-biomarkers from CTCs [36]. Moreover, CTCs are known to harbor genetic and phenotypic discordances from tumor cells in both the PT and metastatic lesions, further blurring the utility of CTCs for biomarker detection [104]. Lastly, CTCs are found in low numbers in the blood and have poor expression of tumor-specific surface markers, which are necessary for enrichment, making them technologically challenging to isolate and study [92].

Chapter 2

Cargo-Free Immunomodulatory Nanoparticles Combined with Anti-PD-1 Antibody for Treating Metastatic Breast Cancer

The material in this chapter has been adapted with minor modifications from the following article:

> Y. Zhang, K.R. Hughes, **R.M. Raghani**, J. Ma, S. Orbach, J.S. Jeruss, L.D. Shea, Cargo-free immunomodulatory nanoparticles combined with anti-PD-1 antibody for treating metastatic breast cancer, Biomaterials. (2021)

2.1 Abstract

The presence of immunosuppressive innate immune cells such as myeloid derived suppressor cells (MDSCs), Ly6C-high monocytes, and tumor-associated macrophages (TAMs) at a tumor can inhibit effector T cell and NK cell function. Immune checkpoint blockade using anti-PD-1 antibody aims to overcome the immune suppressive environment, yet only a fraction of patients responds. Herein, we test the hypothesis that cargo-free PLG nanoparticles administered intravenously can divert circulating immune cells from the tumor microenvironment to enhance the efficacy of anti-PD-1 immunotherapy in the 4T1 mouse model of metastatic triple-negative breast cancer. *In vitro* studies demonstrate that these nanoparticles decrease the expression of MCP-1 by 5-fold and increase the expression of TNF-α by more than 2-fold upon uptake by innate immune cells. Intravenous administration of particles results in internalization by MDSCs and monocytes, with particles detected in the liver, lung, spleen, and primary tumor. Nanoparticle delivery decreased the abundance of MDSCs in circulation and in

the lung, the latter being the primary metastatic site. Combined with anti-PD-1 antibody, nanoparticles significantly slowed tumor growth and resulted in a survival benefit. Gene expression analysis by GSEA indicated inflammatory myeloid cell pathways were downregulated in the lung and upregulated in the spleen and tumor. Upregulation of extrinsic apoptotic pathways was also observed in the primary tumor. Collectively, these results demonstrate that cargo-free PLG nanoparticles can reprogram immune cell responses and alter the tumor microenvironment *in vivo* to overcome the local immune suppression attributed to myeloid cells and enhance the efficacy of anti-PD-1 therapy.

2.2 Introduction

Tumor progression is aided in part by the function of innate immune cells, which can be induced toward an immune suppressive function by tumor-secreted factors [105]. Disease-induced cell types found at the primary tumor or metastatic niche include inflammatory monocytes (CD11b+ Ly6C-hi cells in mice), tumor-associated macrophages (TAMs), and myeloid-derived suppressor cells (MDSCs). Circulating inflammatory monocytes differentiate into tumor-associated macrophages (TAMS) in tissues, and have immunosuppressive phenotypes and induce angiogenesis to aid metastasis [106,107]. Additionally, myeloid cell recruitment has been shown to be critical for metastatic progression [108]. MDSCs are a class of neutrophil that has been implicated in aiding tumor growth and metastasis, especially to the lung [109,110]. These cells normally serve to regulate the immune response to pathogens, but in the context of cancer, MDSCs secrete factors, including immunosuppressive cytokines and reactive oxygen species (ROS), to inhibit anti-tumor T cell and NK cell function [111]. These cells contribute to the failure of immune checkpoint blockade or T-cell immunotherapies [112].

The immunosuppression and pro-tumor functions of myeloid cells have been the targets of numerous therapies to alter either their numbers or phenotypes. Small molecule inhibitors have been applied to inhibit cytokine secretion that recruits myeloid cells [113,114] or T cell function [112,115], or repolarizing cells such as tumor-associated macrophages [116]. Small molecule inhibitors of specific protein activators of MDSCs and TAMs have been shown to reduce their number and abrogate disease [117,118]. Depletion of one or more cell types has also been studied in this context [117,119,120]. However, the large number of cells, cytokines, and other factors that contribute to the immune suppression limit the efficacy of therapies that target a single cell or protein [121]. In addition, myeloid cell phenotypes within various tissues are distinct [122], which motivates the development of therapies that can elicit a tissue-dependent response.

An emerging approach for modulating innate immune cell response in tissues are nanoparticles administered intravenously that target circulating immune cells. Cargo-free polymer nanoparticles (NPs) have been shown to redirect the trafficking of phagocytic innate immune cells upon, and moderate the disease-induced aberrant behavior of these cells. NPs have highly negative surface charge that result in internalization through scavenger receptors including MARCO [123], and the specificity and biodistribution of polymeric NPs can be tuned with changes to the polymer backbone. As such, internalization of NPs is not limited to targeting ligands [124], and they do not induce systemic responses in multiple tissue as with steroids or NSAIDs. The therapeutic benefit of these NPs has been demonstrated in West Nile virus infection, ischemic reperfusion injury [123], traumatic brain injury [125], as well as in spinal cord injury [126]. These injuries are associated with increased inflammation, which contrasts with cancer that is associated with immune suppression to limit immune cell killing of tumor cells [127].

In this report, we test the hypothesis that cargo-free PLG nanoparticles administered intravenously divert circulating immune cells from the tumor microenvironment or metastatic sites, altering the immune responses and enhancing the efficacy of anti-PD1 immunotherapy. In the orthotopic 4T1 mouse model of metastatic triple negative breast cancer, disease-induced myeloid cells rapidly increase in number systemically with disease progression [128] and metastatic 4T1 cells readily colonize the lung due to the host of factors secreted by aberrant monocytes, macrophages, and MDSCs. These myeloid cells have also been shown to directly contribute to resistance to anti-PD-1 and anti-CTLA-4 in the 4T1 model [117]. The cell types and biodistribution of nanoparticles are analyzed, and the impact of the particles on the cell phenotypes are analyzed both *in vitro* and *in vivo*. Particle administration is investigated with respect to the growth of the primary tumor and survival. Finally, the impact of nanoparticles on gene expression within the primary tumor and metastatic site is analyzed. Reprogramming innate immune cell responses within the primary tumor and metastatic tissues represents a new opportunity for this class of nanoparticles that target innate cells in circulation, which has the potential to improve the therapeutic benefit of anti-PD-1 and other immunotherapies.

2.3 Results

2.3.1 Nanoparticle internalization by innate immune cells

PLG nanoparticle internalization by tumor-induced immune cells was initially investigated *in vitro*. By varying the surfactant type and PLG molecular weight, three fluorescently-labeled PLG NP formulations were synthesized (**Figure 2-1A**): PEMA-coated low-molecular weight (PEMA-Low), PEMA-coated high-molecular weight (PEMA-High), and PVA-coated high-molecular weight (PVA-High). These NPs were incubated with blood leukocytes from tumor-bearing mice at 5 μg/mL and 50 μg/mL NP concentration (**Figures 2-1B, 2-S2**). Because PEMA-

High NPs exhibited the maximal internalization at both concentrations, subsequent studies were performed with PEMA-High NPs. Myeloid-derived suppressor cells (MDSCs, $CD11b^+/Ly6C^{lo/-}/Ly6G^+$) and other myeloid cells ($CD11b^+/Ly6C^-/Ly6G^-$) showed increased Cy5.5-NP internalization at 50 μg/mL relative to 5 μg/mL (**Figure 2-1C**), whereas the increased concentration had no effect on the number of Cy5.5-NP^+ monocytes as a percentage of total cells. As MDSCs comprise a large majority of immune cells in circulation, internalization was also quantified as the percentage of Cy5.5-NP^+ cells relative to the number of single cells for each cell subtype (**Figure 2-1D**). At 5 μg/mL, nearly all monocytes are NP^+ (89.4 ± 5.4%) while a lower percentage of MDSCs and other myeloid cells have lower relative internalization (23.7 ± 10.4% and 72.3 ± 14.5%, respectively). When the NP^+ cell numbers are increased at 50 μg/mL, nearly all cells are Cy5.5-NP^+ in all three cell populations (99.3 ± 0.5% of MDSCs, 99.9 ± 0.1% of monocytes, and 99.6 ± 0.2% of other myeloid cells). Taken together, these data demonstrate that monocytes more readily internalize NPs than other myeloid subtypes at low concentrations, yet nearly all MDSCs and other myeloid cells have internalized NPs.

A

	Surfactant	PLG MW	Zeta (mV)	Size (nm)
PEMA-Low	PEMA, 1%	Low	-57.9 ± 0.6	428.6 ± 1.4
PEMA-High	PEMA, 1%	High	-24.1 ± 0.35	896.3 ± 19.05
PVA-High	PVA, 2%	High	-20.1 ± 0.38	249.4 ± 2.23

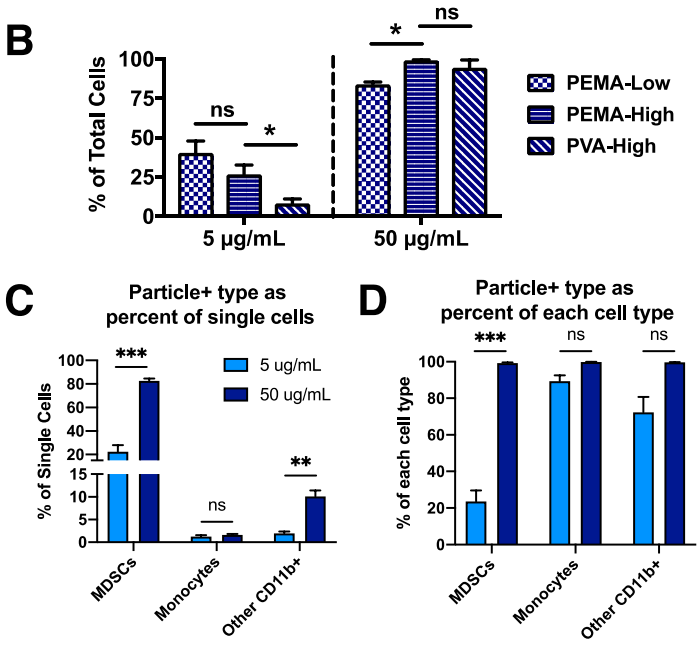

Figure 2-1. Cy5.5-NPs are internalized by innate immune cells and are distributed in disease-relevant tissues. (A) Three NP formulations with combinations of surfactant and PLG molecular weight were tested for internalization *in vitro*. (B) Blood leukocytes from 4T1 tumor-bearing mice at 21 days post inoculation were incubated *in vitro* with each formulation at 5 µg/mL and 50 µg/mL, and internalization was quantified. PEMA-High NPs exhibited high internalization at both concentrations, and subsequent studies were performed with the PEMA-High NPs. Internalization was quantified (C and D) for myeloid cell subtypes (C) as a percentage of all cells and (D) as a percentage of each cell subtype. CD11b+/Ly6Clo/-/Ly6G+ cells (MDSCs) and CD11b+/Ly6C-/Ly6G- cells (other myeloid cells) showed increased internalization with increase in NP concentration, while monocytes did not. These data indicate that monocytes more readily internalize NPs compared to MDSCs and other myeloid cells. A 2-way ANOVA with Tukey's multiple comparisons test was performed (A and B), bars show mean ± SEM for n = 3 biological replicates per condition, where ** $p < 0.01$, *** $p < 0.001$, ns, not significant.

The biodistribution and *in vivo* internalization by myeloid cell subsets was next studied following intravenous injection of Cy5.5-NPs. Assessment of whole-organ fluorescence (**Figure 2-2A, 2-2B, 2-S3A**) indicated that Cy5.5-NPs accumulated primarily in the liver and spleen, and Cy5.5-NPs were detected in these organs through 48 hours post injection. NPs accumulated in the lung at 12 hours, yet the majority was cleared from the lung by 48 hours. Relatively low levels of

Cy5.5-NPs were detected in the tumor. The cell types within these organs that were associated with NPs was quantified by flow cytometry and each NP^+ cell type was shown as a percentage of all NP^+ cells within each organ (**Figure 2-2B, 2-S3B**). Monocytes comprised the largest population of NP^+ myeloid cells in all organs (37.6 ± 7.9%, 46.3 ± 7.9%, 26.6 ± 4.3%, 7.6 ± 2.4% in tumor, lung, spleen, and liver, respectively) compared to MDSCs (15.6 ± 5.3%, 34.8 ± 10.0%, 7.8 ± 2.0%, 3.6 ± 0.7% in tumor, lung, spleen, and liver, respectively) and macrophages (19.5 ± 7.7%, 3.3 ± 0.5%, 3.5 ± 0.8%, 4.0 ± 0.9% in tumor, lung, spleen, and liver, respectively).

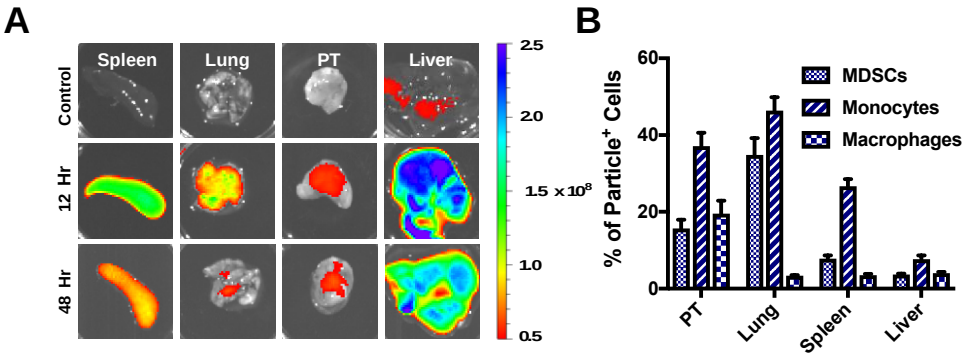

Figure 2-2. In vivo distribution of Cy5.5-NPs. (A) Ex vivo imaging following i.v. injection of 1 mg of Cy5.5-NPs shows they primarily accumulate in spleen and liver, and are detectable for more than 48 hours post injection. (B) Quantification of particle internalization by myeloid cell subsets within tissues as a percentage of total NP+ cells for a given tissue.

2.3.2 Nanoparticle administration alters immune cell distribution in blood and organs

We next investigated whether the intravenously delivered NPs would influence the distribution of innate immune cells in circulation and at the primary tumor or metastatic sites (i.e., lung). The analysis of blood 12 hours following a single dose of NPs revealed that the proportion of MDSCs decreased from 82.5 ± 2.8% to 63.5 ± 13.9% (**Figure 2-3A**). No significant change was observed in the percentage of macrophages ($CD11b^+/F4/80^+$), monocytes, or dendritic cells (DCs, $CD11c^+$) in the blood with NP administration (**Figure 2-3A**). The accumulation of cells within the primary tumor and metastatic sites was analyzed following 6 consecutive days of NP

administration. The quantity of MDSCs as a percentage of all single cells in the lung (**Figure 2-3B**) decreased with NP administration (30.0 ± 3.7% for PBS vs. 21.1 ± 6.2% for NP), consistent with a decrease observed in the blood (**Figure 2-3A**). No significant differences in myeloid cell proportions were observed in the spleen or primary tumor (**Figure 2-3C** and **2-3D**).

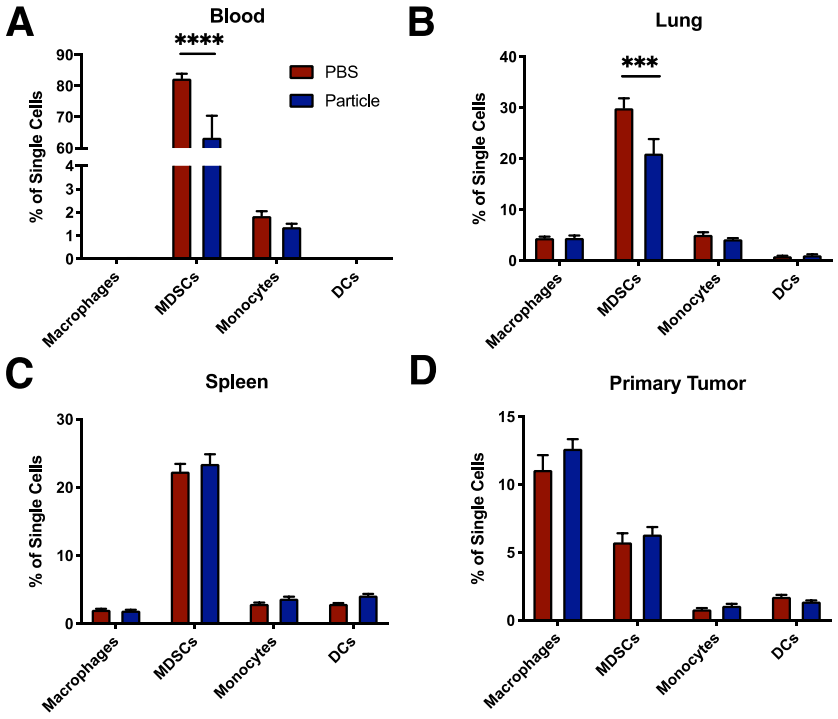

Figure 2-3. In vivo administration of cargo-free NPs reduced the proportion of MDSCs in circulation and at metastatic organs. (A) Tumor-bearing mice at were administered i.v. 1 mg of NPs in 200 µL of PBS or the equivalent volume of PBS only (n = 4 per group), and innate immune cells were quantified in the blood 12 hours post injection by flow cytometry. (B-D) NPs were administered at a dose of 1 mg/200 µL for 6 days to allow for accumulation and uptake of NPs (n = 4 PBS control, n = 5 NP). Flow cytometry quantification of immune cells in the lung (B), spleen (C), and primary tumor (D) was performed on day 10 post inoculation. Decrease in MDSCs observed in the blood (A) and lung (C) with NP administration. A 2-way ANOVA with Tukey's multiple comparisons test was performed (A-D), bars show mean ± SEM, where *** $p < 0.001$, and **** $p < 0.0001$.

2.3.3 Synergistic therapeutic effect observed in nanoparticles combined with anti-PD-1

The therapeutic efficacy of NPs against 4T1 tumor growth and metastasis was next investigated. Mice were inoculated with orthotopic 4T1 tumors and placed in one of four treatment groups: 1) PBS control, 2) anti-PD-1 antibody only, 3) NPs only, and 4) NPs + anti-PD-1 (**Figure**

2-4A). Average tumor size was decreased for combination NPs + anti-PD-1 (V = 1240 ± 298 mm^3, volume increase of 16.0 ± 6.7 compared to initial tumor volume) compared to PBS control (V = 1940 ± 431 mm^3; volume increase by 28.4 ± 12.4; p = 0.038), but was not decreased for either monotherapy (V = 1630 ± 578 mm^3, volume increase by 23.2 ± 8.3 for anti-PD-1; V = 1690 ± 575 mm^3, volume increase by 21.5 ± 5.4 for NPs) (**Figure 2-4B**). Survival, based on body condition and tumor appearance, was monitored after day 22 post inoculation (**Figure 2-4C**). Median survival was 24 days for the PBS and anti-PD-1 groups, 25 days for NPs alone, and 28 days for NPs + anti-PD-1 combination treatment. A survival benefit was observed for the combination treatment cohort compared to cohorts treated with PBS (p = 0.001), and compared to cohorts treated with either anti-PD-1 or NP monotherapy (p = 0.015 and p = 0.030, respectively). Taken

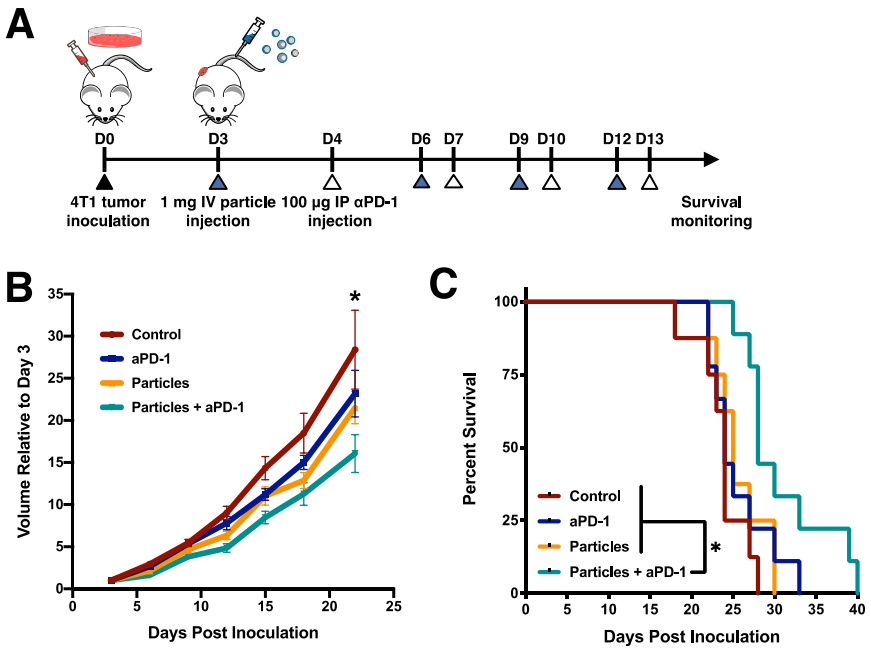

Figure 2-4. NPs + anti-PD-1 combination therapy delays 4T1 tumor growth and reduces metastasis. 4T1-bearing mice were treated with PBS (control), anti-PD-1 (aPD-1), NPs (particles), or combination therapy (particles + aPD-1). (A) Schematic of disease model and treatment. (B) Tumor volumes, and (C) survival curves are shown for the four treatment conditions (control, n = 7; aPD-1, n = 9; particles, n = 8, particles + aPD-1, n = 9), indicating a therapeutic benefit for particles + aPD-1 but not for either monotherapy compared to control. Two-way ANOVA with Tukey's multiple comparisons tests were performed. Bars show mean ± SEM where * $p < 0.05$ compared to control (B), and where * $p < 0.05$ compared to particles + aPD-1 (C).

together, these data indicate an additive or synergistic therapeutic effect by combining NPs and anti-PD-1 antibody.

2.3.4 Nanoparticle internalization results in upregulation of inflammatory pathways

The mechanism by which NP administration may reduce tumor growth and metastasis was investigated *in vitro* by analyzing secretion of multiple cytokines associated with tumor progression following nanoparticle treatment. Mice were first treated with anti-PD-1 antibody post inoculation (**Figure 2-5A**), and splenocytes were then isolated from healthy and tumor-bearing mice (with and without anti-PD-1 treatment) at day 14 post inoculation. Splenocytes from tumor-bearing ($Tumor^+$) mice secreted elevated amounts of the cytokine interleukin 6 (IL-6), granulocyte-macrophage colony-stimulating factor (GM-CSF), monocyte chemoattractant protein

1 (MCP-1), and tumor necrosis factor alpha (TNF-α), but not transforming growth factor beta (TGF-β) relative to those of Tumor- mice (**Figure 2-5B-F**). Treatment of these cells with NPs significantly decreased secretion of MCP-1 (**Figure 2-5D**) and increased TNF- α secretion (**Figure 2-5E**). This effect is amplified with the addition of anti-PD-1 (Tumor$^+$ αPD-1$^+$). No alteration in cytokine expression was observed for NP treatment for production of IL-6 (**Figure 2-5B**) or TGF-β (**Figure 2-5F**) in tumor-bearing mice with or without anti-PD-1. Increased granulocyte-macrophage colony-stimulating factor (GM-CSF) production was observed with NP treatment only in the Tumor$^+$ αPD-1$^+$ group (**Figure 2-5C**). Notably, NP treatment increased TNF-α production by more than 2-fold in tumor-bearing mice both with and without anti-PD-1 (**Figure 2-5E**). The production of MCP-1 is also greatly increased in tumor-bearing mice, yet there is a nearly 5-fold decrease in secreted MCP-1 with NP treatment in both the Tumor$^+$ and Tumor$^+$ αPD-1$^+$ groups. We sought to identify the source of the produced cytokines, and thus Gr1$^+$ cells were sorted by MACS and cytokine analysis was performed. Gr1$^+$ cells were the focus as they are the predominant cell type in the disease model. These studies indicate an increased expression of TNF-α by the Gr1$^+$ cells (**Figure 2-S4**), consistent with the analysis of single cell data sets. However, the increase in MCP-1 was not observed for the Gr1$^+$ cells, indicating an alternative cell type. These data indicate that NPs can alter the production of inflammatory cytokines and that anti-PD-1 contributes to additional changes in cytokine levels.

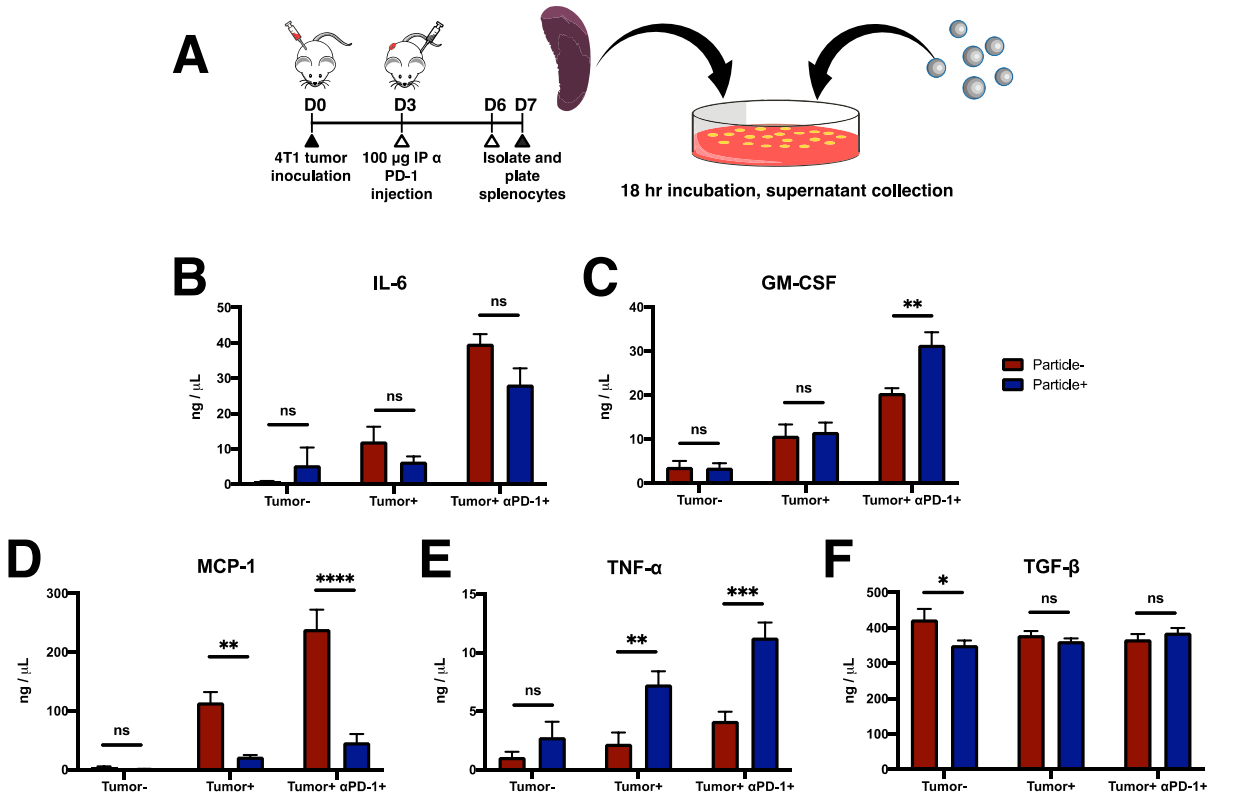

Figure 2-5. Reprogramming of inflammatory response by NP treatment *in vitro*. (A) Schematic and timeline of the study. Splenocytes from tumor-bearing mice that were treated with or without aPD-1 and incubated with NPs. (B-F) Cytokine secretion as measured by ELISA for splenocytes isolated from healthy (tumor-), tumor-bearing (tumor+), and *in vivo* aPD-1-treated (tumor+ aPD-1+) mice. Splenocytes were treated *in vitro* with (particle+) or without (particle-) NPs. Notably, there was a large decrease in the production of the MDSC-recruiting chemokine MCP-1 (D) and an increase in the production of proinflammatory TNF-*α* (C). 2-way ANOVA with Tukey's multiple comparisons tests were performed. Bars show mean ± SEM where * $p < 0.05$, ** $p < 0.01$, *** $p < 0.001$, **** $p < 0.0001$ compared to particle- control (n = 4 per condition).

2.3.5 Tissue-specific deactivation of disease-relevant pathways in vivo

Gene expression within the primary tumor, spleen, and the lung, the primary metastatic site was analyzed at day 14 post inoculation to assess the impact of NP and anti-PD-1 treatment on these tissues. Gene expression at the spleen was analyzed to provide a relative measure of systemic immune changes, which could then be compared to the tissue specific responses within the primary tumor and lung. Differential gene expression was evaluated for each tissue compared to the PBS control group (**Figures 2-6A - 2-6C**). In addition, pathway changes were investigated using Gene

Set Enrichment Analysis (GSEA) for a total of 5,944 gene sets were examined (**Figure 2-S5**). Furthermore, we subcategorized the pathway changes into those that would be supportive of tumor progression versus those that would inhibit tumor progression (**Figure 2-S6**). The spleen and tumor had a substantially larger number of pathways that were predicted to have upregulated activity relative to those that would be downregulated, though the number of pathways that would be predicted to be supportive of tumor progression relative to those that would inhibit tumor progression were more similar. Gene sets that showed the greatest enrichment (positive or negative) for immune cells in all data sets were obtained and condensed into a list of 14 disease-relevant pathways (**Figures 2-6D, 2-6E**). Pathways with normalized enrichment score (NES) > 1.3 or NES < -1.3 were considered differentially expressed compared to untreated control. Relative to no treatment, the spleen and lung had a similar NES for 9 of the 14 pathways, with the differences associated with innate and adaptive immune cell responses. NP treatment resulted in downregulation of pathways associated with pro-tumor innate cells. The impact of NPs was distinct within the lung, the primary metastatic site, relative to the spleen or primary tumor. In the lung, the number of pathways predicted to have downregulated activity was substantially larger than the number predicted to be upregulated, which also associated with an increased in the activity of pathways associated with anti-tumor activity relative to pro-tumor activity. For the 14 common pathways, only 4 were similar between the lung and the spleen or primary tumor.

The RNAseq data was also analyzed by comparing the NP + anti-PD-1 condition to NP alone in order to more effectively isolate the impact of the additional anti-PD-1 treatment. A list of 15 disease-relevant pathways were identified (**Figure 2-6F**). As before, the spleen and primary tumor had many similarities, and the lung was the most distinct with most pathways having a negative NES. With the primary tumor, an increased expression was observed for many pathways

associated with activation of the immune system for both adaptive and innate immune cells, which is consistent with the decreased tumor growth that was observed and also the expected effects of treatment with anti-PD-1. Within the lung, most of these 15 pathways had a negative NES. Based on the differential response of the lung relative to the primary tumor and spleen, we also analyzed the cell types present within the lung at day 14 for differences in cell types for the conditions (**Figure 2-S7**). For NP treatment with and without anti-PD-1, the number of neutrophils, macrophages, T cells, B cells, and NK cells was similar, suggesting that the RNAseq results indicate a differential phenotype and do not result from the accumulation of differential cell types. Analysis of the tumor cell numbers within the lung indicate an accumulation on the order of 100 cells within the lung, indicate of early stage metastasis, that was not significantly different between conditions (**Figure 2-S8**).

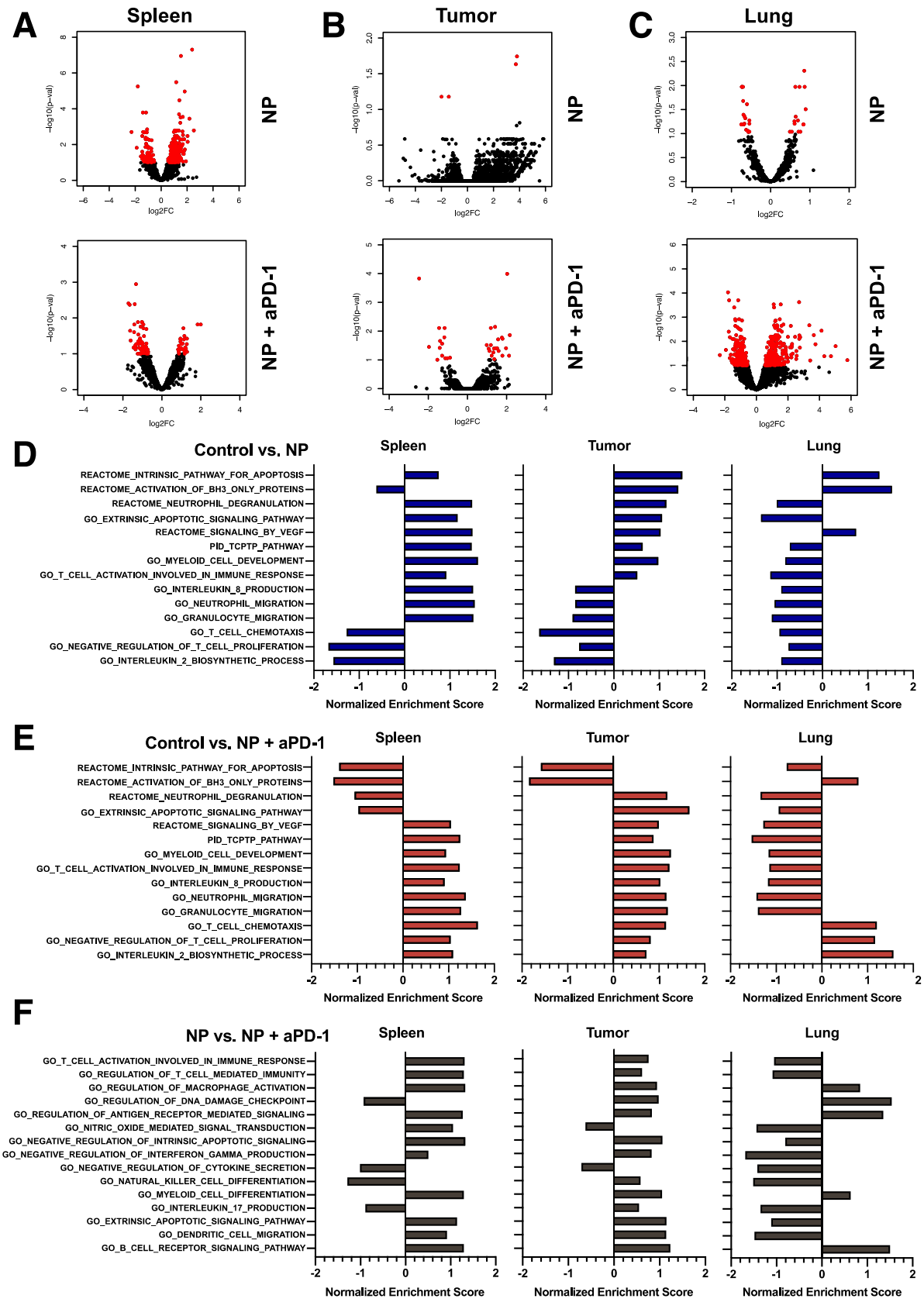
A
Spleen
B
Tumor
C
Lung
NP
NP + aPD-1
−log10(p−val)
log2FC
D
Control vs. NP
E
Control vs. NP + aPD-1
F
NP vs. NP + aPD-1
REACTOME_INTRINSIC_PATHWAY_FOR_APOPTOSIS
REACTOME_ACTIVATION_OF_BH3_ONLY_PROTEINS
REACTOME_NEUTROPHIL_DEGRANULATION
GO_EXTRINSIC_APOPTOTIC_SIGNALING_PATHWAY
REACTOME_SIGNALING_BY_VEGF
PID_TCPTP_PATHWAY
GO_MYELOID_CELL_DEVELOPMENT
GO_T_CELL_ACTIVATION_INVOLVED_IN_IMMUNE_RESPONSE
GO_INTERLEUKIN_8_PRODUCTION
GO_NEUTROPHIL_MIGRATION
GO_GRANULOCYTE_MIGRATION
GO_T_CELL_CHEMOTAXIS
GO_NEGATIVE_REGULATION_OF_T_CELL_PROLIFERATION
GO_INTERLEUKIN_2_BIOSYNTHETIC_PROCESS
GO_REGULATION_OF_T_CELL_MEDIATED_IMMUNITY
GO_REGULATION_OF_MACROPHAGE_ACTIVATION
GO_REGULATION_OF_DNA_DAMAGE_CHECKPOINT
GO_REGULATION_OF_ANTIGEN_RECEPTOR_MEDIATED_SIGNALING
GO_NITRIC_OXIDE_MEDIATED_SIGNAL_TRANSDUCTION
GO_NEGATIVE_REGULATION_OF_INTRINSIC_APOPTOTIC_SIGNALING
GO_NEGATIVE_REGULATION_OF_INTERFERON_GAMMA_PRODUCTION
GO_NEGATIVE_REGULATION_OF_CYTOKINE_SECRETION
GO_NATURAL_KILLER_CELL_DIFFERENTIATION
GO_MYELOID_CELL_DIFFERENTIATION
GO_INTERLEUKIN_17_PRODUCTION
GO_EXTRINSIC_APOPTOTIC_SIGNALING_PATHWAY
GO_DENDRITIC_CELL_MIGRATION
GO_B_CELL_RECEPTOR_SIGNALING_PATHWAY
Normalized Enrichment Score

Figure 2-6. Tissue-specific *in vivo* reprogramming by NP and aPD-1 treatment. (A-C) Gene expression by RNAseq was performed on spleen, tumor, and lung tissue from mice treated with PBS, NPs, or NPs + aPD-1 (n = 3 per condition), and differential gene expression between the control and NP groups or the control and NP + aPD-1 groups were analyzed. Phenotypic differences were analyzed by Gene Set Enrichment Analysis. (D and E) Pathway enrichment for NP and NP and aPD-1 treated mice as shown by normalized enrichment score (NES) compared with PBS for the given gene sets. (F) Pathway enrichment for NP + aPD-1 compared with NP alone was also analyzed. Pathways with NES > 1.3 or NES < -1.3 were considered differentially expressed. Changes in the tumor largely reflected systemic changes as seen in the spleen, with positive enrichment of immune cell function, whereas the lung showed negative enrichment in many of these pathways.

2.4 Discussion

In this study, cargo-free PLG NPs were investigated for systemic delivery and therapeutic efficacy in the 4T1 mouse model of metastatic breast cancer. Innate immune cells, such as MDSCs, inflammatory monocytes, and TAMs have been revealed to support pro-tumor functions at the primary tumor and metastatic niche. The cells have been widely studied for their potential as biomarkers for early diagnostics of cancer and metastasis [129–133]. Furthermore, the therapeutic benefit of immunotherapies such as immune checkpoint blockade (ICB) and CAR T-cells, which primarily aim to improve the adaptive anti-tumor immune response, are limited by the presence of these immunosuppressive innate cells [117,119,120]. As such, targeting of these innate immune cells has emerged as a potential cancer immunotherapy. The data presented here demonstrate that NPs delivered systemically alter the phenotype of the pro-tumor innate immune cells at the primary tumor, resulting in a therapeutic benefit when combined with anti-PD-1 that is targeting the adaptive immune cells.

Previous studies have targeted innate immune cells with antibodies or small molecules against cell surface receptors or their ligands. MDSC depletion with antibodies either against Gr1 or Ly6G has been reported to have a therapeutic benefit in multiple cancer models [134,135]. In the 4T1 model, diversion or depletion of MDSCs has resulted in a survival benefit following resection of the primary tumor [128,136]. Inhibiting MDSC activation resulted in total elimination of tumors in mice treated with combination anti-PD-1 and anti-CTLA-4 [117]. Alternatively, small

molecule inhibitors of myeloid cell recruitment and activation have also proven to be effective for targeting specific myeloid cells and improving the efficacy of immuno-, chemo-, and radio-therapies. However, there have been several reports of adverse effects of existing therapies. Stopping CCL2 inhibition has been shown to accelerate breast cancer metastasis [137]. CSF1R inhibition delays tumor growth [118], yet also promoted metastasis by diminishing the amount of IL-15 and reducing the number of NK cells [138]. The NPs reported here do not deplete the immune cell as can occur with antibodies, and do not contain an active pharmaceutical ingredient. No adverse effects were observed for NP treated animals in these studies, suggesting that NPs may provide an opportunity to enhance outcomes and improve safety by avoiding off target effects. These NPs are based on a formulation that completed both Phase I and Phase II clinical trials in celiac disease (NCTG03486990, NCT03738475), supporting the safety of these particles for translation. In addition, human MDSCs cannot be targeted with the same antibodies due to differences between mouse and human surface proteins [109,139,140]. NPs may provide an opportunity to modify human MDSCs based on a similar functionality between human and mice.

Administration of cargo-free PLG NPs intravenously in the cancer model leads to their subsequent association with monocytes, MDSCs, and other myeloid cells (**Figure 2-2B**), which results in a reduction in the percentage of myeloid cells present in the blood and lung (**Figure 2-3**). These NPs have been previously employed in animal models of trauma and autoimmune disease, and have been able to reduce inflammation that is associated with loss of function [126,141]. Intravenous administration leads to NP accumulation primarily in the spleen and liver, and to a lesser extent in the lung for the first 48 hours post injection. Previous reports have suggested that intravenous NP administration diverted inflammatory cells to the spleen [123,142], while others have observed granulocyte trafficking to the liver in several inflammatory disease

models [143]. While NP administration reduced levels of MDSCs within the blood and lung, the primary tumor had stable levels of MDSCs, which were the lowest relative to other tissues at approximately 5% of single cells. This relatively low abundance would suggest a low level of MDSC recruitment. Furthermore, the lifetime of MDSCs can be up to 4 times longer in tumors relative to blood [144], which is also consistent with a low level of recruitment and may explain why the nanoparticles that divert a fraction of the circulating cells did not substantially impact the abundance of MDSCs within the primary tumor.

Herein, the NPs were applied to a model of cancer progression, which is typically associated with immune suppression to enable the tumor cells to escape destruction by the immune system. The NPs can target the innate cells and the ICB can primarily target the adaptive immune cell responses. A greater percentage of Ly6C-hi monocytes was observed to internalize NPs relative to MDSCs and other myeloid cells, though no significant decrease in monocytes was observed in tissues. These monocytes are thought to be precursors to TAMs [106], and previous studies found decreased metastatic seeding in the lung when monocyte recruitment was inhibited [145]. The lower level of association with MDSCs is consistent with a decreased capacity for phagocytosis [146], yet confirms previous findings that MDSCs can still be targeted through particle internalization [147]. The difference in NP uptake may also be explained in part by physicochemical properties of the NPs. Preferential internalization by specific cell types was reported to be a function of the surfactant used for NP manufacturing [148] or polymer properties [141]. In addition, nanoparticle size and surface charge influence internalization by myeloid cells [149], and selectivity can be achieved without targeting moieties [150,151].

Reduced primary tumor growth was observed in the 4T1 model with combination NP and anti-PD-1 treatment (**Figure 2-4**). Interestingly, the NP administration was applied for only 12

days, yet administration impacted tumor growth over longer time frames. NP internalization induces phenotypic changes in the myeloid cells, with the response dependent upon the status of the immune system. PLG nanoparticles have been applied to reduce inflammation in spinal cord injury, yet the NPs appear to induce inflammatory pathways both *in vitro* and *in vivo* in the 4T1 model (**Figure 2-5**). *In vitro* studies of NP internalization indicated upregulation of two immunostimulatory cytokines TNF-α and GM-CSF. These cytokines have relatively nuanced roles in cancer progression. Neutralization of systemic GM-CSF with "cytokine sponges" has been reported to enhance the efficacy of anti-PD-1 treatment [152]. Conversely, combinations of GM-CSF, IL-6, and TNF-α have also been shown to inhibit human T cell activation *in vitro*, though solid tumors that contained MDSCs were found to consistently downregulate GM-CSF [139]. NP treatment *in vitro* also resulted in a decrease in the production of MCP-1 (CCL2), which is a critical cytokine associated with MDSC function [145]. Reviewing single cell data from the 4T1 model, macrophages and monocytes appear to be the predominant cell type expressing MCP-1 [153]. Signaling within the tumor microenvironment is complex, and the survival advantage provided by these particles warrant further investigation in the mechanisms of action.

NP treatment led to substantial changes in the gene expression systemically and within the primary tumor, which may contribute to the delayed tumor growth and the survival benefit. The percentage of MDSCs within the primary tumor was not significantly reduced with NP treatment, yet the phenotype of the immune cells was altered both *in vivo* (**Figure 2-6**) and *in vitro* (**Figure 2-S4**), consistent with a report that MDSC alteration unrelated to recruitment can have a significant impact in the 4T1 model [154]. MDSCs are increasingly being appreciated for their ability to modulate and contribute to tumor development, as they secrete a variety of cytokines that are associated with pro- and anti-inflammatory phenotypes. The influence of these cytokines on cancer

progression is complex. ARG-1, inducible NO synthase, reactive oxygen species, S100A8/9, and PD-L1 are generally immunosuppressive in their ability to inhibit DC, NK and T cell activity, while S100A8/9, TGF-β, IL-10 promote the function of Tregs and TAMs, which are present at a metastatic niche [155–158]. TNF-α is implicated in tumor progression in a variety of contexts, and has been observed to contribute to MDSC necroptosis [159–161]. Due, in part, to their role in cancer progression, MDSCs have become a target of biomaterial strategies to modulate multiple stages of tumorigenesis [162–165]. MDSCs share a considerable number of phenotypic and functional roles with neutrophils [166,167], which have been reported to exhibit altered trafficking, phenotype, and cytokine secretion following various size-, charge-, and shape-dependent biomaterial interactions [168–171]. The mechanisms by which these highly-negatively charged NPs specifically influence MDSC function have not been fully elucidated, yet are likely to involve multiple complex interactions that modulate the cell phenotype. As seen in **Figure 2-6**, NP delivery alters a number of innate immune cell processes such as myeloid cell differentiation, cytokine secretion, and signaling that can impact multiple aspects of the adaptive immune response. Addition of anti-PD-1 along with NP administration provided an opportunity to target both the innate and adaptive immune suppression. The addition of anti-PD-1 with NP administration further enhanced pathways associated with myeloid cell function and also enhanced a number of pathways associated with T cell and natural killer cell responses. Anti-PD-1 led to downregulated negative regulation of T cell proliferation, which is consistent with findings that PD-1 downregulates T cell proliferation [172]. The impact of the NP and anti-PD-1 within the lung was distinct, which may be due to the relatively small numbers of tumor cells in the organs at the time points analyzed.

In conclusion, we report that PLG NPs delivered systemically to target circulating immune cells improve the efficacy of ICB. The NPs are well-tolerated and the absence of an active pharmaceutical ingredient may reduce off target effects. The NPs reprogram innate immune cell phenotypes by altering their trafficking and expression of key cytokines, which altered the microenvironment of the primary tumor. Modulating the innate cell responses by the NPs combined with ICB therapy that targets the adaptive responses contributes to an improved therapeutic outcome. PLG NPs that target circulating innate immune cells may provide novel therapeutic strategies in cancer, used either alone or to complement current or emerging T-cell-targeted immunotherapies.

2.5 Methods

2.5.1 Nanoparticle fabrication

Particles were synthesized as previously described [173,174]. Briefly, high-molecular weight (acid-terminated, inherent viscosity 0.55-75 dL/g, Lactel) or low-molecular weight (acid-terminated, inherent viscosity 0.15-0.25 dL/g, Lactel) PLG polymer were dissolved at 20% w/v in dichlormethane. The dissolved polymer was added to either 1% w/v (poly(ethylene-alt-maleic anhydride) (PEMA, MW 400,000, Polysciences, Inc) or 2% w/v polyvinylalcohol (PVA, MW 30,000-70,000, Polysciences, Inc) solution and the mixture was sonicated using a Cole-Parmer CPX130 Ultrasonic Processor to form the nanoparticles. The nanoparticle solution was poured immediately into stirring 0.5% w/v PEMA or 0.5% w/v PVA and organic solvent was evaporated overnight. The nanoparticles were then pelleted by centrifugation, the remaining solution was removed, and the nanoparticle pellet was resuspended in DI water. Nanoparticles were lyophilized for storage following three of these washes in DI water. To fabricate fluorescent nanoparticles, acid-terminated 50:50 Poly(DL-Lactide-co-Glycolide)(PLG) polymer (acid-terminated, inherent

viscosity 0.55-75 dL/g, Lactel) was first conjugated with cyanine 5.5 amine dye (Lumiprobe) using N-(3-Dimethylaminopropyl)-N'-ethylcarbodiimide hydrochloride (EDC) (Sigma-Aldrich)/N-hydroxysuccinimide (NHS) (Thermo Fisher Scientific) chemistry. Unconjugated polymer and cyanine 5.5-conjugated polymer were then combined at 99:1 weight ratio. Polymer solution was used to make nanoparticles as described above.

2.5.2 Tumor cell culture and inoculation

4T1-luc2-tdTomato cells (Perkin Elmer) were expanded in RPMI 1640 + GlutaMAX (Thermo Fisher Scientific) with 10% FBS for 5 days at 37°C and 5% CO_2 prior to inoculation. Cells were removed from culture flasks by incubation with trypsin for 10 minutes at 37°C and resuspended in RPMI 1640. Cells were then pelleted by centrifugation at 300 x g and washed with DPBS, and resuspended at 1 x 10^7 cells/mL of DPBS. Orthotopic tumor inoculations were performed by injection of 5 x 10^5 tumor cells resuspended in 50 μL DPBS (Life Technologies) into the fourth right mammary fat pad of 8- to 10-week-old female BALB/c mice (Jackson Laboratory). The cell line was confirmed to be pathogen free and authenticated by short tandem repeat DNA analysis and compared to the ATCC STR profile database (DDC Medical).

2.5.3 Nanoparticle and anti-PD-1 treatment

Nanoparticles were resuspended in DPBS (Life Technologies) at 1 mg in 200 μL and passed through a 35 μm filter mesh prior to intravenous administration via tail vein injection. Control animals received 200 μL of DPBS intravenously. *InVivo*Mab anti-mouse anti-PD-1 (CD279) antibody (clone RMP1-14, Bio X Cell) was diluted in DPBS to a final concentration of 1 mg/mL immediately prior to i.p. injection. For therapeutic efficacy studies, NPs and anti-PD-1 were administered once every 3 days, for a total of 4 doses. For short-term nanoparticle

biodistribution studies, a single dose of Cy5.5-NPs at 1mg in 200 µL of PBS was administered prior to organ explant at 12 or 48 hours post-inoculation. For studies of NP accumulation in tissues, Cy5.5-NPs were administered at a dose of 1 mg/200 µL for 6 days to allow for accumulation of NPs and to observe potential NP-induced cell trafficking (n = 4 PBS control, n = 5 NP). Organs were explanted at day 10 post inoculation and innate immune cell distribution was quantified by flow cytometry. For studies of NPs and blood-based immune cell distribution, a single dose of NPs at 1 mg/200 µL was administered and flow cytometry analysis of blood was performed 12 hours post injection.

2.5.4 Tumor size measurement and survival monitoring

Tumors were measured using standard electronic calipers (VWR) while mice were anesthetized with 2% v/v% isoflurane. Tumor volume was calculated as $V = 0.5 \times L \times W^2$, where L is the length of the longest dimension of the tumor and W is the length of the tumor perpendicular to the longest dimension. Mice were monitored for tumor size and body conditioning to determine survival. Mice were euthanized if any of the following criteria were met: tumor size of > 2cm in any dimension, ulceration of more than 50% of the visible tumor area, partial paralysis due to tumor invasion of hind limb muscle, labored breathing, ascites, lethargy, or visible weight loss.

2.5.5 Ex-vivo fluorescence and bioluminescence imaging

Short-term nanoparticle distribution was measured in explanted whole organs following a single particle injection, with analysis of the organs after 12 or 48 hours using an IVIS Lumina LTE imaging system (Caliper Life Science). Fluorescence signal intensity at 675/700 Ex/Em is reported as photon flux in total photon count/cm^2/steradian. Metastatic tumor burden of luciferase-expressing tumor cells in explanted lungs was measured by bioluminescence imaging with the

IVIS. Briefly, lungs were incubated in 50 μM d-luciferin (Caliper) at room temperature for 10 minutes prior to imaging in the IVIS. Bioluminescence signal intensity is reported as integrated light flux (photons/sec) as calculated by the Living Image Software (Caliper Life Sciences).

2.5.6 Flow cytometry

Flow cytometry was performed on primary cells obtained from explanted organs. Spleens, lungs, primary tumors, and livers were minced and enzyme digested with Liberase TL or TM (Roche), then filtered through a 70 μm cell strainer (Corning) to obtain a cell suspension. Whole blood was collected by cardiac puncture using a 23 guage needle (BD) attached to a 1 mL BD Luer-Lok syringe and mixed with 10 v/v% 25 mM EDTA (Life Technologies). Red blood cell lysis of whole blood, spleens, and lungs was performed with ACK Lysing Buffer (Life Technologies). Cells were pelleted by centrifugation at 400 x g for 5 minutes and resuspended in MACS buffer. NP^+ cells were identified by Cy5.5 fluorescence signal. Nonspecific staining was blocked with anti-CD16/32 (Biolegend) and samples were stained for innate immune markers with anti-mouse CD45 AF700, F4/80 PE-Cy7, Ly6G PacBlue, Ly6C FITC (Biologend), and CD11b BV510 (BD Biosciences). For adaptive immune markers, samples were stained with anti-mouse CD45 AF700, CD4 V500, CD8 FITC, CD19 PacBlue, and CD49b PE-Cy7 (Biolegend). Stained samples were analyzed using the MoFlo Astrios Flow Cytometer or CytoFLEX (Beckman Coulter), and data were processed using FlowJo (BD) with the gating strategies shown in **Figure 2-S1**.

2.5.7 In vitro nanoparticle uptake and ELISA

Single cell suspensions were isolated from spleens and whole blood of tumor-bearing mice at 14 or 21 days post tumor inoculation as described above. For nanoparticle uptake assays, cells

were resuspended in RPMI 1640 media with 10% FBS and seeded in 24-well plates at 1 x 10^6 cells per well. NPs were resuspended in DPBS at 1 mg/mL and added to the wells. Uptake was characterized following a 30 minute incubation at 37ºC by flow cytometry as described above. For cytokine secretion assays, cells were resuspended in RPMI 1640 media and seeded in 96-well plates at 2.5 x 10^5 cells per well. For the evaluation of cytokine secretion by $Gr1^+$ cells, $Gr1^+$ splenocytes were sorted using the Myeloid-Derived Suppressor Cell Isolation Kit (Miltenyi Biotec), and cells were counted and resuspended in media. NPs were resuspended as described above and added to each well. Following incubation for 18 hours, cells were pelleted at 1,000 x g for 5 minutes and the supernatant was removed and diluted 4x for quantification of cytokine secretion by ELISA, which was performed by the Cancer Center Immunology Core at the University of Michigan.

2.5.8 Gene expression analysis by RNA-seq

Explanted tissues were flash-frozen by submerging them in isopentane on dry ice, and homogenized in TRIzol reagent (Thermo Fisher Scientific). RNA was extracted from each tissue sample with the Direct-zol RNA spin column kit (Zymo Research). Purified RNA concentration was measured by UV spectroscopy using a Nanodrop 2000c (Thermo Scientific) to confirm all samples had concentrations ≥ 10 ng/μL. RNA quality control, QuantSeq 3' mRNA-seq library prep and quality control, and sequencing were performed by the Advanced Genomics Core at the University of Michigan. Samples were sequenced using the Illumina NextSeq 550 sequencer, and sequences were aligned to Gene Symbols. Raw sequencing counts were normalized and differential gene expression was calculated in R and using DESeq2 [175] [176]. For pathway analysis, mouse gene symbols for counts obtained through RNA-seq were first converted to human gene symbols using the biomaRt package in R. Gene Set Enrichment Analysis (GSEA) was

performed on DESeq2-normalized counts and the corresponding human gene symbols for a total of 5,944 MsigDB gene sets (Hallmark, Reactome, PID, and Gene Ontology (GO)). A positive normalized enrichment score (NES) indicates enrichment in the treated cohort compared with PBS control. In comparisons between the two treatment groups, a positive NES indicates enrichment in the combination (NP + anti-PD-1) treatment group compared with the nanoparticle (NP) treatment group.

2.5.9 Statistical analysis

One-way or two-way ANOVA and Tukey's multiple comparisons tests were performed on groups with more than 2 conditions. Two-tailed unpaired t test was used for single comparisons between two conditions. Median survival and survival curves were analyzed with the log-rank (Mantel-Cox) test for statistical significance. Following normalization of RNA-seq gene expression data with DESeq2, genes with adjusted p-value < 0.1 were considered differentially expressed. Statistical analyses were performed using Prism 8 (GraphPad Software) and R. A p-value < 0.05 was considered to be statistically significant and all values are expressed in mean ± standard deviation (SD). Error bars on plotted data represent standard error of the mean (SEM).

2.6 Supplementary Figures

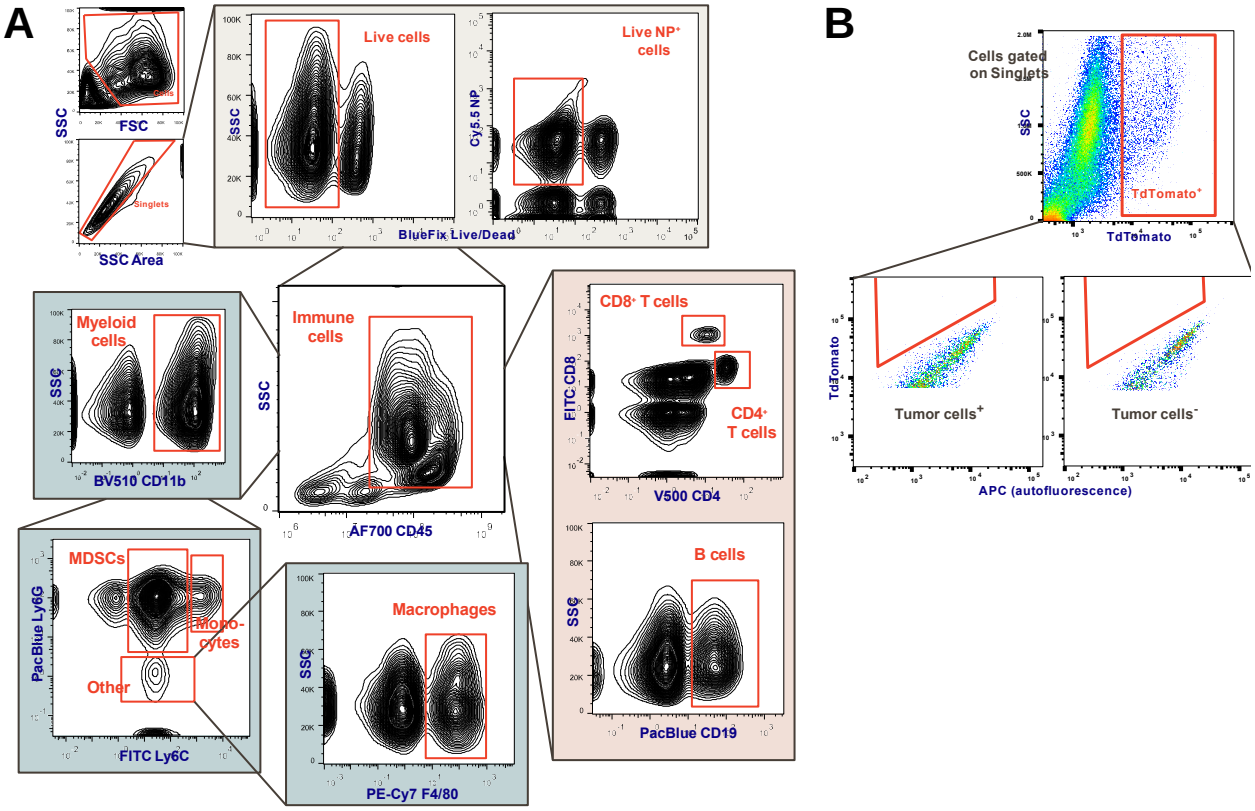

Figure 2-S1. Flow cytometry analysis of tissues to identify immune cell types and tumor cells. Gating strategies are shown for (A) immune flow and (B) tumor flow. Immune cell samples were gated on singlets and identified by AF700 CD45 staining (A, top). Immune cell populations were split into 2 panels and stained separately with innate cell markers (A, bottom left) and adaptive cell markers (A, bottom right). Quantification of Td-Tomato-expressing tumor cells was performed on unstained cell samples, and tumor cells were identified as the Td-Tomato+ APC/autofluorescence- population as shown above.

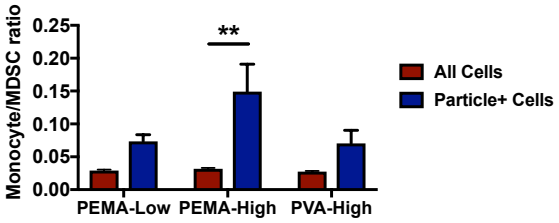

Figure 2-S2. Uptake specificity can be tuned by changing surfactant and polymer molecular weight.

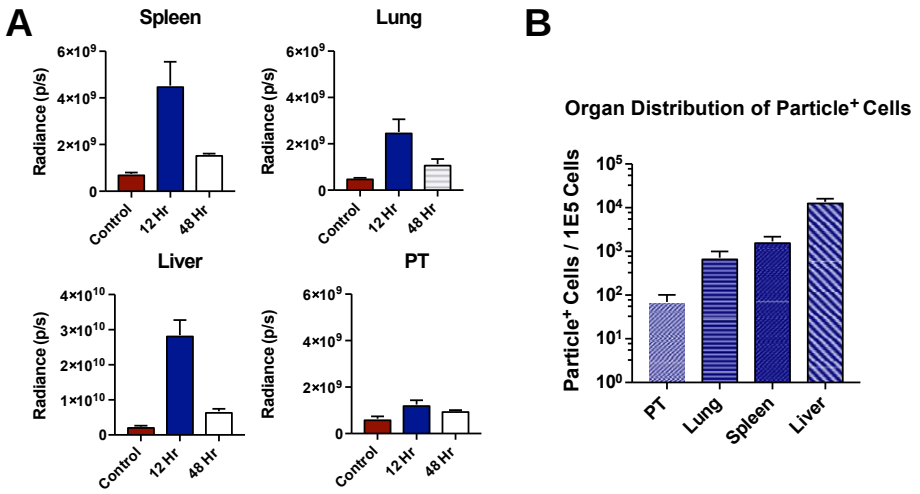

Figure 2-S3. Quantification of Cy5.5-NP signal by IVIS (A, n = 3 NP+, n = 2 PBS) and (B) flow cytometry.

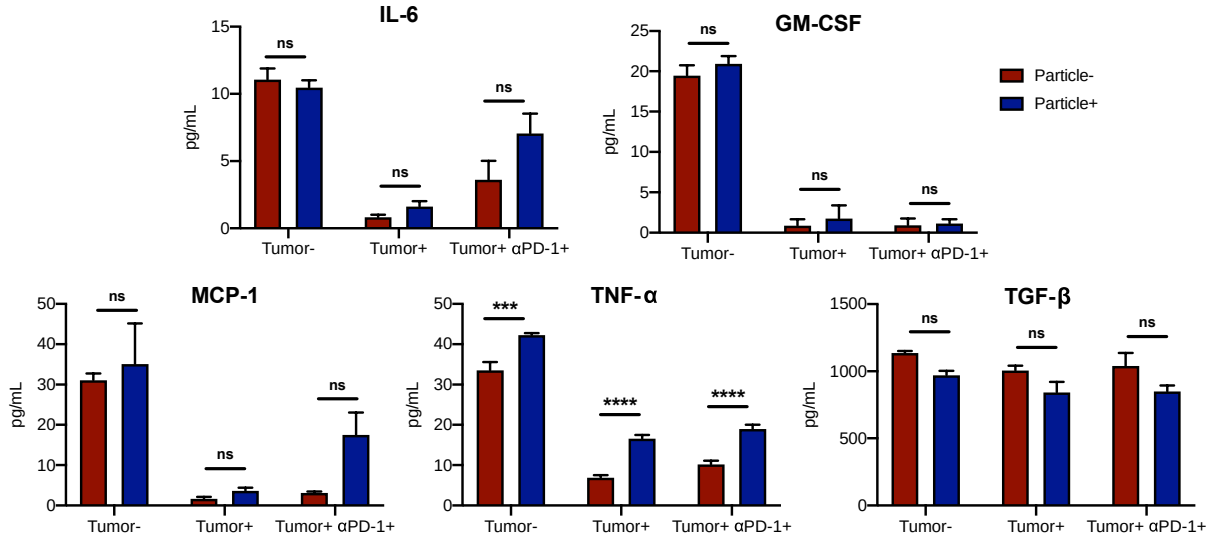

Figure 2-S4. Cytokine secretion as measured by ELISA for Gr-1+ splenocytes isolated and sorted from healthy, tumor-bearing, and *in vivo* anti-PD-1 treated mice. 2-way ANOVA with Tukey's multiple comparisons tests were performed. Bars show mean ± SEM where *** $p < 0.001$, **** $p < 0.0001$ compared to particle- control (n = 3 in Tumor- cohort, n = 4 in Tumor+ and Tumor+ aPD-1+ cohorts).

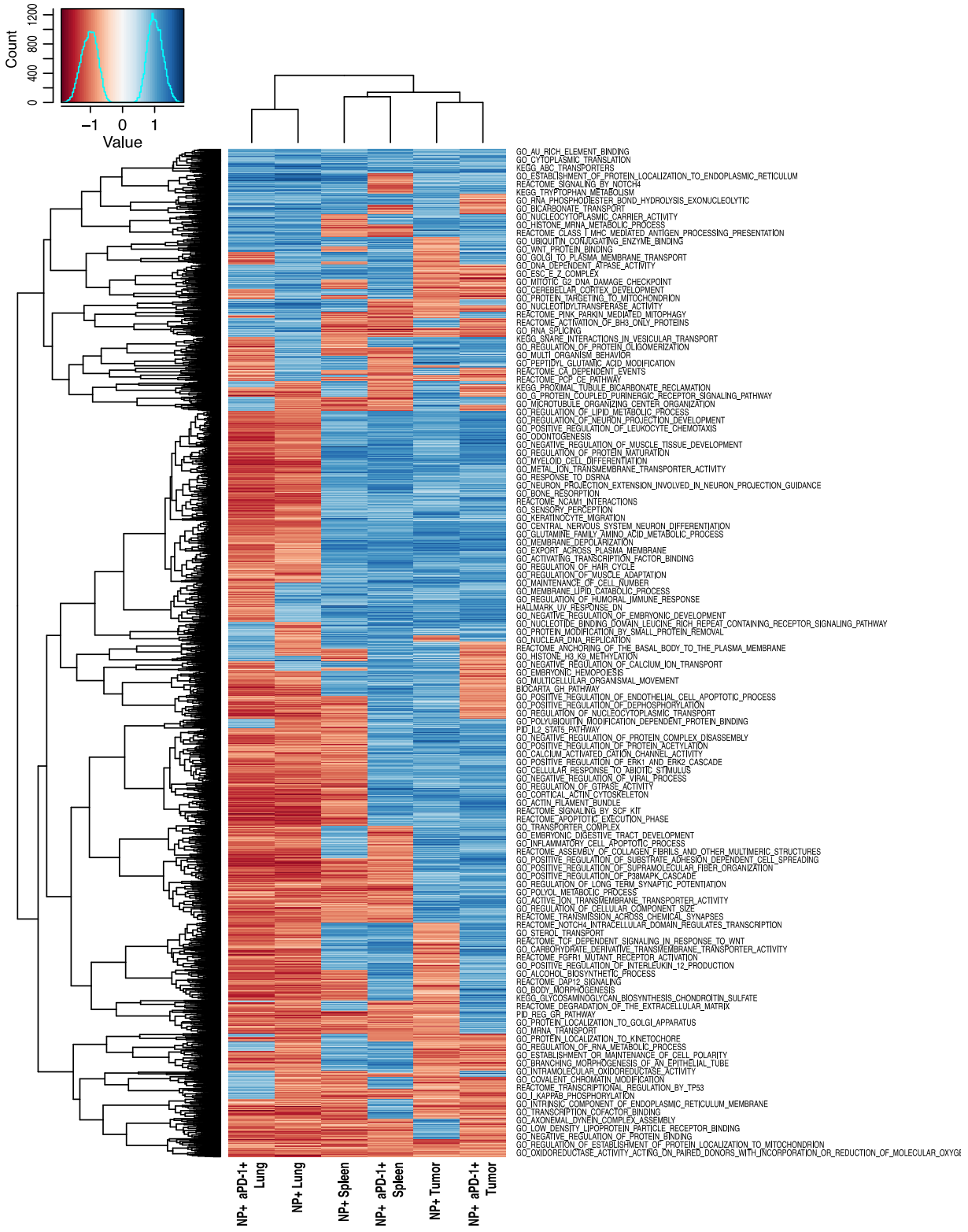

Figure 2-S5. Gene set enrichment (GSEA) heatmap for a set of 5,944 pathway changes for lung, spleen, and tumor compared with tissues from PBS-treated mice. Pathway changes in the spleen were more similar to those in the tumor. The lung showed broad downregulation of immune-related pathways.

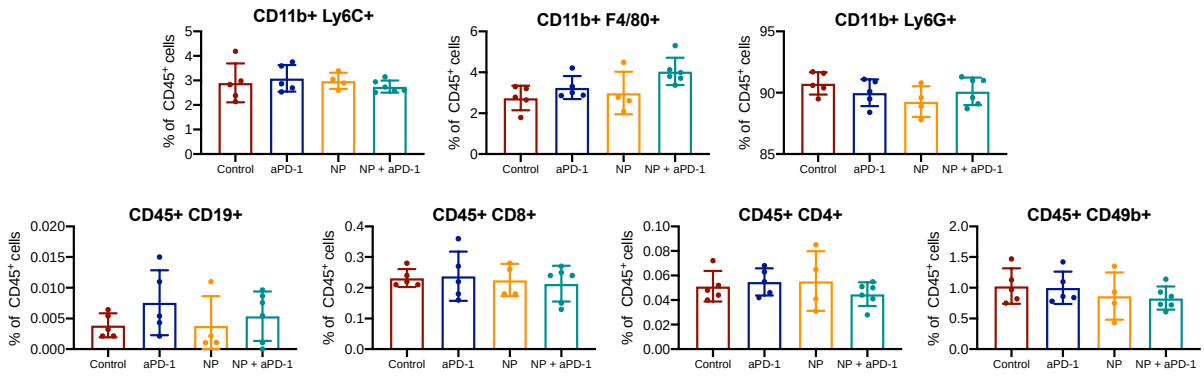

Figure 2-S6. Flow cytometry analysis of immune cell types (CD11b+ Ly6C+ monocytes, CD11b+ F4/80+ macrophages, CD11b+ Ly6G+ MDSCs, CD19+ B cells, CD8+ T cells, CD4+ T cells, and CD49b+ NK cells) present at the lung on Day 14 post inoculation.

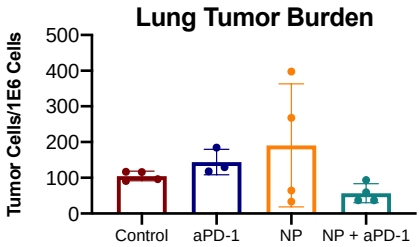

Figure 2-S7. Number of tumor cells at the lung at Day 14 post inoculation (n = 4 per group) as quantified by flow cytometry.

Chapter 3

Cargo-Free Nanoparticles Alleviate Myeloid Cell-Induced Immunosuppression and Inhibit Metastatic Colonization

The material in this chapter has been adapted with minor modifications from the following article:

R.M. Raghani *, J.A. Ma*, Y. Zhang, S. Orbach, J. Wang, M. Zeinali, S. Nagrath, T. Murthy, A. Elhofy, J.S. Jeruss, L.D. Shea, Cargo-free nanoparticles alleviate myeloid cell-induced immunosuppression and inhibit metastatic colonization, *In Preparation*.

* These authors contributed equally to this work

3.1 Introduction

Few therapies exist to effectively treat metastatic disease, and as such, distant recurrence often marks the disease stage where treatment no longer has curative intent, and disease progression leads to mortality [3]. The stark disparity in outcomes between primary and metastatic disease necessitates investigating novel strategies for targeting the microenvironments that support metastatic colonization and the subsequent progression of disease. Aberrant monocytes, neutrophils, and macrophages have been shown to suppress anti-tumor immunity during cancer progression [15–19,21,22]. Recently, novel immunotherapy approaches targeting pro-tumor myeloid cells in metastatic cancer have begun to emerge with the goal of promoting an anti-tumor immune response [49–52]. Cargo-free nanoparticles have been shown to be immunomodulatory and their function tunable by modifying their physical and chemical properties [61–63]. Upon intravenous delivery, nanoparticles are largely taken up by myeloid cells, such as macrophages,

neutrophils, and dendritic cells, and nanoparticle administration has been shown to both alter myeloid cell phenotype and redirect myeloid cell trafficking away from sites of inflammation [64,65]. Our lab previously demonstrated that naked nanoparticles can mitigate pathological inflammation by targeting myeloid cells in models of traumatic injury and autoimmune disease, [66,67].

In this report, we investigate the hypothesis that cargo-free PLG nanoparticles administered intravenously can reduce metastatic colonization of the lungs by targeting the immunosuppressive, myeloid cell mediators of metastatic progression. In an orthotopic murine model of metastatic triple negative breast cancer (4T1), metastatic 4T1 cells seed and colonize the lungs over the course of disease progression, orchestrated in part by the recruitment of aberrant myeloid cells to the lungs [26,177]. The impact of nanoparticles on circulating tumor cells, pulmonary metastasis, and the lung microenvironment are analyzed *in vivo*. Gene expression changes among distinct leukocyte populations within the metastatic niche, resulting from nanoparticle administration, are investigated with single cell RNA sequencing (scRNA-seq). Finally, the efficacy of nanoparticle delivery on tumor cell clearance is studied in a T-cell-deficient model (RAG-1 KO) and as an adjuvant therapy in a primary tumor resection model. Our cargo-free nanoparticles provide a novel platform for modulating cancer-associated myeloid cells and enhancing anti-tumor T-cell surveillance, and as such, demonstrate great potential as an adjuvant therapy for treating metastatic breast cancer.

3.2 Results

3.2.1 Nanoparticle administration reduces tumor growth and metastatic dissemination

We investigated the efficacy of PLG nanoparticles (NPs) to inhibit tumor progression in the 4T1 model of murine, metastatic triple negative breast cancer (mTNBC). As neutrophils and

macrophages are known to promote tumor development, we first investigated the hypothesis that NP immunomodulation would disrupt the growth of primary tumors [178]. Mice were orthotopically inoculated with 4T1 cells and intravenously injected with NPs starting 1, 2, and 4 days post-tumor inoculation to study how NPs disrupt tumor formation at varying stages of engraftment (**Figure 3-1A**). 4T1 tumor cells are hypothesized to begin engrafting 1 day after inoculation, complete engraftment by 2 days, and will have established into palpable tumors by 4 days post-inoculation. At 21 days after inoculation, mice injected with NPs starting 1 day after inoculation demonstrated a 54% reduction in tumor volume ($p<0.05$) compared to mice injected with saline (**Figure 3-1B**). Initiating NP administration day 2 post-tumor inoculation showed a 37% reduction in primary tumor size ($p<0.05$). However, while mice injected with NPs starting 4 days after inoculation trended towards smaller tumors (32% reduction in 21 day tumor size), this difference was not significantly different from mice receiving saline ($p=0.068$). Mice treated with NPs starting 1 day after inoculation had significantly smaller tumor volumes at day 21 compared to mice treated starting 2 days (28% reduction, $p<0.05$) or 4 days (33%, $p<0.05$) after inoculation. As such, we concluded that earlier administration was more effective at disrupting tumor growth.

NP administration is also effective at reducing tumor cell dissemination and metastasis. During the metastatic cascade, tumor cells must extravasate from a primary tumor, survive in circulation, and home to a metastatic niche, which is most commonly in the lung in the 4T1 model. Mice treated with NPs trended toward reduced numbers of circulating tumor cells at 21 days after inoculation ($p=0.06$), with an 86% reduction in total CTCs (**Figure 3-1C**) and a 95% reduction in CTCs in clusters with CD45+ immune cells ($p=0.16$) (**Figure 3-S1B**). Notably, NP administration significantly reduced the formation of metastatic lesions (**Figure 3-1D**). NP administration starting 1 day after inoculation completely blocked formation of metastases, and NP administration starting

2 days after inoculation resulted in a 76% reduction in lung metastatic burden ($p<0.01$). Earlier NP administration trended towards increased efficacy in decreasing metastatic burden. Mice treated with NPs 4 days after inoculation demonstrated decreased metastatic burden (70% decrease, $p<0.05$) but trended towards higher burdens than mice treated 1 day after inoculation (51% increase, $p=0.063$). These findings demonstrate that NP administration reduces metastasis and tumor cell dissemination *in vivo*, suggesting that NPs have systemic effects on multiple steps of the metastatic cascade. Furthermore, because of the efficacy of early NP delivery, all subsequent studies were performed initiating NP administration 1 day post-tumor inoculation.

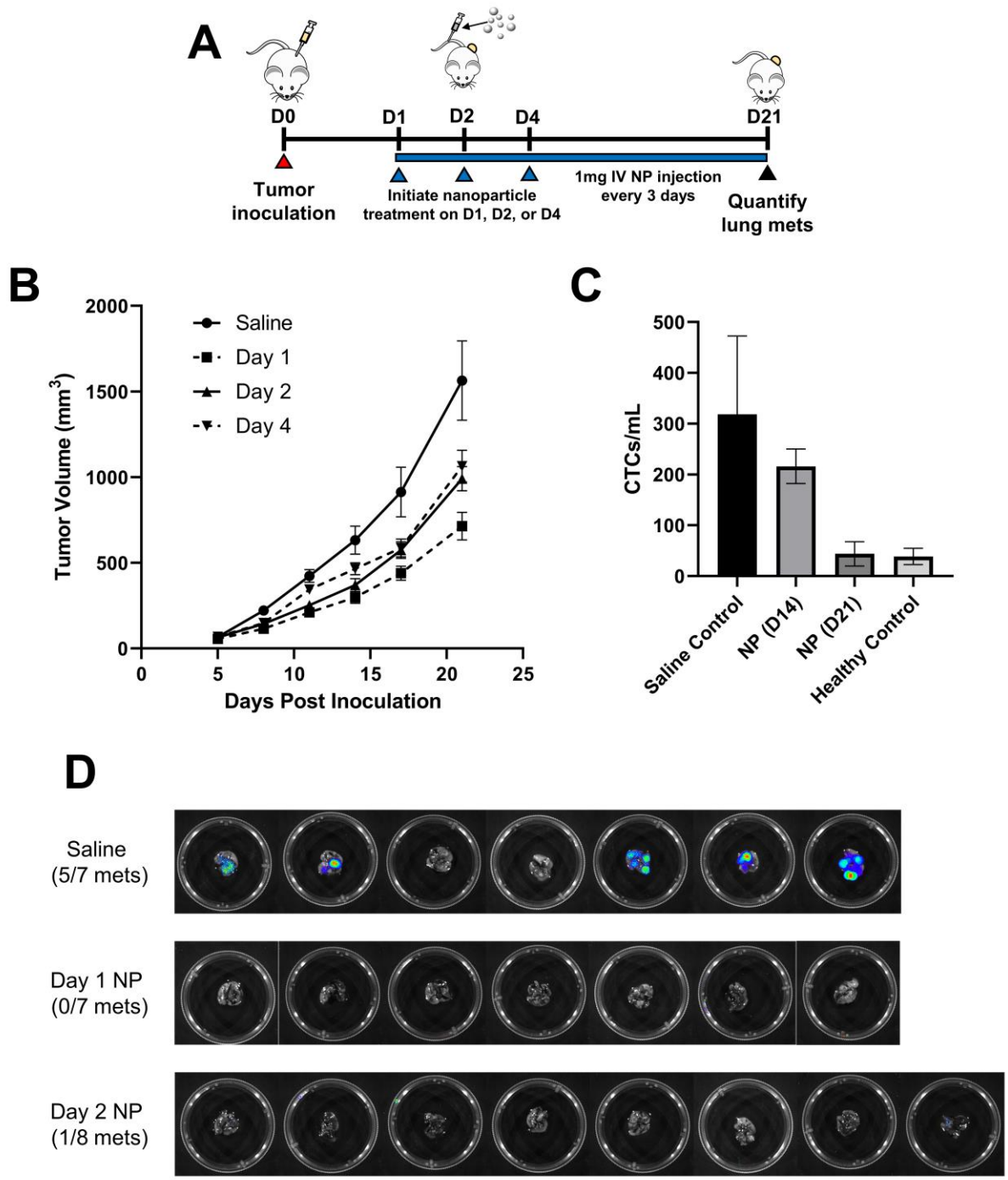

Figure 3-1. *In vivo* administration of PLG nanoparticles reduces primary tumor growth and metastatic colonization of the lungs. (A) Balb/c mice were inoculated with 4T1 tumor cells and received intravenous NP administration every 3 days starting on D1, D2, or D4 post-tumor inoculation, or saline as the control. (B) PT volumes were recorded longitudinally for three weeks following orthotopic 4T1 inoculation. (C) Circulating tumor cells in the peripheral blood were quantified for tumor-bearing mice receiving NPs on D14 and D21 post-tumor inoculation. The peripheral blood of tumor-bearing mice (saline control) and naïve Balb/c mice (healthy control) receiving saline was also analyzed. (D) Lung metastases were quantified with bioluminescent imaging on D21 post-tumor inoculation. Two-tailed unpaired t-tests assuming unequal variance were performed for single comparisons between two conditions. Bars show mean ± SEM.

3.2.2 Immune cell composition altered at lung microenvironment with nanoparticle administration

We next investigated the mechanisms by which NPs influence the composition and phenotype of the metastatic niche. As NPs are primarily phagocytosed by myeloid cells, such as neutrophils and monocytes, we hypothesized that NPs reprogram the pro-tumor metastatic microenvironment [68]. We performed single cell RNA sequencing (scRNA-seq) on cells isolated from the lungs of tumor-bearing mice receiving either saline or NPs to identify the immune populations at the metastatic niche that are altered with NP administration (**Figure 3-2A**). Neutrophils, monocytes, endothelial cells, and B cells were the predominant populations in both NP-treated and saline control mice. In control mice, neutrophils made up 65.5% of all cells in the lung, followed by endothelial cells (10.6%), monocytes (7.7%), and B cells (3.3%) (**Figure 3-2B**). Lungs from NP-treated mice had a substantially lower proportion of neutrophils (38.1%), and an increased proportion of monocytes (13.8%), endothelial cells (11.4%), and B cells (11.3%). T cells (6.7%), stromal cells (5.2%), and dendritic cells (4.6%) also increased in NP-treated mice comparison to saline (2.4%, 2.7%, and 1.2%, respectively), suggesting that nanoparticle administration resulted in a lower accumulation of neutrophils and increased presence of other cell populations.

Neutrophils, monocytes, and dendritic cells demonstrated the largest changes in proportion and gene expression. As such, these myeloid cells, which are capable of NP uptake, were sub-clustered to identify differences in immune cell phenotypes resulting from NP administration. In neutrophils, NP administration was associated with a decrease in pro-tumor subpopulations and a large increase in the proportion of inflammatory, interferon-associated neutrophils (**Figure 3-2C**). A 9-fold increase in IFN-associated neutrophils and a 2-fold increase in the proportion of

neutrophil progenitors was demonstrated in NP-treated lungs compared to the saline control. NP administration also resulted in a 2-fold decrease in the proportion of neutrophils identified as pro-tumor and mature, and a 2.5-fold decrease in the proportion of neutrophils identified as transitional. Monocytes similarly demonstrated a 1.5-fold decrease in transitional monocytes and a 2.5-fold increase in the proportion of non-classical monocytes in the lungs of NP-treated mice (**Figure 3-2D**). There was also a 2.5-fold increase in cells identified as IFN-associated monocytes with NP administration, but these made up a small proportion of monocytes (2.2% in NP-treated mice). Dendritic cells shifted from largely classical DCs to activated DCs, with a 4.5-fold decrease in the proportion of cDCs and a corresponding 4-fold increase in the proportion of activated DCs and 3.5-fold increase in inflammatory DCs with NP administration (**Figure 3-2E**). Collectively, these data demonstrate that NP administration decreases neutrophil accumulation in the lung and promotes inflammatory, activated phenotypes in myeloid populations.

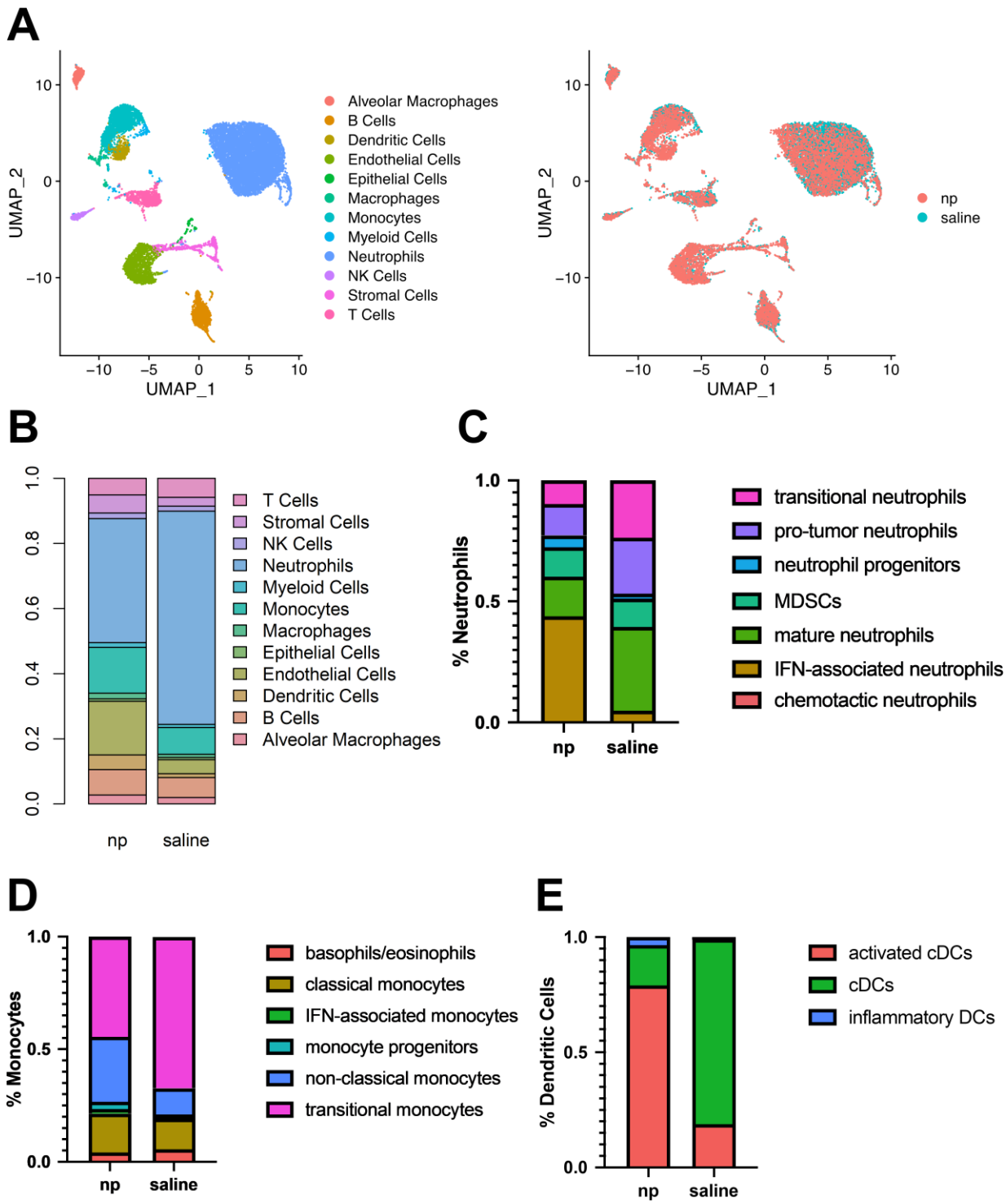

Figure 3-2. *In vivo* remodeling of lung microenvironment by single cell RNA sequencing. (A) Clustering by different cell populations (left) and nanoparticle versus saline (right). (B) Histogram of cell proportions at the lung of mice receiving either NPs or saline control. Histogram of (C) neutrophil, (D) monocyte, and (E) dendritic cell subsets at the lungs of mice receiving NPs versus saline.

3.2.3 Nanoparticle delivery results in upregulation of inflammatory pathway-associated genes among myeloid cell populations at the lungs

NP administration resulted in significant changes in gene expression among neutrophils, monocytes, and dendritic cells (**Figures 3-3A - 3-C**). In neutrophils, genes associated with inflammation and interferon gamma signaling (Igtp, Gbp2, Isg15, Ifi47, Stat1, and Irf1) were highly upregulated compared to neutrophils in control mice. Similar increases were observed in monocytes, with increases in Stat1, Gbp2b, Cxcl2, and CD74 expression. In NP-treated dendritic cells, genes associated with phagocytosis and antigen presentation (Id2, Fpr2, Tnfaip2, Gbp2, Prdx5, and Cxcl2) were significantly upregulated compared to the saline control.

Gene set enrichment analysis (GSEA) was performed to investigate the functional effects of gene expression changes among these identified populations. All cell populations saw significant upregulation of pathways associated with IFN and TNF signaling (**Figure 3-3D**). The Hallmark Interferon Gamma Response (M5913) was the top upregulated pathway in neutrophils and monocytes, and the second-most upregulated pathway in dendritic cells. The Hallmark Interferon Alpha Response pathway was also highly upregulated in these cells as the third-most and second-most upregulated pathway in neutrophils and monocytes, respectively. TNFa signaling, as identified in GSEA by both the Hallmark TNFA signaling via NFkB and GO Response to Tumor Necrosis Factor gene sets, was also shown to be highly upregulated in neutrophils, monocytes, and dendritic cells. These pathways were the fifth-most, third-most, and top upregulated pathways respectively. Together, these data indicate that nanoparticle administration skews myeloid cells in the lung towards more inflammatory, anti-tumor phenotypes.

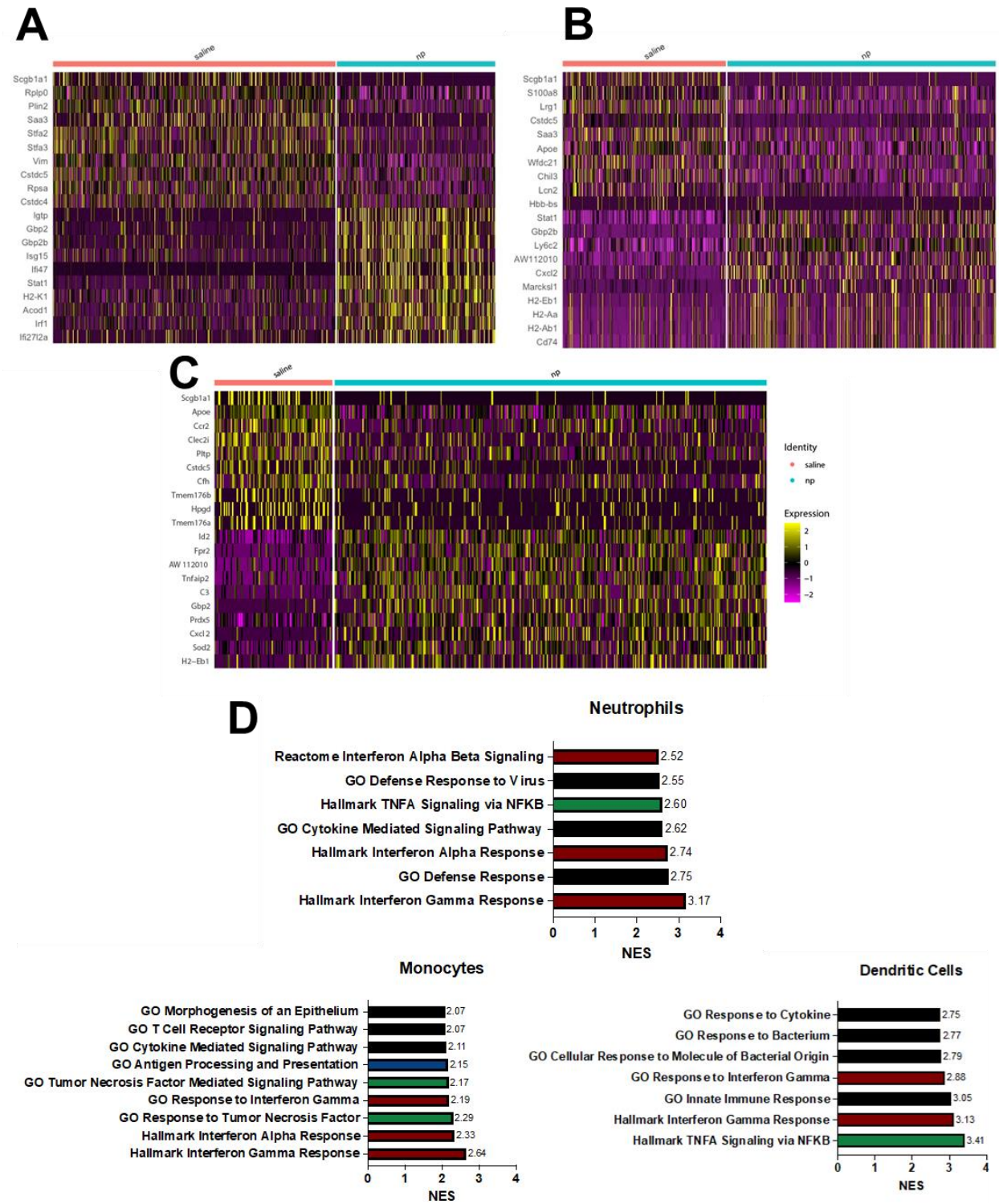

Figure 3-3. Nanoparticle administration induces inflammatory, anti-tumor phenotype among myeloid cells at the lungs. Differentially expressed genes among (A) neutrophils, (B) monocytes, and (C) dendritic cells in tumor-bearing mice that received either intravenous saline or NPs. (D) Gene set enrichment analysis was used to probe differentially regulated pathways among neutrophils, monocytes, and dendritic cells.

3.2.4 Administration of nanoparticles alters the composition and secretome of immune cells

As immune cells at the lung metastatic niche are recruited from circulation from the blood, we investigated how NPs influenced the composition of immune cells in the peripheral blood [179]. Mice injected with NPs had a significantly increased proportion of monocytes and a corresponding decreased proportion of neutrophils in circulation (**Figure 3-4A**). However, the absolute magnitude of change was small, corresponding to a 2.1% increase in monocytes and 2.5% decrease in neutrophils. We thus sought to investigate whether nanoparticles influenced the phenotypes of cells in the blood and at the lung. Plasma isolated from nanoparticle treated mice demonstrated a 2-fold reduction in MPO-DNA complexes, indicative of a reduction in NETosis and suggesting altered myeloid cell phenotypes (**Figure 3-4B**). Cells from the lungs and blood were isolated into CD45+ and CD45- fractions and cultured for 18 hours, and the resulting supernatant was analyzed by ELISA. NP administration broadly decreased the secretion of cytokines and chemokines in both the CD45+ and CD45- fractions (**Figures 3-4C – 3-4E**). CD45+ immune cells demonstrated significant reductions in the secretion of IL1b, IFNg, IL-4, IL-13, and CCL2. CD45- stromal cells also displayed broad reductions in cytokine and chemokine secretion, demonstrating 2-fold to 3-fold decreases in the secretion of IL-1b, IL-4, IL-6, IL-13, CCL3, and CCL4. Interestingly, NP treatment reduced the secretion of IFNg by CD45- cells in the lung to levels below the detection limit, and conversely resulted in a 1.6-fold increase in the secretion of TNFa. While cells in the blood trended towards reductions in the secretion of IFNg and TNFa, NP administration did not significantly alter the secretion of cytokines or chemokines in CD45+ or CD45- cells in the blood, with the exception of a 1.7-fold increase in CCL3 secretion by CD45- cells. Taken together, these data show that nanoparticles alter the ratios of blood-derived immune

cells and broadly reduce the secretion of cytokines and chemokines and may abrogate pathological inflammation in the lung.

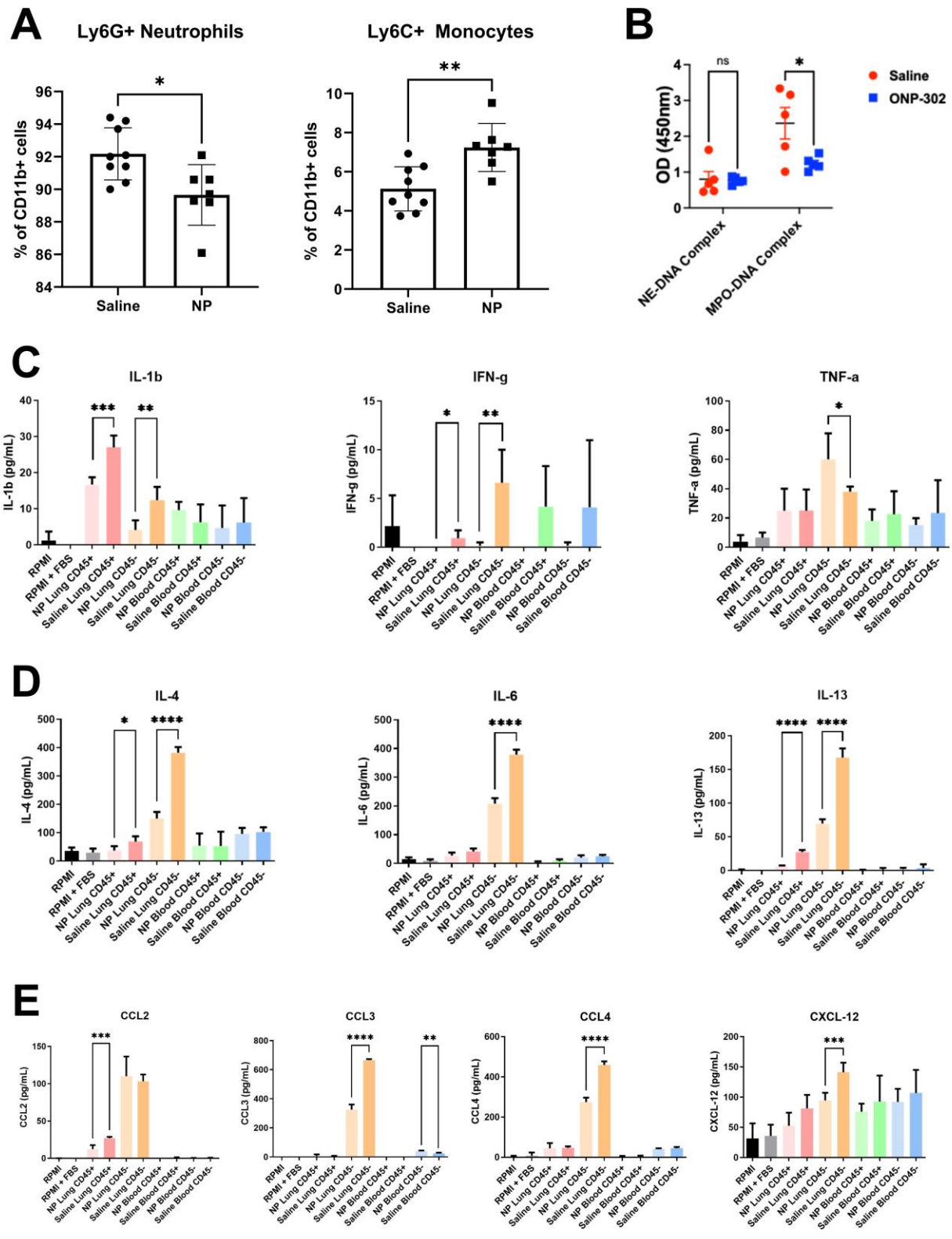
A
Ly6G+ Neutrophils
% of CD11b+ cells
Saline
NP
Ly6C+ Monocytes
% of CD11b+ cells
Saline
NP
B
OD (450nm)
ns
Saline
ONP-302
NE-DNA Complex
MPO-DNA Complex
C
IL-1b
IL-1b (pg/mL)
IFN-g
IFN-g (pg/mL)
TNF-a
TNF-a (pg/mL)
RPMI
RPMI + FBS
NP Lung CD45+
Saline Lung CD45+
NP Lung CD45-
Saline Lung CD45-
NP Blood CD45+
Saline Blood CD45+
NP Blood CD45-
Saline Blood CD45-
D
IL-4
IL-4 (pg/mL)
IL-6
IL-6 (pg/mL)
IL-13
IL-13 (pg/mL)
E
CCL2
CCL2 (pg/mL)
CCL3
CCL3 (pg/mL)
CCL4
CCL4 (pg/mL)
CXCL-12
CXCL-12 (pg/mL)

Figure 3-4. Immune cell composition and secretome modulated in the periphery as a result of nanoparticle administration. (A) Ratio of Ly6G+ neutrophils and Ly6C+ monocytes in peripheral blood analyzed in 4T1-bearing mice that received either NPs or saline (% of CD11b+ myeloid cells). (B) NETosis in plasma investigated through quantification of NE-DNA and MPO-DNA complexes. (C) CD45+/- fractions were magnetically sorted form the peripheral blood and lungs and cultured *in vitro*. Secretome was analyzed with ELISA for analytes associated with (C) Th1, (D) Th2, and (E) chemokine responses. Two-tailed unpaired t-tests assuming unequal variance were performed for single comparisons between two conditions, * $p < 0.05$.

3.2.5 Efficacy of nanoparticles as an adjuvant therapy and their abrogated efficacy in a T-cell-deficient model

The role of T cells in the clearance of metastases following NP administration was investigated using a T-cell-deficient model *in vivo*. RAG-1 KO and Balb/c mice were inoculated with orthotopic 4T1 tumors and received either NP treatment or saline control. Primary tumor volumes were longitudinally recorded, which revealed a statistically significant difference between Balb/c and RAG-1 KO mice receiving nanoparticles starting at 11 days-post tumor inoculation (**Figure 3-5A**). This trend continued during disease progression, with the average PT volume of RAG-1 KO mice receiving nanoparticles to be 2.5 times that of NP-receiving Balb/c mice at 20 days post tumor inoculation. Interestingly, starting around 16 days post-tumor inoculation, the average PT volume of saline-treated RAG-1 KO mice significantly surpassed the growth of saline-treated Balb/c mice. Most importantly, there was no statistical difference, across all recorded time points, in the longitudinal primary tumor volumes of NP-receiving RAG-1 KO and those receiving saline. This data demonstrates that without mature T-cells, nanoparticles did not reduce the growth of the primary tumor.

The impact of nanoparticles on the metastatic colonization of the lungs was next investigated by imaging the lungs of tumor-bearing RAG-1 KO mice. Lungs were collected from nanoparticle or saline-treated Balb/c and RAG-1 KO mice 21 days after tumor inoculation. Bioluminescent imaging of these lungs revealed no statistical difference in metastases between

RAG-1 KO mice receiving nanoparticles or saline (**Figure 3-5B, 3-5C**). As previously shown, a significant reduction in pulmonary metastases was observed in Balb/c mice receiving NPs, as compared to those receiving saline. Notably, while 20/20 RAG-1 KO mice had developed lung metastases by 21 days after inoculation, in the immunocompetent Balb/c mice receiving saline, 14/17 mice had pulmonary metastases (**Figure 3-1E, Figure 3-5C**). Collectively, this data indicates that the NP-mediated reduction in lung metastases is abrogated in a murine model lacking mature T-cells.

We next investigated the hypothesis that NPs promote tumor cell clearance in a PT resection model, with the goal of studying the impact of NP administration on metastatic progression in the absence of the PT. Balb/c mice were inoculated and split into three cohorts receiving saline control, neoadjuvant nanoparticle treatment (NP administration pre-resection), or adjuvant nanoparticle treatment (NP administration post-resection) (**Figure 3-5D**). Excitingly, nanoparticle administration completely abrogated lung metastases in both the neoadjuvant and adjuvant cohorts, as compared to the saline cohort (**Figure 3-5E**). This study, in which NPs were delivered after the formation of established metastases, indicates that nanoparticle treatment leads to the clearance of pulmonary metastases. Taken together, these data indicate that T-cells are necessary for the nanoparticle-mediated reduction of pulmonary metastases and that established metastatic lesions are cleared with nanoparticle treatment delivered in the adjuvant setting.

A

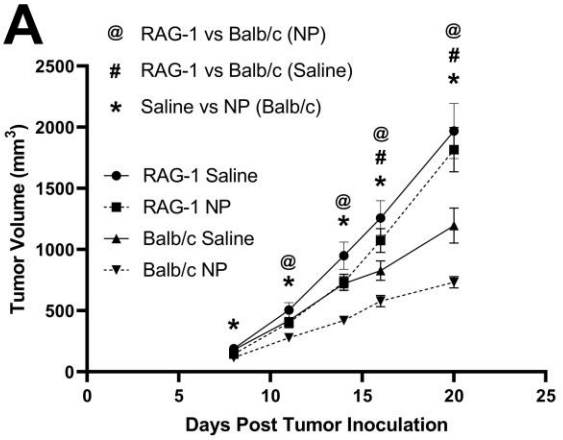

B

Group	Incidence of Metastasis
RAG-1 Saline	10/10
RAG-1 NP	10/10
Balb/c Saline	9/10
Balb/c NP	1/10

C

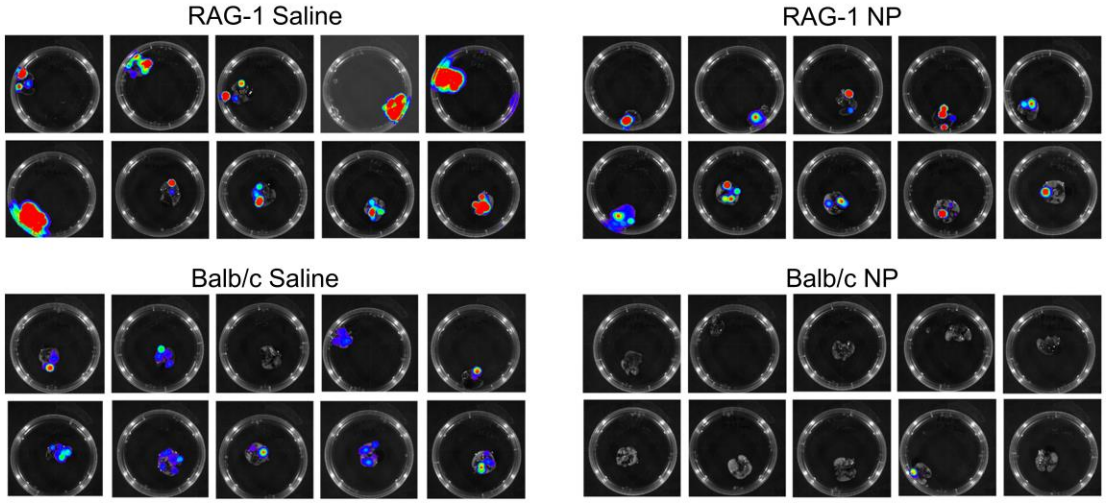

D

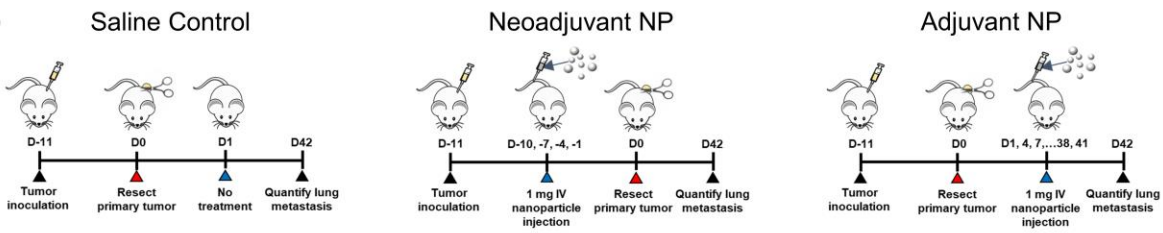

E

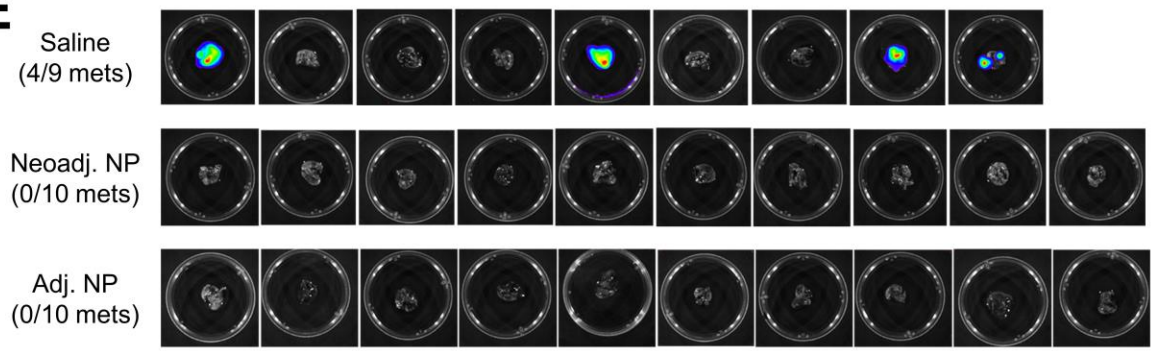

Figure 3-5. Nanoparticle-mediated clearance of metastatic tumors dependent on T-cells. (A) Longitudinal primary tumor growth in tumor-bearing Balb/c or RAG-1 KO mice that received either saline or NPs. (B) Proportion of immunocompetent (Balb/c) or T-cell-deficient (RAG-1 KO) mice with pulmonary metastases at D21 post-tumor inoculation and (C) BLI of the lungs. (D) Schematic of resection study. NPs were administered either before (neoadjuvant) or after (adjuvant) PT resection. (E) Lung BLI of Balb/c mice receiving nanoparticles or saline in PT resection study.

3.3 Discussion

In this study, immunomodulatory cargo-free PLG NPs were investigated for therapeutic efficacy in the neoadjuvant and adjuvant setting for treating metastasis in the 4T1 murine model of TNBC. Immunotherapy has emerged as a powerful tool for localized and metastatic disease, with its continued development being supported by the nearly 6,300 active clinical trials investigating immunomodulatory agents in cancer that have begun since 2020 [180,181]. However, despite the durable responses in some patients and FDA approvals, the majority of TNBC patients are not responsive to checkpoint inhibition. In the randomized, open-label, phase 3 trial (KEYNOTE-119) of the checkpoint inhibitor pembrolizumab in mTNBC patients, investigators observed a 9.6% objective response rate [78]. Interestingly, there is mounting evidence demonstrating that checkpoint blockade resistance is driven, in part, by immunosuppressive components of the tumor microenvironment, including myeloid cells [182]. This report details an immunomodulatory nanoparticle platform that can reprogram innate immune cells to skew the immunosuppressive microenvironment toward an inflammatory, anti-tumor milieu.

We found that primary tumor growth was reduced as a result of neoadjuvant NP administration. Clinically, the majority of TNBC patients receive neoadjuvant chemotherapy with the goal of reducing PT volume prior to surgical resection [183]. In the KEYNOTE 522 trial, 64.8% of patients receiving a combination of pembrolizumab and chemotherapy demonstrated a

pathologic complete response. Notably, this combination of immunotherapy and chemotherapy substantially improved the PCR relative to either treatment alone (51.2% for chemotherapy or 21.4% for pembrolizumab as monotherapies). We have previously reported that cargo-free PLG NPs improved the efficacy of checkpoint inhibition in reducing PT growth, when delivered as a combination therapy [68]. These naked NPs function by a distinct mechanism from either chemotherapy or checkpoint blockade, and may present an opportunity to further improve the PCR when administered as a neoadjuvant therapy. And, whereas other nanoparticle approaches deliver chemotherapeutic agents, these cargo-free nanoparticles demonstrated efficacy by modulating immune responses without delivering a payload [184,185].

Adjuvant NP administration, following PT resection in a murine model of TNBC, led to clearance of pulmonary metastases. For many cancer types, metastatic disease marks the stage where treatment no longer has curative intent, and disease progression leads to mortality. While significant advances have been made in the treatment of localized breast cancer, few therapies exist to effectively treat metastasis [3]. As such, breast cancer diagnoses have a 99% five-year survival rate for localized disease, yet survival drops to 29% for progression to metastatic disease [1]. The disparity in outcomes between primary and metastatic disease necessitates investigating novel strategies for targeting the microenvironments that support metastatic colonization and the subsequent progression of disease. Immunotherapies have been pursued with the goal of stimulating an anti-tumor immune response to treat metastasis. To investigate the efficacy of immunomodulatory, drug-free NPs in clearing metastatic lesions, we administered NPs in the adjuvant setting, in which therapy is delivered after surgical resection. This allows for an intervention to be studied in the clinical context of established metastatic lesions without a PT. Excitingly, we observed that adjuvant NP therapy led to the clearance of pulmonary metastases.

These results support the cargo-free NP platform as a potential opportunity for treating metastatic lesions in advanced TNBC.

NP administration alters the immune cell composition at the metastatic niche, in part through altered cytokine secretion that impacts recruitment from circulation. Neutrophils suppress effector cell responses in the metastatic niche, and targeting these cells has been shown to inhibit metastasis [52,186,187]. While nanoparticle administration resulted in modest changes in immune cell composition in peripheral blood, we observed large changes in neutrophil accumulation at sites of disease that cannot be explained by systemic changes in composition alone. We found that nanoparticle administration drastically reduced the secretion of monocyte and neutrophil-attracting chemokines at the lung, suggesting that nanoparticles induce tissue-specific changes in immune cell recruitment. In particular, the nanoparticle-induced downregulation of CCL2 secretion by CD45+ cells and CCL3 by CD45- cells in the lung may disrupt the continued accumulation of immunosuppressive myeloid cells at metastatic niches. CCL2 and CCL3 have been found to promote the recruitment and retention of monocytes and monocyte-derived macrophages, and CCL3 has been shown to promote the accumulation of neutrophils at metastatic sites [25,188,189]. CXCL12, which was downregulated in the CD45- lung cells with nanoparticle treatment, has also been implicated in the recruitment and retention of neutrophils to the metastatic niche and associated with metastasis [190,191]. Overall, these findings suggest that NP administration reduces the secretion of inflammatory chemokines and inhibits the recruitment of metastasis-supporting myeloid cells to the lung, thereby inhibiting the formation of an immunosuppressive metastatic niche.

Alterations in the immune cell composition at metastatic sites following NP administration can disrupt the immunosuppression that is associated with disease progression and maintain an

anti-tumor inflammatory environment. The accumulation of immunosuppressive myeloid cells in the periphery and at the metastatic niche correlate with poor clinical outcomes and immunotherapy resistance [47,192]. Myeloid cells, especially neutrophils, are associated with immunosuppression in advanced metastases, with potent suppression of T cell cytotoxicity through the secretion of reactive oxygen species and expression of surface markers such as PD-1 [43,44]. In the lungs of nanoparticle-treated mice, inflammatory gene expression pathways and inflammatory myeloid cell subsets were upregulated in comparison to the lungs of saline-treated mice. Signaling pathways associated with IFNg and TNFa were significantly upregulated in neutrophils, monocytes, and dendritic cells. IFNg signaling has been associated with anti-tumor cytotoxicity in neutrophils and maturation of monocytes and dendritic cells, leading to the activation of tumoricidal NK and T cells, respectively [193–196]. Similarly, TNFa has been associated with neutrophil cytotoxicity and tumoricidal polarization of monocyte-derived macrophages [197,198]. Notably, while TNFa secretion increased with nanoparticle administration, IFNg secretion conversely decreased, suggesting that the upregulation of genes associated with IFNg signaling may be directly associated with nanoparticle delivery. This connection is further supported by the presence of clusters of neutrophil and monocyte subpopulations that that are highly expressing IFNg-associated genes, which are primarily present in nanoparticle-treated mice.

T cell activity was critical to the nanoparticle-induced clearance of metastatic tumor cells. T cell immunity is a critical component of tumor surveillance, and cancer-induced T cell dysfunction is a major mechanism of immune escape [199]. The infiltration of immunosuppressive myeloid cells induces T cell anergy and the development of regulatory T cells, and previous therapeutic strategies targeting immunosuppressive myeloid cells have demonstrated success in enhancing anti-tumor T cell activity [200,201]. The delivery of nanoparticles following the

metastatic seeding completely suppressed the development of metastatic lesions after resection, suggesting that nanoparticles reprogram the metastatic niche to promote the active clearance of metastatic tumor cells. As nanoparticles potently inhibited tumor growth and metastasis in immunocompetent mice, but were ineffective in T cell deficient mice, this clearance is likely to be driven by T cells. While the induction of inflammatory gene expression programs in neutrophils may induce anti-tumor neutrophil cytotoxicity, the lack of response in T cell-deficient mice demonstrates that tumor clearance by innate immune cells alone is insufficient, and that T cells are essential in the nanoparticle mechanism of action [202]. Interestingly, nanoparticle administration significantly increased DC activation and expression of genes associated with antigen presentation, motivating further study on how cargo-free nanoparticles directly stimulate adaptive immunity.

In conclusion, we report that cargo-free PLG NPs augment PT resection by abrogating distant recurrence when administered either as a neoadjuvant or adjuvant therapy. The NPs modulated the immune microenvironment of the lungs, a metastatic site in TNBC, skewing suppressive immune cells toward inflammatory, anti-tumor phenotypes. NP administration enhanced T-cell-mediated tumor cell clearance, and their efficacy was nullified in a T-cell-deficient model. These promising results support proposing a clinical trial to provide a novel, immunomodulatory neoadjuvant/adjuvant therapy to mitigate recurrence during surgical resection in treating TNBC.

3.4 Methods

3.4.1 Nanoparticle fabrication

ONP-302 nanoparticles were manufactured by COUR Pharmaceuticals Development Company, Inc. Nanoparticles were made from poly(lactic-co-glycolic) acid (PLGA) (Lactel®, Durect Corporation) using a double emulsion technique. Briefly, a water-in-oil emulsion

containing a proprietary mixture of PLGA and surfactants was prepared. Solvents were removed by evaporation, yielding negatively charged nanoparticles which were then washed, filtered, and concentrated by tangential flow filtration. ONP-302 nanoparticles were then formulated with buffering agents and cryoprotectants and lyophilized. The physiochemical properties of nanoparticles were characterized by dynamic light scattering (DLS) and scanning electron microscopy (SEM).

3.4.2 Tumor cell culture and animal inoculations

4T1-luc2-tdTomato murine triple negative breast cancer cells (PerkinElmer) were cultured in RPMI 1640 Medium (Gibco) containing 10% fetal bovine serum (FBS, Avantor) for 5 days (37C, 5% CO_2) prior to orthotopic inoculation. Tumor cells were enzymatically lifted from the tissue culture flask with trypsin (Gibco) for 10 minutes at 37C and resuspended in culture medium. Cells were centrifuged at 500xg for 5 minutes and resuspended in Dulbecco′s phosphate buffered saline (DPBS) (Gibco) at a concentration of 2E6 cells/mL. The tumor cell line was previously confirmed to be pathogen free and authenticated by short tandem repeat DNA analysis and compared to the ATCC STR profile database (DDC Medical). Orthotopic inoculations were performed by injecting 50 uL of the cell suspension, containing 1E5 4T1 tumor cells, to the fourth right mammary fat pad of 12-week-old female Balb/c mice (Jackson Laboratory strain #000651). In addition to the immunocompetent Balb/c strain, Rag1 KO (Jackson Laboratory strain #003145) mice were used as they are homozygous for the Rag1tm1Mom mutation and thus do not produce mature T cells.

3.4.3 Nanoparticle administration

Nanoparticles were intravenously injected into the lateral tail veins of mice. Nanoparticles were resuspended in a mixture of sterile water for injection (Intermountain Life Sciences) and sterile DPBS . Nanoparticles were first resuspended in water at 40 mg/mL, and diluted with DPBS to 10 mg/mL for a final ratio of 1 parts water to 3 parts DPBS. Nanoparticles were administered at a dose of 1 mg in 100 uL of solution every 3 days. Control mice received 100 uL of DPBS. Nanoparticles were injected starting 1, 2, or 4 days after tumor inoculation for primary tumor growth studies. In tumor resection studies, the neoadjuvant group received nanoparticles starting 1 day after inoculation, and additional doses every 3 days until tumor resection at 11 days, for a total of 4 doses. Mice in the adjuvant group did not receive nanoparticles prior to resection, and initiated dosing 1 day after resection with nanoparticles every 3 days until the endpoint at 42 days after resection. For all other studies, nanoparticles were administered starting 1 day after tumor inoculation and continued every 3 days until the study endpoint.

3.4.4 Tumor volume measurements

Tumor size was recorded using standard electronic calipers (VWR) while mice were anesthetized with 2% v/v% isoflurane. Primary tumor volume was calculated ($V = 0.5 \times L \times W^2$, L: length of longest dimension of the tumor, W: length perpendicular to the longest tumor dimension) as previously described [68].

3.4.5 Ex-vivo bioluminescent imaging

Metastatic burden at the lungs and liver was measured with explanted whole organs at terminal endpoint using an IVIS Lumina LTE imaging system (Caliper Life Science). The formation of metastatic lesions at these explanted tissues was quantified by bioluminescence

imaging with the IVIS Lumina LTE imaging system (Caliper Life Science). Tissues were incubated in DPBS containing 630 uM d-luciferin (Caliper) at 37C for 10 minutes and subsequently imaged with the IVIS. The bioluminescent imaging of luciferase-expressing 4T1 cells were calculated by the Living Image Software (Caliper Life Sciences) and visualized as flux (photons/sec) from the tissues.

3.4.6 Circulating tumor cell quantification and association with immune cells

Circulating tumor cells (CTCs) were isolated and quantified using the Labyrinth microfluidic platform [203]. CTCs are separated from leukocytes by size, as white blood cells are smaller than 4T1 cells and path differently in the microfluidic system. Briefly, blood samples were collected from mice treated with nanoparticles at 14 and 21 days after tumor inoculation, from tumor-bearing mice injected with saline at 14 days after inoculation, and naive mice without tumors. Due to sample volume requirements, blood from two mice were pooled per sample. Blood was first processed with Ficoll separation to separate red blood cells, then run through the Labyrinth at a flow rate of 1800 uL/min. CTCs accumulated primarily in the second outlet, representative of larger cells, and leukocytes were isolated in the first outlet. To quantify CTCs and leukocytes, samples were taken from each outlet, diluted in 1:7.5 in PBS, and stained with DAPI. Two slides were imaged from each outlet for each sample for technical replicates. Representative images of CTCs and leukocytes are shown in **Figure 3-S1E**.

3.4.7 Single-cell RNA-sequencing

Saline- or NP-treated lungs were extracted from mice 14 days post-tumor inoculation. The tissues were minced with scalpel blades, enzymatically digested with liberase TM (Roche), processed through a cell strainer, and underwent erythrocyte lysis with ACK buffer (Gibco) for 5

minutes. Library preparation of the resulting single cell suspension was conducted with the 10x Chromium platform. Samples were sequenced on the NovaSeq 6000 at the University of Michigan Advanced Genomics Core at an average depth of 50,000 reads per cell. Raw reads were mapped by CellRanger to output count matrices with subsequent clustering and differential gene expression performed using the Seurat (v2) pipeline [204]. Cells containing < 500 genes, > 5000 genes, or > 7.5% mitochondrial genes were filtered out from the final data set. Cluster cell types were classified using the markers shown in **Figure 3-S2A**. The clusters defined as neutrophils, monocytes, and dendritic cells were further analyzed to identify specific subsets using the gene expression outlined in **Figures 3-S2B - 3-S2D**.

3.4.8 Gene Set Enrichment Analysis (GSEA)

Within the neutrophils, monocytes, and dendritic cells, differentially expressed genes between the NP-treated and saline-treated cells were identified using Seurat. The resulting gene lists were converted to human orthologs with biomaRt. Gene fold-changes were used as the ranking variable to assemble pre-ranked gene lists. GSEA (pre-ranked gene list) was used to identify enriched pathways sampling from hallmark, KEGG, REACTOME, and gene ontology (GO) databases from the Molecular Signatures Database (MSigDB). The top 10 pathways up-regulated in the NP-treated samples were reported for each cell type with redundant pathways removed by leading edge analysis.

3.4.9 Flow cytometry, magnetic activated cell sorting, and enzyme-linked immunosorbent assay

Lungs and whole blood of tumor-bearing mice were isolated at 14 days-post tumor inoculation. Lungs were mechanically and enzymatically digested as previously detailed [68].

Tissues were processed through a 70 um cell strainer (Corning) to filter. Single cell suspensions of the lungs and blood were then prepared by erythrocyte lysis in ACK buffer, (Fisher) washing in DPBS supplemented with 2 mM EDTA and 0.5% bovine serum albumin, and centrifugation at 500xg for 5 minutes. Blood cells were treated with anti-CD16/32 (1:100, clone 93, Biolegend) to block nonspecific staining and samples stained with antibodies against Alexa Fluor 700 anti-CD45 (1:100, clone 30-F11, Biolegend), Brilliant Violet 510 anti-CD11b (1:25, clone M1/70, Biolegend), Brilliant Violet 711 anti-Ly6G (1:20, clone 1A8, Biolegend), and FITC anti-Ly6C (1:100, clone HK1.4, Biolegend), as well as with DAPI (Biolegend) for viability, and analyzed on the BioRad ZE5 Cell Analyzer. Data analysis was performed using FlowJo (BD). Cells from the blood and lungs were labeled with magnetic microparticle-conjugated antibodies against CD45 (Miltenyi Biotec) and sorted. The CD45-positive fraction, representing immune cells, and CD45-negative fraction, consisting of non-immune cells, were resuspended at 1E6 cells/mL in media and cultured in a 96-well plate for 16-18 hours at 2.5E5 cells/well. Following incubation, cells were centrifuged at 1000xg for 5 min. Supernatant was collected and frozen at -80C. The levels of IL-1b, IL-4, IL-6, IL-13, IFNg, TNFa, TGFb, CCL2, CCL3, CCL4, and CXCL12 in supernatant were quantified via ELISA performed by the Cancer Center Immunology Core at the University of Michigan. Separately, ELISAs for NE-DNA and MPO-DNA complexes were formed on blood plasma to quantify NETosis. Blood was collected in EDTA blood collection tubes (BD) and centrifuged at 2000xg for 5 minutes to separate plasma, which was frozen at -80C until analysis.

3.4.10 Statistical analysis

Two-tailed unpaired t-tests assuming unequal variance were performed for single comparisons between two conditions, namely nanoparticle and control. Median survival and

survival curves were analyzed using a simple survival analysis (Kaplan-Meier) with log-rank (Mantel-Cox test) for statistical significance. Significant differentially expressed genes in the scRNA-seq analysis was determined with the Wilcoxon rank-sum test using default Seurat settings. The significance of GSEA pathway scores were determined with Student's t-tests using the Bonferroni multiple hypothesis correction ($a = 0.01$). Prism 9 (GraphPad), Excel (Microsoft), and R were used for performing statistical analyses, with $p < 0.05$ considered to be statistically significant. Error bars on plotted data are calculated as standard error mean (SEM).

3.5 Supplementary Figures

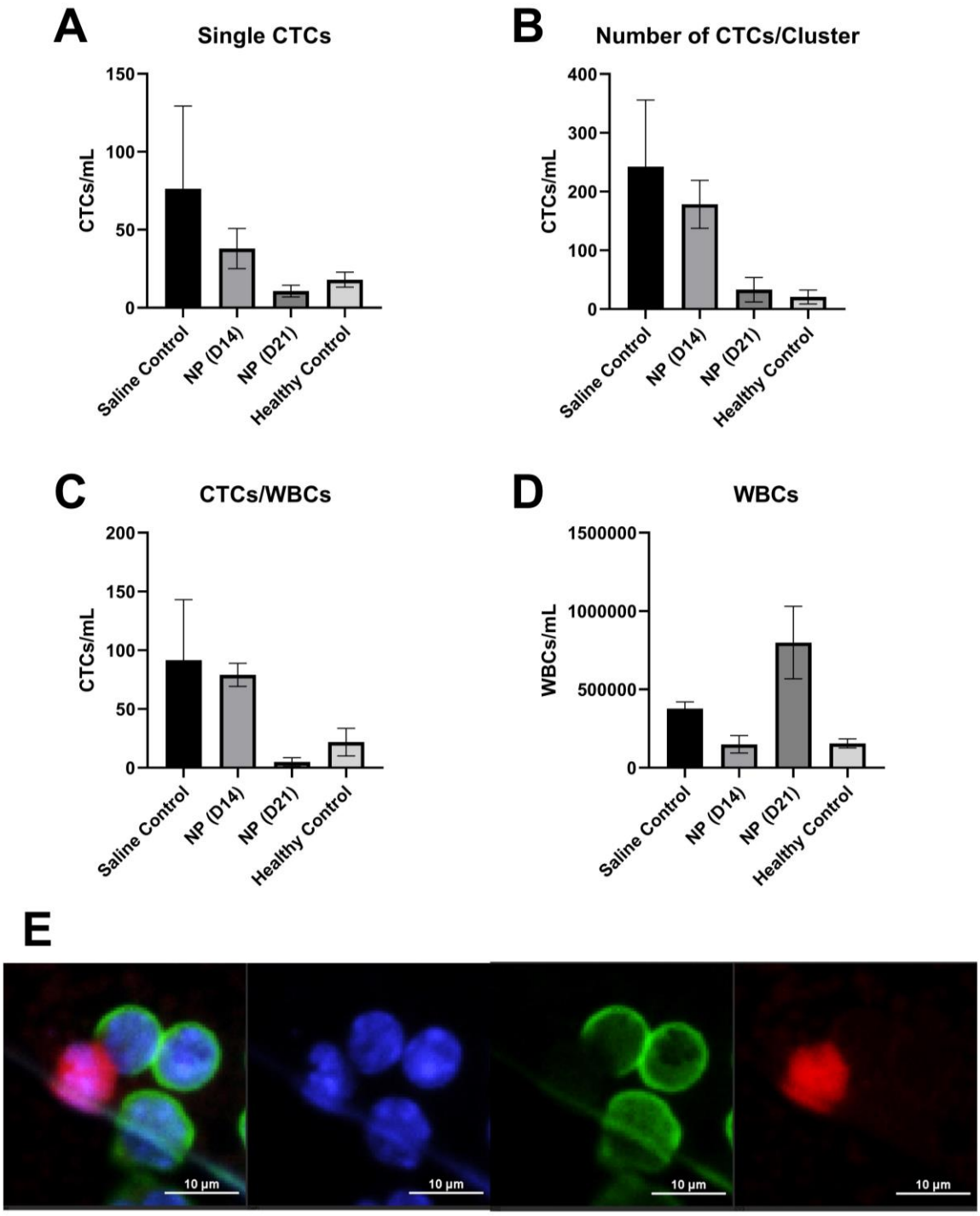

Figure 3-S1. Nanoparticles reduces circulating tumor cells in peripheral blood. Quantification of (A) single CTCs, (B) number of CTCs/cluster, (C) ratio of CTCs to white blood cells, and (D) quantity of WBCs. Quantification normalized to blood volume. (E) Representative images of cells in peripheral blood. Blue – DAPI, Green – CD45+, Red – tdTomato.

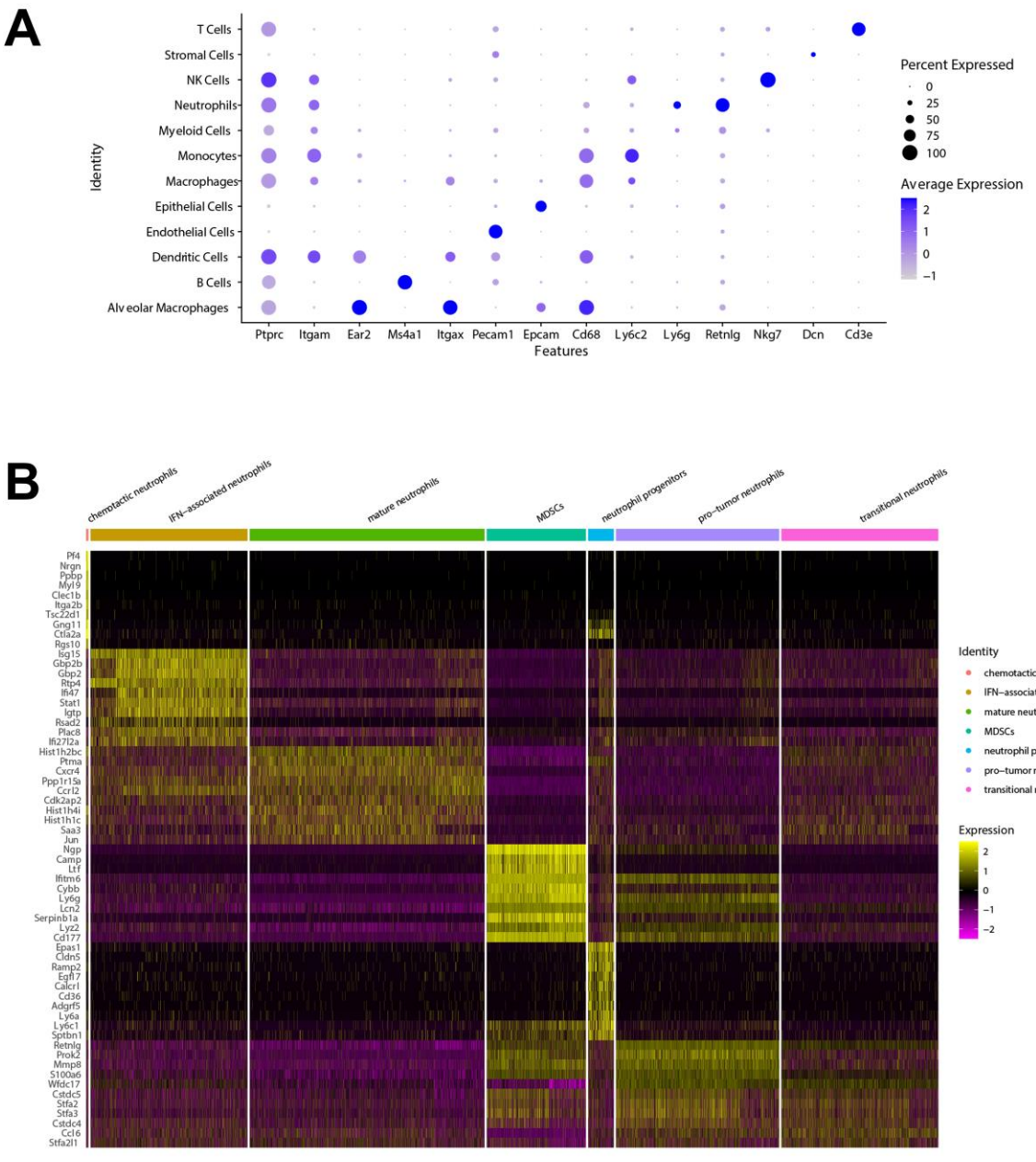
A
T Cells
Stromal Cells
NK Cells
Neutrophils
Myeloid Cells
Monocytes
Macrophages
Epithelial Cells
Endothelial Cells
Dendritic Cells
B Cells
Alveolar Macrophages
Identity
Ptprc
Itgam
Ear2
Ms4a1
Itgax
Pecam1
Epcam
Cd68
Ly6c2
Ly6g
Retnlg
Nkg7
Dcn
Cd3e
Features
Percent Expressed
0
25
50
75
100
Average Expression
2
1
0
−1
B
chemtactic neutrophils
IFN−associated neutrophils
mature neutrophils
MDSCs
neutrophil progenitors
pro−tumor neutrophils
transitional neutrophils
Identity
chemotactic neutrophil
IFN−associated neutrophils
mature neutrophils
MDSCs
neutrophil progenitors
pro−tumor neutrophils
transitional neutrophils
Expression
2
1
0
−1
−2

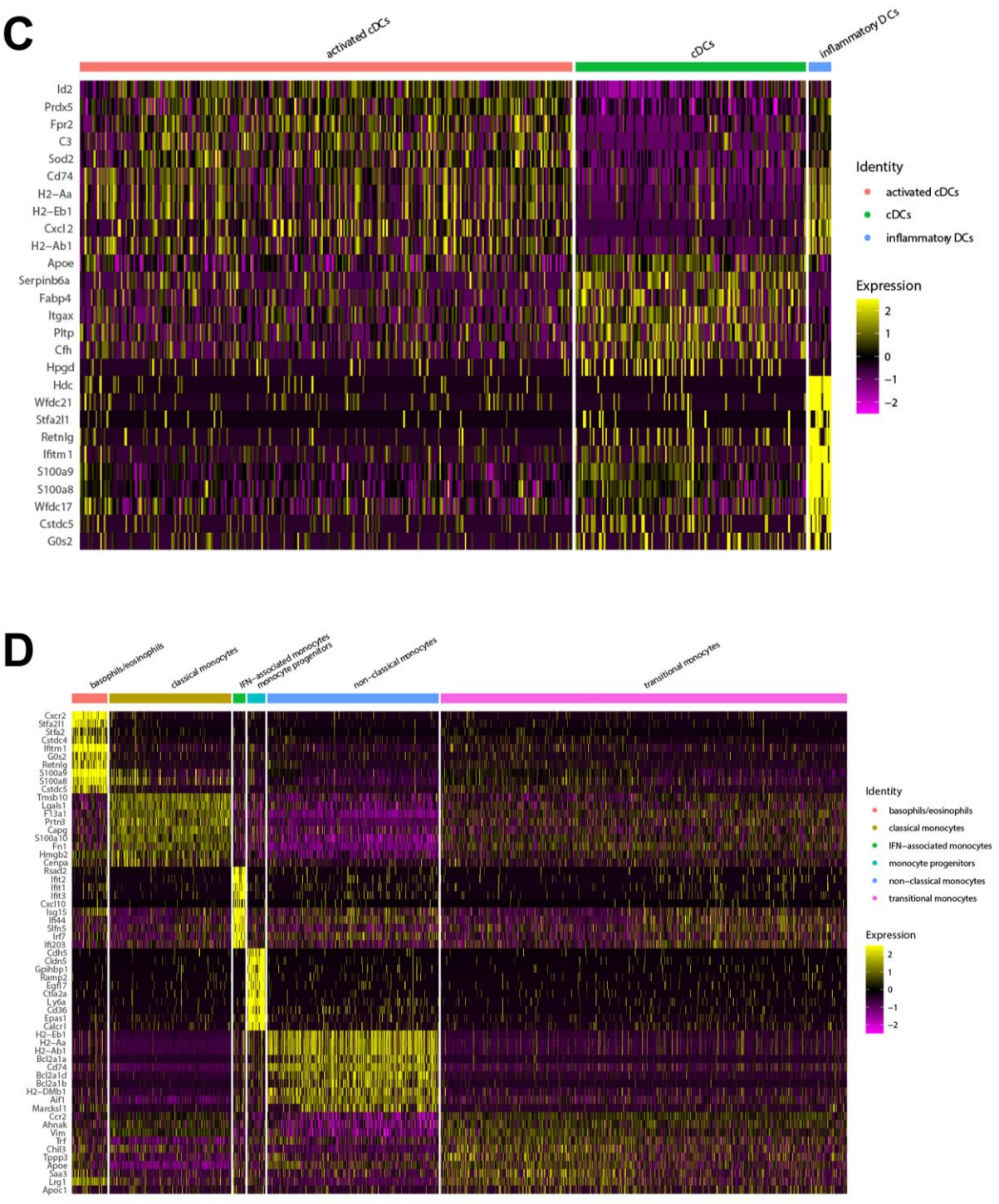

Figure 3-S2. Gene expressions of lung-derived cell populations by single cell RNA sequencing. (A) Average gene expression of cell types. Gene expression of (B) neutrophils, (C) dendritic cells, and (D) monocytes by subpopulations.

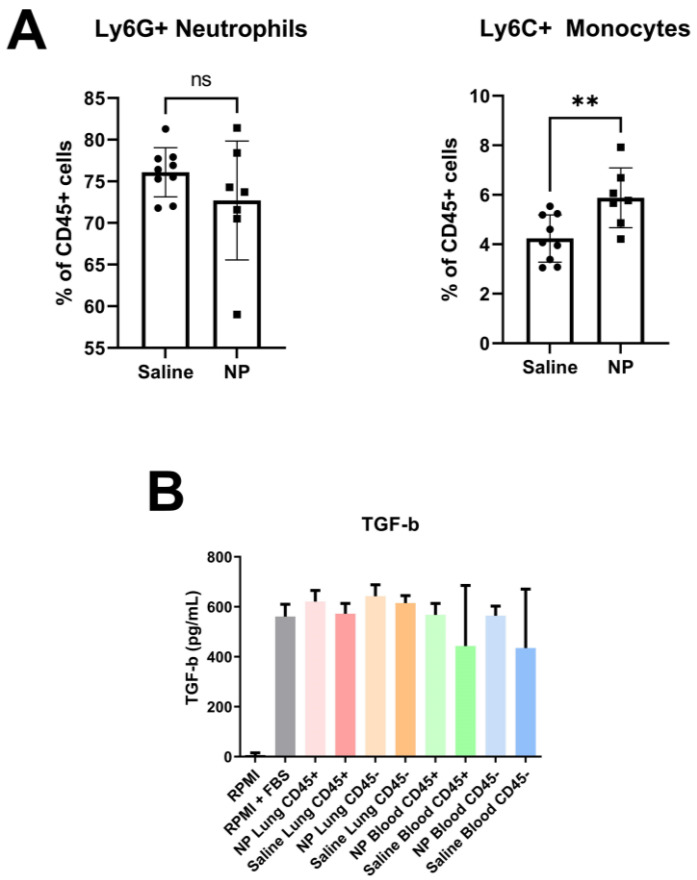

Figure 3-S3. Peripheral immune cell responses to nanoparticle administration. (A) Ratio of Ly6G+ neutrophils and Ly6C+ monocytes in peripheral blood analyzed in 4T1-bearing mice receiving either NPs or saline (% of CD45+ immune cells). (B) Quantification of TGF-β secretion by CD45+/- cells sorted from the lungs or peripheral blood.

A

Group	Incidence of Metastasis
RAG-1 Saline	3/10
RAG-1 NP	0/10
Balb/c Saline	0/5
Balb/c NP	0/5

B

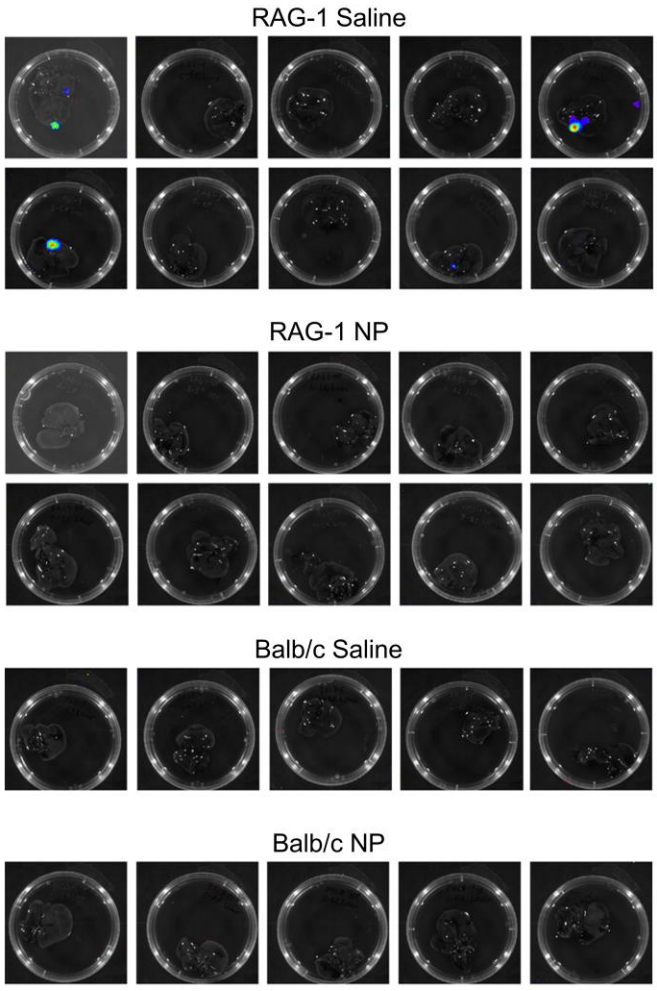

Figure 3-S4. Quantification of liver metastases in T-cell-deficient model. (A) Incidence of liver metastases in tumor-bearing Balb/c or RAG-1 KO mice receiving either saline or NPs. Liver metastases quantified on D21 post-tumor inoculation. (B) Luminescent images of livers.

Chapter 4

Engineered Immunologic Niche Monitors Checkpoint Blockade Response and Probes Mechanisms of Resistance

The material in this chapter has been adapted with minor modifications from the following article:

> **R.M. Raghani**, G. Escalona, I.A. Schrack, J.A. Ma, K.M. DiLillo, P. Kandagatla, R. Urie, J.T. Decker, A.H. Morris, K.B. Arnold, J.S. Jeruss, L.D. Shea, Engineered immunologic niche monitors checkpoint blockade response and probes mechanisms of resistance, *In Preparation*.

4.1 Introduction

The treatment of triple negative breast cancer (TNBC) with (ICB) has shown improvements in patient outcomes [71]. In a phase 3 clinical trial of anti-PD-1 (aPD-1) in mTNBC patients, ICB was found to perform similarly as effective, with reduced grade 3-4 adverse events, as compared to the gold standard chemotherapy [78]. Additionally, in the phase 3 trial of neoadjuvant/adjuvant aPD-1 in early-stage TNBC patients, investigators found improved pathological complete responses and reduced disease progression in the patients receiving ICB [81]. However, while ICB-sensitive breast cancer patients have incredible responses, the majority of TNBC patients are resistant to ICB. As such, there is a great need for biomarkers to stratify patients based on ICB-response.

We tested the hypothesis that probing dynamics at an engineered immunologic niche would provide unique analytes correlative of ICB-response. The niche implant integrates with the host

through tissue infiltration throughout the biomaterial architecture, and the microenvironment of this immunologic niche is dynamically modified during disease initiation and progression [205,206]. Our lab has previously shown that the immune milieu of the implant can be longitudinally probed for monitoring 1) initiation and progression of disease, and 2) response to a primary tumor (PT) resection, in a murine model of triple negative breast cancer, or nanoparticle administration, in a murine model of relapsing multiple sclerosis [207,208]. As such, we hypothesized that dynamic gene expressions in immune cells at the immunologic niche could provide insight into immunotherapy response in TNBC. Divergent responses in disease progression, as a result of checkpoint inhibition, were investigated by monitoring primary tumor growth and survival. Gene expressions were probed at the immunologic niche to identify genes that correlate with treatment response after therapy. Pathway analyses, gene sequencing of myeloid cells, and flow cytometry of immune cell populations were conducted to investigate cell types and differentially regulated pathways underlying the divergent therapy responses. Finally, we analyzed gene expressions prior to treatment to investigate analytes correlative of predicting therapy response, before initiating therapy. Longitudinally interrogating an engineered immunologic niche, to monitor changes associated with ICB-response, presents a new opportunity to stratify therapy candidates and investigate mechanisms underlying treatment resistance.

4.2 Results

4.2.1 Divergent disease progression and survival in response to treatment with checkpoint blockade therapy

We first investigated divergent ICB-responses in a murine model of advanced TNBC. Balb/c mice were orthotopically inoculated (D0) with triple negative 4T1 tumor cells at the fourth right mammary fat pad. Mice were split into two cohorts and received either intraperitoneal (IP)

administrations of aPD-1 or isotype control every other day starting on day 9 post-tumor inoculation, for a total of four doses (D9, D11, D13, D15; **Figure 4-1A**). Waiting for at least a week post-tumor inoculation to initiate ICB allowed for the formation of established primary disease prior to starting treatment. Longitudinal PT volumes were recorded and mice were monitored for survival.

While mice receiving aPD-1 trended toward reduced PT growth, no significant difference was found between the aPD-1 and isotype control cohorts (**Figure 4-S1A**, $p > 0.05$). The aPD-1 cohort was then stratified based on ICB-response. Mice whose PT growth was less than the established cutoff for fold change in PT volume on D21 post-tumor inoculation, as compared to the baseline (D7), were categorized as ICB-sensitive (**Figure 4-S2**). The ICB-resistant mice were categorized as those with a fold change in PT volume above this cutoff. Interestingly, when categorizing the ICB cohort based on ICB-response, ICB-sensitive mice had significantly reduced PT growth versus the ICB-resistant mice on days 11, 13, 15, and 19 post-tumor inoculation (**Figure 4-1B**, $p < 0.05$). Mice that were sensitive to ICB also had significantly reduced PT growth compared to the isotype control cohort, and ICB-resistant mice had indistinguishable progression of versus the isotype control (**Figure 4-1B**). In addition to changes in PT growth, ICB-sensitive mice had significantly improved survival compared to the ICB-resistant cohort (**Figure 4-1C**, $p < 0.05$). Following the observation that tumor-bearing Balb/c mice treated with aPD-1 had divergent PT growth and survival in response to ICB, we asked if these divergent immune responses could be monitored at the immunologic niche by investigating implant-derived gene expressions with bulk RNA sequencing (RNA-seq).

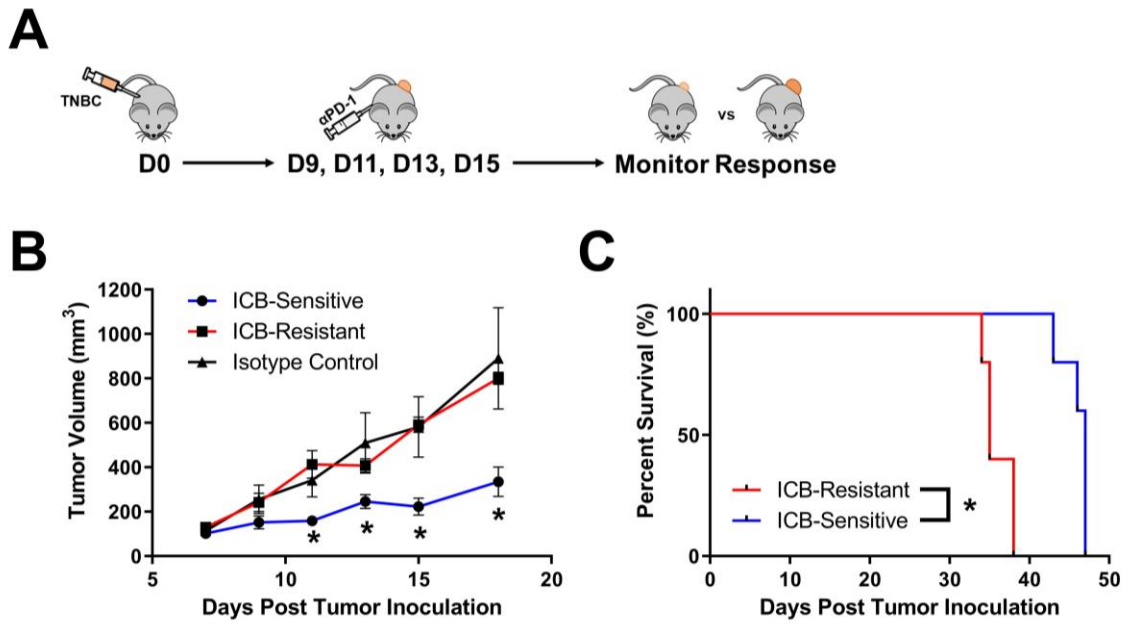

Figure 4-1. Treatment with ICB yields divergent responses in PT growth and survival. (A) Schematic of orthotopically inoculating Balb/c mice with 4T1 tumor cells and administering anti-PD-1. (B) Longitudinal primary tumor volumes in tumor-bearing mice receiving either anti-PD-1 or isotype control. (C) Survival of 4T1-bearing Balb/c mice receiving anti-PD-1. ICB-sensitivity and resistance stratified based on cutoff for fold change of primary tumor volume on D21 post-tumor inoculation to D7. Two-tailed unpaired t-tests assuming unequal variance were performed for single comparisons between two conditions. Bars show mean ± SEM. * $p < 0.05$.

4.2.2 Therapy response alters gene expression at immunologic niche after therapy

Next, we performed bulk RNA-seq on RNA from the immunologic niche to investigate implant-derived gene expressions for longitudinally monitoring ICB-response. We have previously shown that the gene expressions of immune cells at the engineered, immunologic niche can be probed for monitoring progression of BC and response to a PT resection [207]. Microporous polycaprolactone (PCL) scaffold implants (thickness – 2mm, diameter – 5mm) with interconnected pores (250–425 mm) were surgically inserted into the dorsal subcutaneous space of Balb/c mice 14 days prior to tumor inoculation (D-14) to allow for tissue infiltration and integration with the host (**Figure 4-2A**). The microporous architecture facilitates cell colonization throughout the entirety of the implant, and we have previously shown that immune changes at the

immunologic niche are reflective of dynamics in disease progression [207,208]. Mice were orthotopically inoculated with 4T1 tumor cells (D0) and an immunologic niche implant was biopsied (D7) once the primary disease was established to analyze the immune response at baseline, prior to initiating ICB therapy (**Figure 4-2A**). Four doses of aPD-1 were administered IP every other day starting on D9 post-tumor inoculation. Niche implants were biopsied at D14 and D21 for analyzing immune changes during therapy (D14) and after the conclusion of ICB therapy (D21) (**Figure 4-2A**). PT volumes were longitudinally recorded and survival monitored to stratify mice into ICB-sensitive and ICB-resistant cohorts. Biopsied immunologic niche tissues were immediately flash frozen in isopentane. Frozen implants were homogenized in Trizol and RNA subsequently isolated from homogenate using the Direct-zol™ RNA Kit. The isolated RNA was diluted to the desired concentration and submitted to the University of Michigan Advanced Genomics Core for analysis with total RNA (ribo-depletion) library preparation and bulk RNA-seq performed on the Illumina NovaSeq™ S4 at PE150 (45-60 million reads/sample). Raw counts, as prepared from demultiplexed fastq files by the Advanced Genomics Core, were converted to normalized counts using DEseq2 [209].

To investigate immunologic niche-derived genes for monitoring ICB-response, we first screened the bulk RNA-seq data with T-tests comparing the differential gene expressions after therapy (D21, after Tx). This analysis identified 242 differentially expressed genes (DEGs) between the ICB-sensitive and ICB-resistant cohorts (**Figures 4-S3A - 4-S3C**). Principal component analysis (PCA) was used for dimensionality reduction to visualize how the cohorts clustered based on the expressions of these 242 DEGs after Tx (Figure 4-S3A - 4-S3C). As the first two components were found to be responsible for the majority of the variance, only PCA1 and PCA2 were visualized for the remaining analyses (**Figures 4-S3A – 4-S3B**). Elastic net-based

coefficient reduction, favoring group selection ($\alpha = 0.05$), was then implemented to identify the most biologically relevant genes from this 242-gene panel. This α value was utilized to retain highly correlated variables, as covarying features are valuable for identifying genes with related mechanistic insight. We employed cross validation with 2000 random resampling iterations and selected features that were chosen in more than 85% of iterations to ensure robustness of the identified gene signature. The EN analysis of after Tx DEGs identified a panel of 22 genes (**Figure 4-S3E**). Hierarchical clustering of the multivariate gene expressions grouped the cohorts based on their response after Tx (Figure 4-S3E). PCA-based dimensionality reduction of the implant-derived gene expressions from this 22 gene panel clustered mice separately based on ICB-response after Tx (**Figure 4-S3F**). Notably, 13/22 of the genes were upregulated in the ICB-sensitive mice, whereas 9/22 of the EN-identified genes were upregulated in the ICB-resistant mice. After observing that the gene expressions at the immunologic niche could be monitored after therapy to glean insight into ICB-response, we asked if normalizing the implant-derived gene expressions from each mouse to their baseline before Tx could probe for dynamic changes in ICB-response.

4.2.3 Delta analysis of gene expressions monitors for unique ICB-response dynamics

We next tested the hypothesis that a delta analysis, or normalization to baseline (D7), of the immunologic niche-derived gene expressions could more effectively illuminate dynamics in ICB-response. Delta counts were first calculated by normalizing the DEseq2-normalized counts for each gene after Tx (D21) to the DEseq2-normalized counts before Tx (D7), for each mouse. T-tests were then performed between cohorts for the delta counts of each gene to screen for DEGs ($p < 0.05$). This initial screen identified 237 DEGs between ICB-sensitive and ICB-resistant cohorts (**Figures 4-2B - 4-2C**). Visualization of the DEseq2-normalized gene expressions by PCA showed separate clustering of the mice not only after Tx, but also before Tx (**Figure 4-2B**).

Notably, PCA clustering of the delta counts (expressions normalized to D7) showed separation of the cohorts based on ICB-response after Tx (D21 expressions normalized to D7, **Figure 4-2C**), as well as during Tx (D14 normalized to D7, **Figure 4-S4D**). Performance metrics were calculated for sensitivity, specificity, and categorization efficacy for the 237-gene delta-panel (Figure 4-S4C).

The 237-gene delta panel was then analyzed with EN to identify the most relevant DEGs for monitoring ICB-response. Through 2000 iterations of cross validation, the EN analysis of the delta DEGs identified a signature of 16 genes. Excitingly, PCA-based clustering of the 16-gene delta signature showed excellent separation of the ICB-sensitive and ICB-resistant cohorts (**Figure 4-2E**). Hierarchical clustering of the 16-gene panel separated cohorts based on ICB-response (**Figure 4-2D**). Notably, 6/16 genes increased in expression from baseline (D7) to after Tx (D21) among the ICB-sensitive cohort, whereas the remaining 10 genes decreased (**Figure 4-2D**). Performance metrics were calculated for the EN-identified delta-panel (**Figure 4-S4C**). The delta panel more effectively separated ICB-sensitive from ICB-resistant than the after panel. It is worth noting that when visualizing the PCA-based clustering of ICB-sensitive and resistant cohorts (using DEseq2-normalized counts versus the delta counts), the delta panel (**Figure 4-2B**) differentially clustered cohorts before Tx, whereas the after panel (**Figure 4-S3C**) did not. Following the exciting findings that implant-derived gene expressions provide dynamic information for monitoring divergent ICB-responses, we wanted to investigate how inflammatory pathways were being differentially regulated in response to ICB.

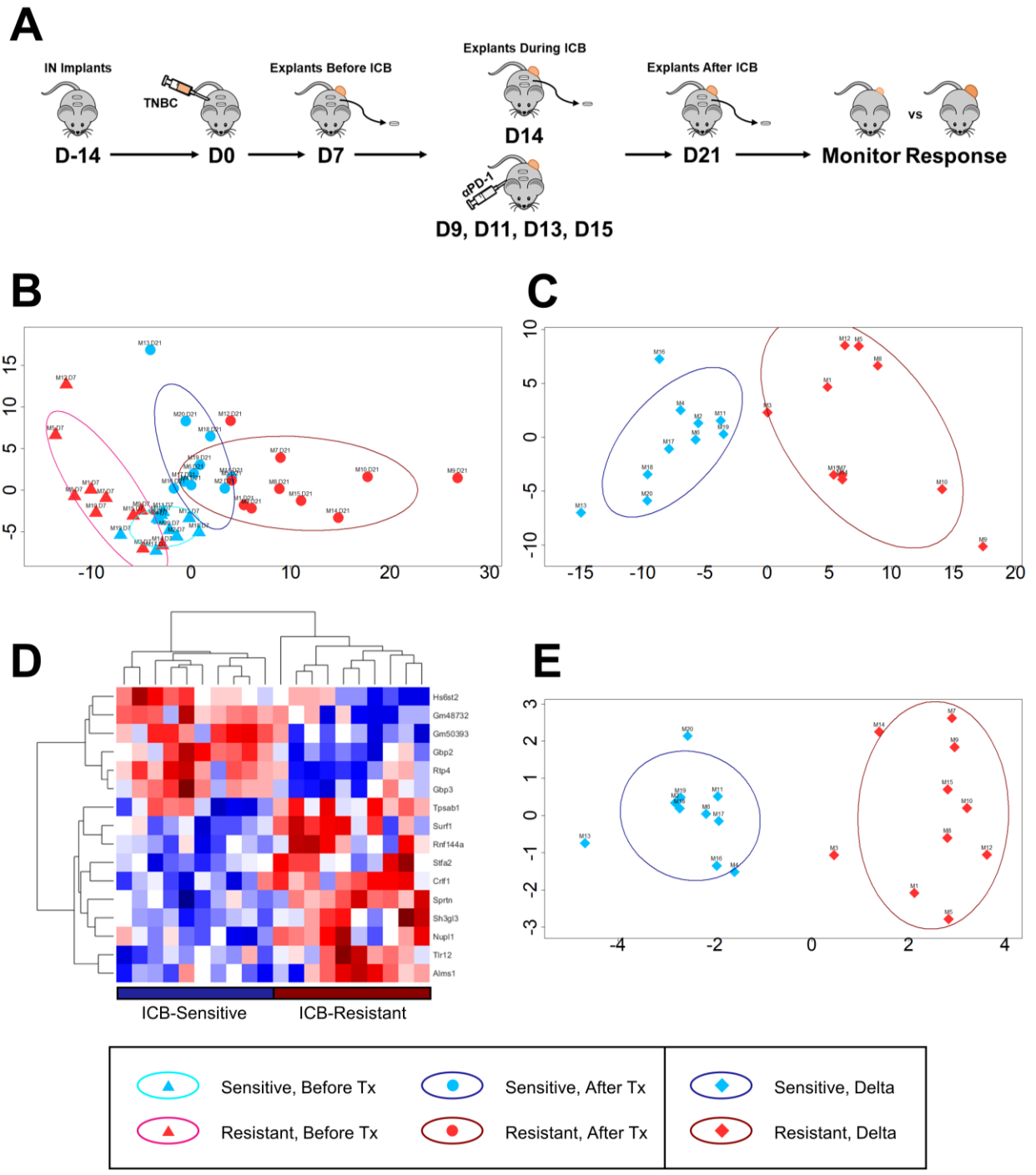

Figure 4-2. Bulk RNA sequencing of IN implant identifies differentially expressed, delta-normalized genes correlative of ICB-response. (A) Schematic of implanting mice with IN, inoculating with 4T1, explanting IN, administering anti-PD-1, and monitoring ICB-response. (B) Clustering of DEseq2-normalized gene expressions with principal component analysis. Clustering represents panel of 237 differentially expressed genes. (C) Clustering of delta (D21 – D7) normalized gene expressions (panel of 237 genes). (D) Heat map of EN-identified monitoring signature of 16 differentially expressed genes. (E) Clustering of ICB-sensitive and ICB-resistant mice based on 16-gene panel. (B-E) Analyses performed on delta-normalized counts. (C-E) Visualization performed on delta-normalized counts.

4.2.4 Immune cell pathways are differentially regulated between ICB- sensitivity and resistance

Gene expressions were analyzed with gene set enrichment analysis (GSEA) to assess differentially regulated pathways associated with divergent ICB-responses [210]. GSEA was performed on implant-derived DEseq2-normalized counts from cohorts after Tx. Pathway changes were examined for a total of 4726 identified gene sets. We first set a normalized enrichment score (NES) cutoff of NES > 1 to find the most differentially regulated pathways, identifying 2100 pathways above this cutoff. Then, we subcategorized the pathways to search for those of the immune system, excluding irrelevant inflammatory pathways (e.g. WP_MIRNAS_INVOLVEMENT_IN_THE_IMMUNE_RESPONSE_IN_SEPSIS). The 143 differentially regulated pathways were broadly categorized into general immune, cytokine/chemokine, myeloid cell, and lymphocyte pathways (**Figure 4-3**). The GSEA analysis of the RNA-seq data identified differentially regulated immune pathways including those associated with cytokine signaling, chemokine regulation, leukocyte proliferation, leukocyte migration, leukocyte differentiation, leukocyte cell-cell adhesion, leukocyte chemotaxis, inflammatory responses, leukocyte cytotoxicity, and aberrant inflammation (**Figure 4-3A**). The most differentially regulated cytokine/chemokine pathways were for those associated with interferon gamma (IFNγ), Type 1 IFN (IFNα, IFNβ), IFN signaling in cancer, interleukin 12 (IL-12), IL-11, IL-10, IL-8, IL-6, IL-4/IL-13, IL-2, and IL-1 (**Figure 4-3B**). The majority of these cytokine/chemokine pathways upregulated in the ICB-sensitive cohort are those responsible for anti-tumor, pro-inflammatory responses. We found that myeloid cell pathways, including those for neutrophil, monocyte, and macrophage function, were differentially regulated between ICB-sensitive and ICB-resistant (**Figure 4-3C**). Pathways for innate immune cell chemotaxis, myeloid

cell differentiation, and degranulation were downregulated at the immunologic niche of ICB-resistant mice. The most differentially regulated lymphocyte pathways were those associated with T-cell activation, T-cell differentiation, T-cell proliferation, NK cell function, T-cell migration, T-cell cytokine production, Th1 response, Th17 response, aberrant T-cell morphology, B-cell activation (**Figure 4-3D**). Specifically, pro-inflammatory pathways, including activation of T-cells, B-cells, and NK-cells were upregulated in the ICB-sensitive cohort. Much of the downregulated cytokine/chemokine pathways in the ICB-resistant cohort have been shown to originate from myeloid cells and play a role in suppressing T-cell responses. In light of the differentially regulated cytokine/chemokine and myeloid cell pathways, we hypothesized that myeloid cell phenotype and function were responsible for differences between the ICB-sensitive and ICB-resistant cohorts at the immunologic niche. To test this hypothesis, we implanted immunologic niche scaffolds (D-14), inoculated the mice with 4T1 tumor cells (D0), administered aPD-1 IP (D9, D11, D13, D15), and explanted the engineered niches a week after completing ICB (D21). ICB-response was determined as detailed in the previous studies. The implants were mechanically and enzymatically digested to derive a single cell suspension. Immunologic niche-derived cells were pooled from all mice within either the ICB-sensitive or ICB-resistant cohorts and processed separately. Cells were labelled with magnetic microbead-conjugated anti-CD11b antibodies. Labelled single cell suspensions were passed through a magnetic activated cell sorting (MACS) column to sort the positive fraction containing CD11b+ myeloid cells. The negative fraction, containing non-myeloid cells such as fibroblasts, was additionally collected. CD11b+ myeloid cell and CD11b- cell suspensions from the ICB-sensitive and ICB-resistant cohorts were lysed in Trizol and RNA isolated. CD11b+ ICB-sensitive, CD11b+ ICB-resistant, CD11b- ICB-sensitive, and CD11b- ICB-resistant RNA was submitted to the AGC for bulk RNA-seq. We are

awaiting the results of this study. Following the pathway analyses that showed that T-cell and myeloid cell pathways at the immunologic niche were differentially regulated between ICB-sensitivity and ICB-resistance cohorts after Tx, we asked how leukocyte populations were changing more broadly at the immunologic niche, PT, and spleen.

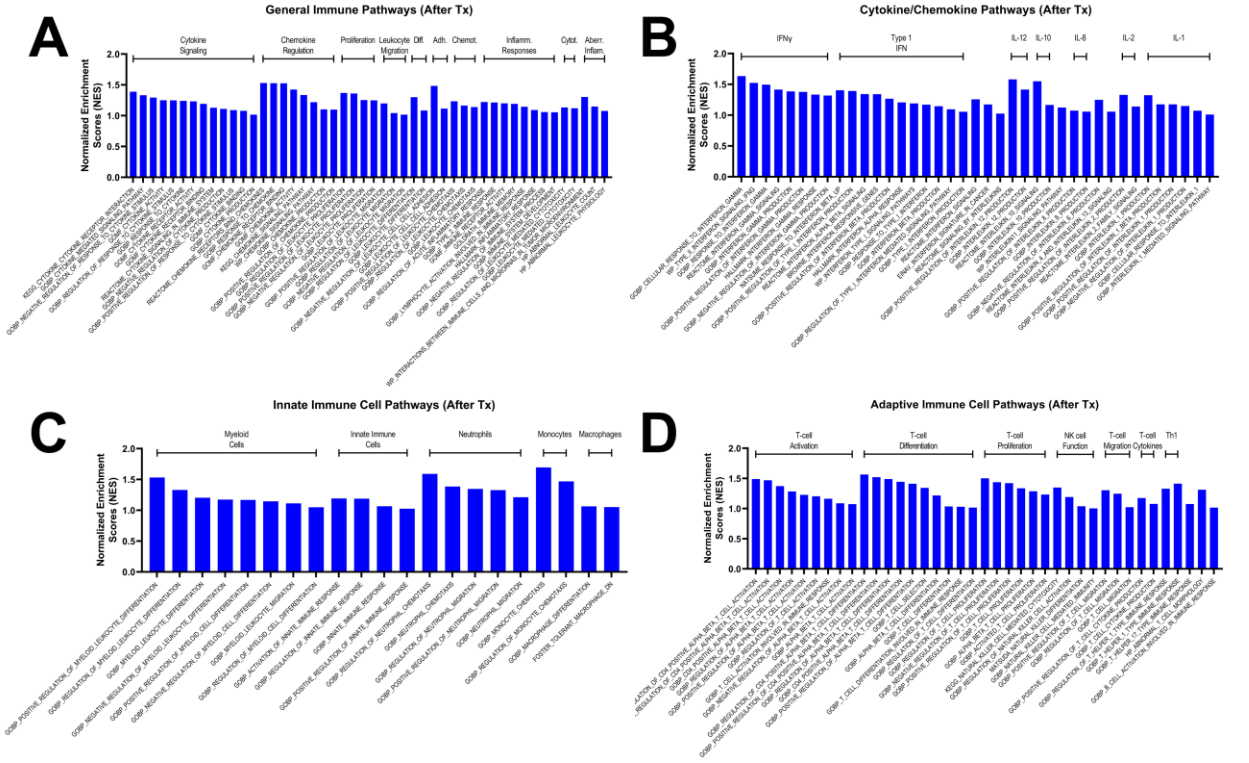

Figure 4-3. Lymphocyte and myeloid cell pathways differentially regulated between ICB-sensitive and ICB-resistant mice at IN implant. Pathways associated with (A) general immune, (B) cytokine/chemokine, (C) myeloid cell (innate immune cell), and (D) lymphocyte (adaptive immune cell) responses. Normalized enrichment scores (NES) represent pathways upregulated in ICB-sensitivity, cutoff of NES > 1 utilized for GSEA analysis.

4.2.5 Ratios of leukocyte populations skewed at immunologic niche as result of therapy response

The impact of ICB on systemic immune responses, comparing immune populations at the immunologic niche, PT, and spleen, was next investigated. The PT is regularly biopsied in the clinic and the spleen functions as a surrogate for the blood. Mice with implants were orthotopically

inoculated and received aPD-1. Tissues were isolated from mice after Tx (D21) and processed into single cell suspensions. Cells were labelled with fluorophore-conjugated antibodies and analyzed with flow cytometry. No significant difference was observed between the proportion of monocytes (CD11b+ Ly6C+), neutrophils (CD11b+ Ly6G+), and macrophages (CD11b+ F4/80+) at the PTs of ICB-sensitive and resistant mice (**Figure 4-4B**). While some trends were observed, there was no significant difference between the proportions of monocytes, neutrophils, and macrophages at the immunologic niche (IN Implant) of these mice (**Figure 4-4B**). Notably, the PT of ICB-sensitive mice had significantly increased infiltration of cytotoxic T lymphocytes (CD8+) versus the ICB-resistant PTs (**Figure 4-4C**). This observation at the PT is in line with the goal of a T-cell-targeted immunomodulatory therapy. Reduced proportions of both B-cells (CD19+) and NK-cells (CD49b+) were found at the immunologic niche of ICB-sensitive mice (**Figure 4-4C**). Interestingly, the immunologic niche had enriched populations of both myeloid cells (neutrophils, monocytes, macrophages) and lymphocytes (T-cells, B-cells, NK-cells), in comparison to the PT (**Figures 4-4B - 4-4C**). In the context of immuno-oncology, many have found meaningful immunological insight by investigating the ratios of myeloid cells to lymphocytes [211]. As such, the ratios of infiltrated myeloid cells to lymphocytes were calculated (**Figure 4-4D**). Excitingly, the ratio of macrophages to NK-cells, neutrophils to NK-cells, neutrophils to B-cells, and neutrophils to T-cells were significantly increased at the immunologic niche of ICB-sensitive mice versus ICB-resistant mice (**Figure 4-4D**). Differences in the myeloid cell to lymphocyte ratio, between the ICB-sensitive and ICB-resistant cohorts, was not observed at the PT and spleen. Following the observation that the engineered implants capture unique immune cell dynamics after Tx, and that implant-derived genes can be monitored for ICB-response, we asked if the immunologic niche could be probed before Tx for predictive gene expressions.

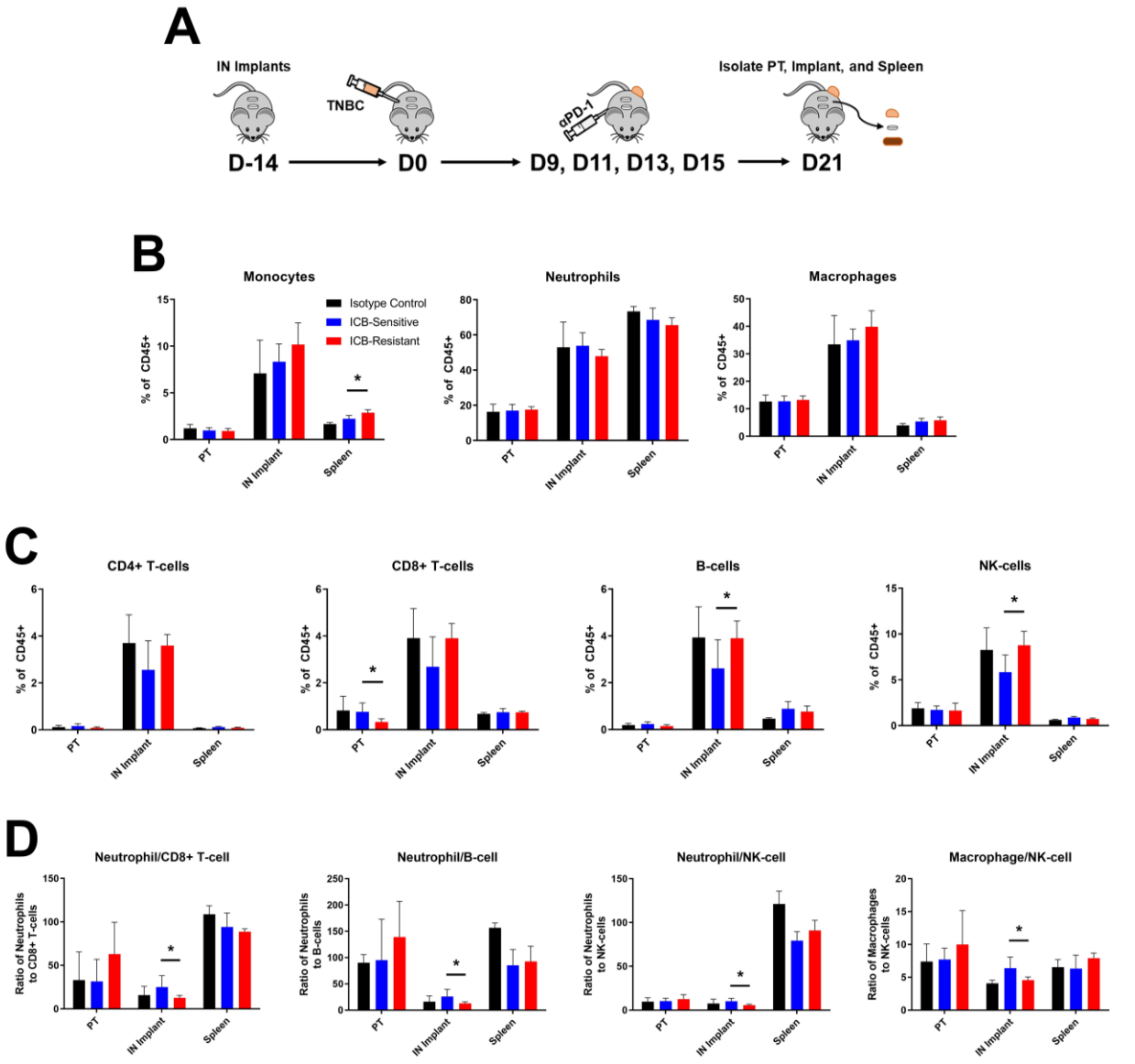

Figure 4-4. IN Implant captures divergent lymphocyte and myeloid cell responses as result of ICB-sensitivity versus resistance. (A) Schematic of implanting mice with IN, inoculating with 4T1, administering anti-PD-1, and isolating PT, IN implant, and spleen for analysis with flow cytometry. Flow cytometry analysis of tissues isolated on D21 post-tumor inoculation with fluorophores labelling (B) myeloid cells and (C) lymphocytes. Cell proportions quantified as % of CD45+. (D) Ratio of myeloid cells-to-lymphoctes. Two-tailed unpaired t-tests assuming unequal variance were performed for single comparisons between two conditions. * $p < 0.05$.

4.2.6 Gene expressions predictive of ICB-response

The delta analysis showed that dynamic gene expression changes can be monitored at the implant for ICB-response (**Figure 4-2**). Interestingly, the PCA-based clustering of the DEseq2-

normalized counts from the delta panel showed mildly separate clustering between ICB-sensitive and resistant before Tx (**Figure 4-2B**). As such, we wanted to test the hypothesis that a unique set of predictive genes could be identified before initiating Tx (D7). The DEseq2-normalized counts before Tx (D7) were first screened with T-tests between the gene expression of ICB-sensitive and resistant, identifying 331 DEGs (**Figure 4-5A**). PCA of these before Tx DEGs showed differential clustering of sensitive and resistant cohorts (**Figure 4-5A**). EN was them employed to identify a 16-gene panel of DEGs before Tx. Clustering of the implant-derived gene expressions from the before Tx-panel showed superb categorization of ICB-sensitivity and resistance prior to administering ICB (**Figure 4-5C**). Notably, 12/16 genes were upregulated in the mice, before Tx, that would become sensitive to ICB and hierarchical clustering categorized the cohorts based on predicted ICB-response (**Figure 4-5B**). Performance metrics were calculated for sensitivity, specificity, and categorization efficacy (**Figure 4-S5D**). Interestingly, the categorization metrics indicated that the before Tx gene signature more effectively predicted ICB-response than the delta gene signature for monitoring ICB-response (**Figure 4-S4C**). Based on the exciting observations that a multivariate panel of genes was predictive of ICB-response prior to Tx, we investigated differentially regulated pathways underlying these differences.

GSEA was performed on the implant-derived gene expressions before Tx. Differentially regulated pathways were examined for 4880 identified gene sets. An NES > 1 cutoff was used to identify the 2671 most differentially regulated pathways. Immune system-associated pathways were then subcategorized, excluding irrelevant inflammatory pathways. The 207 differentially regulated immune pathways were broadly categorized into general immune, cytokine/chemokine, myeloid cell, and lymphocyte pathways (**Figures 4-5D - 4-5G**). The 81 general immune system pathways differentially regulated between ICB-sensitivity and resistance included pathways

associated with inflammatory responses, cytokine signaling, aberrant inflammation, migration, chemokine regulation, chemotaxis, proliferation, leukocyte transendothelial (T.E) migration, leukocyte cell-cell adhesion, leukocyte degranulation, leukocyte differentiation, immune receptor signaling, leukocyte cytotoxicity, and leukocyte homeostasis (**Figure 4-5D**). The 23 most differentially regulated cytokine/chemokine pathways included those associated with Type 1 IFN (IFNα, IFNβ), IFNγ, and TNF signaling (**Figure 4-5E**). The 47 myeloid cell-associated pathways included those of neutrophils, macrophages, innate immune cell responses, mast cells, and monocytes (**Figure 4-5F**). Interestingly, pathways including myeloid cell homeostasis, myeloid cell differentiation, and neutrophil-mediated immunity were upregulated, whereas macrophage tolerance and macrophage M1 vs M2 pathways were downregulated at the implant before Tx (**Figure 4-5F**). Finally, the most differentially regulated lymphocyte pathways between ICB-sensitive and ICB-resistant before Tx were pathways associated with T-cell differentiation, T-cell activation, T-cell proliferation, B-cell activation, T-cell migration, NK cell function, T-cell cytokine production, aberrant T-cell function, T-cell receptor signaling, Th1 response, Th17 response, and adaptive immune cell responses (**Figure 4-5G**). Some of these pathways upregulated at the immunologic niche of ICB-sensitive mice before Tx included modulators of T-cell receptor signaling (TCR) and the somatic diversification of immunoglobulins involved in immune responses (**Figure 4-5G**). Collectively, these studies point to the clinical utility of the immunologic niche for 1) predicting ICB-response prior to initiating therapy, 2) monitoring ICB-sensitivity during therapy, and 3) illuminating the role of differentially regulated immune cell pathways responsible for divergent ICB-responses.

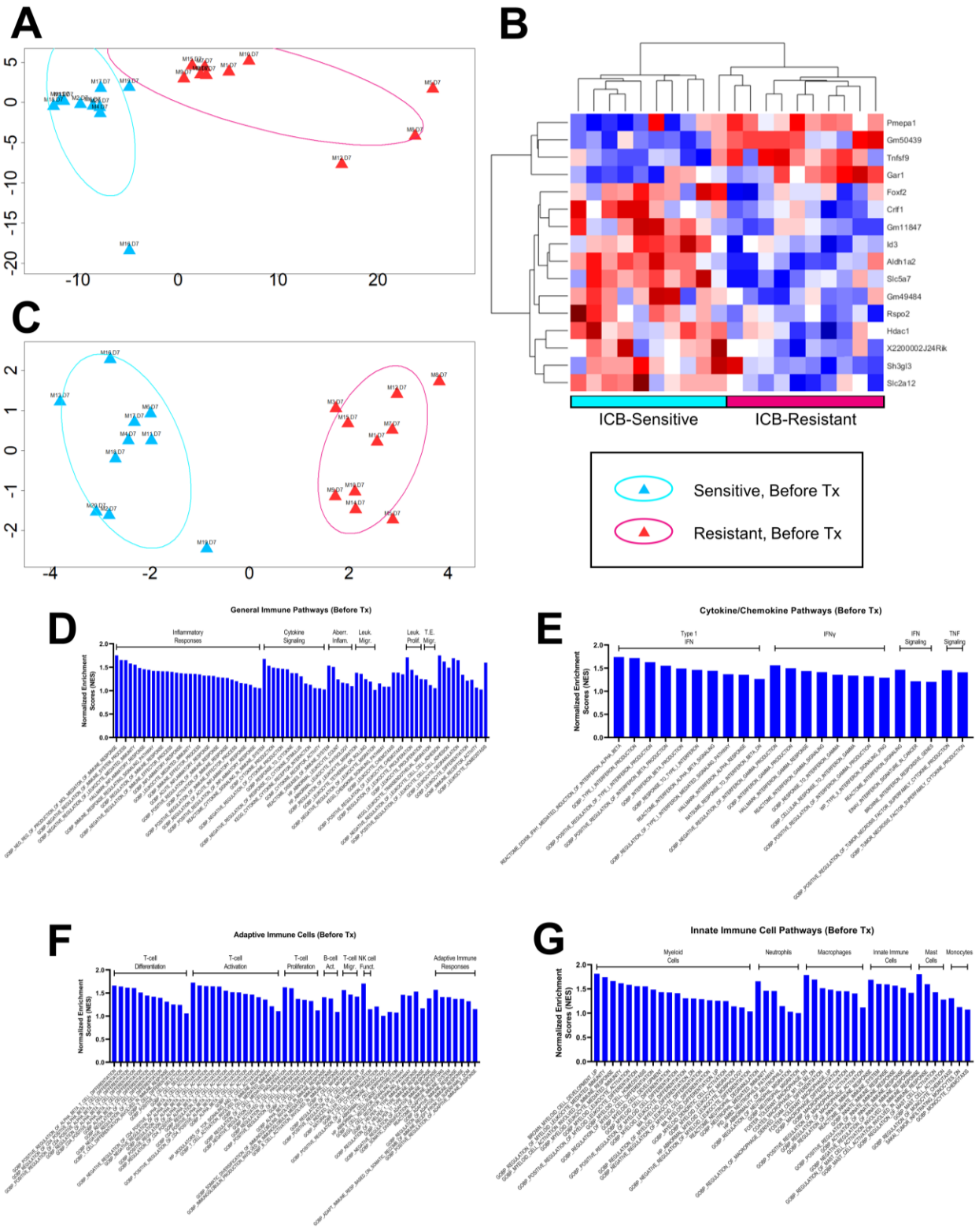

Figure 4-5. Analysis of IN-derived analytes before administering therapy identifies predictive signature for ICB-response. (A) PCA-based clustering of DEseq2-normalized gene expressions. Clustering represents panel of 331 differentially expressed genes. (B) Heat map of EN-identified predictive signature of 16 genes. (C) Clustering of mice before administering therapy based on 16-gene predictive signature. GSEA analysis of gene expressions before

therapy for (D) general immune, (E) cytokine/chemokine, (F) myeloid cell (innate immune cell), and (G) lymphocyte (adaptive immune cell) pathways. Cutoff of NES > 1 used for GSEA analysis.

4.3 Discussion

In this study, the immunologic niche was investigated as a diagnostic for ICB-response. Checkpoint inhibitors have been approved for both metastatic and early TNBC, and while profound responses have been elicited in ICB-sensitive patients, many are resistant to ICB. The clinical utility of ICB in TNBC has been greatly limited by an inability to 1) identify patients with a high likelihood of ICB-sensitivity prior to initiating therapy and 2) monitor ICB-response during therapy. Much of this is due to the inherent limitations of a PT biopsy, which represents a restricted snapshot of biomarkers confined to the local microenvironment. Groups have investigated liquid biopsy-derived biomarkers to address this challenge. While liquid biopsies have shown some clinical utility in monitoring CTC burden and identifying chemotherapy options, they have shown insufficient success in identifying immunotherapy-associated biomarkers [98–103]. This may be in part, because of the differences in the phenotype and function of immune cells between those in the blood and those that have extravasated into a tissue [92]. The immunologic niche provides a unique opportunity to study immune cells that have extravasated systemic vasculature to a site that can be longitudinally probed.

We demonstrated that immunologic niche-derived gene expressions could be probed to monitor ICB-response. Biomarker expression at a PT is often discordant with biomarker expression at metastatic foci, which provides significant complications when making clinical decisions from PT-derived biomarkers, especially when treatments for metastatic BC are informed by a PT biopsy that may have been collected many years prior [212]. In BC, metastatic foci are typically localized to the lungs, liver, bone marrow, or brain. As a result of the anatomical

constraints of these tissues, radiographic imaging is the gold standard for monitoring therapy response in treating metastatic disease. For the majority of chemo- and radiotherapies, change in metastatic lesion size is indicative of therapy response, where an increase or decrease in the size of a lesion indicates therapy resistance or sensitivity. Pseudoprogression and hyperprogression following ICB are unique phenomena that confound the ability to correlate lesion size with immunotherapy response [213]. Pseudoprogression is characterized by the radiographic appearance of lesion growth, as a result of immune cell infiltration in ICB-sensitive patients. This initial growth is subsequently followed by tumor regression as a result of an anti-tumor immune response [213]. The inability to delineate between true progression of disease, as a result of ICB-resistance, and pseudoprogression among ICB-sensitive patients highlights the clinical need for a technology to profile the immune response to ICB. Additionally, a small proportion of patients experience hyperprogression, or a rapid progression of disease following the initiation of ICB [213]. Radiographic imaging alone cannot differentiate pseudoprogression from hyperprogression when lesion enlargement is observed. In this report, a multivariate gene signature was identified for monitoring ICB-response at the immunologic niche implant. Engineered niche-derived biomarkers were analyzed by normalizing gene expressions during or after therapy to gene expressions before the initiation of ICB. The immunologic niche was shown to provide insight into dynamic immune system responses to ICB, and implant-derived gene expressions were monitored to glean ICB-response both during and after ICB. A technology like this has the potential to augment radiographic imaging for monitoring ICB-response.

An implant-derived gene signature was also identified for predicting ICB-response prior to therapy. The standard of care for predicting ICB-response has been limited to PD-L1 expression, leukocyte infiltration, and tumor mutational burden [82]. Clinical trials have found improved

response rates among BC patients with high TMB and TNBC patients with PD-L1+ tumors, however this is not predictive of ICB-response and has performed poorly at identifying ICB-sensitive patients. Selecting TNBC patients with PD-L1+ tumor infiltrating lymphocytes has binned specific subpopulations that have the best ICB-response, but even the majority of this subpopulation is ICB-resistant [79]. The FDA has recently approved ICB in early TNBC, administered in the neoadjuvant/adjuvant setting to augment surgical resection of the PT. In this setting, neoadjuvant ICB is delivered prior to resection with the goal of reducing PT volume and then adjuvant ICB is administered following resection to mitigate recurrence [81]. Not all patients require adjuvant ICB, and as of yet, there is no way to stratify the patients that would benefit from ICB following surgical resection. Taking the adverse side effects associated with ICB and cost to the medical system into account, there is a great clinical need for identifying which patients would benefit from ICB. Analysis of implant-derived gene expressions prior to ICB identified multivariate analytes predictive of ICB-response before initiating therapy.

Flow cytometry and gene pathway analyses of the engineered niche revealed the contribution of myeloid cell dysfunction in ICB-resistance. The phase 2 TONIC trial of nivolumab (aPD-1) in mTNBC patients investigated induction strategies for modulating the tumor microenvironment prior to ICB [214]. Interestingly, this study found the highest ORR among the doxorubicin (35%) and cisplatin (23%) induction cohorts, and also detected an upregulation of genes associated with PD-1/PD-L1, Th1 cell, myeloid cell, T-cell cytotoxicity, and IFNg pathways, as a result of pre-ICB induction. In pre-clinical studies, doxorubicin and cisplatin have both been shown to be immunomodulatory, in part through their targeting of suppressive myeloid cells [215,216]. Probing the gene expression at the immunologic niche identified differentially regulated myeloid cell pathways, suggesting that myeloid cells may contribute to ICB-resistance.

Additionally, the flow cytometry characterization of cells at the implant showed significantly different ratios of myeloid cells to lymphocytes between ICB-sensitive and ICB-resistant mice. Together with the findings from the TONIC trial, these studies illuminate the potential role of suppressive myeloid cells in ICB-resistance, as well as the efficacy of improving ICB-sensitivity by alleviating this suppression. The immunologic niche could serve as a diagnostic for monitoring suppressive mechanisms underlying ICB-resistance and to motivate the use of induction strategies to skew ICB-resistance to ICB-sensitivity. The landmark first-in-human clinical trial, QUILT-3.067, is an ongoing study with the goal of evaluating the safety and efficacy of combining multimodal induction therapies with ICB to improve ICB-sensitivity by targeting multiple arms of the immune system [217]. This unique trial combines chemoradiation, IL-15 cytokine administration, tumor-associated antigen vaccine, high-affinity NK cell therapy, and avelumab in patients with refractory, metastatic, or unresectable TNBC tumors. Initial results from the small cohort of patients (n=9) suggests greatly improved overall response, disease control response, and complete response rates, as compared to ICB monotherapy. This trial points to the mounting evidence that myeloid and NK-cells, among other immune cells, play a role in suppressing anti-tumor immune cell responses. Interestingly, in this report we found that pathways for myeloid and NK-cell function were differentially regulated between the ICB-sensitive and resistant cohorts. Both the phase 2 induction and QUILT-3.067 trials highlight the value for a diagnostic that could provide insight into targetable immunosuppressive mechanisms underlying ICB-resistance.

The immunologic niche implant collects enriched populations of monocytes, macrophages, T-cells, B-cells, and NK-cells versus both the PT and spleen, which functions as a surrogate for the blood. Isolating key immune cells, due to their low numbers in the blood, has been an immense technological challenge for the clinical utility of liquid biopsies as a cancer immunotherapy

diagnostic [92]. Our lab has previously shown that biopsies of the immunologic niche can be utilized for enriching cells that can be probed for analytes indicative of systemic immune dysregulation [207,208]. The gene expression from these cells can be studied to glean insight into differentially regulated pathways, which may provide additional insight into ICB-resistance-associated mechanisms. This is especially exciting, given that combination therapies have been shown to increase ICB response rates [43]. Insight into dysregulated immune pathways underlying ICB-resistance could motivate selecting chemo-, immuno-, or radiation therapies to skew ICB-resistant patients as an induction strategy prior to ICB.

In conclusion, we report that the immunologic niche implant can be probed to investigate divergent responses to checkpoint blockade. Engineered niche-derived gene expressions were computationally identified for monitoring ICB-response during and after therapy. Probing the implant identified divergent immune cell pathways and significantly different myeloid cell-to-lymphocyte ratios between ICB-sensitivity and resistance, implicating the contribution of aberrant myeloid cell function in ICB-resistance. Finally, an immunologic niche-derived gene signature was identified that is predictive of ICB-response prior to the initiation of therapy. The ability to longitudinally biopsy an accessible site for ICB-response-associated biomarkers in real time, as well as to investigate mechanisms underlying ICB-resistance, could dramatically innovate how clinicians utilize ICB for cancer management.

4.4 Methods

4.4.1 Microporous PCL scaffold fabrication and subcutaneous implantation

To fabricate microporous implants, polycaprolactone (PCL) was mixed with a salt porogen (NaCl, 250-425 um), pressed into molds (5mm wide, 2mm thick), the polymer sintered at 135C, and porogen-leached as previously described [207,208]. PCL implants were disinfected and stored

at -80C until surgery. Immunologic niches were implanted in the dorsal subcutaneous space of 8-week old female Balb/c mice (Jackson Laboratories). All procedures were performed in accordance with the institutional guidelines and protocols approved by the University of Michigan Institutional Animal Care and Use Committee. Mice were anesthetized with isofluorane prior to subcutaneous implantation with PCL implants. Mice received subcutaneous injections of carprofen (5 mg/kg) immediately before surgery and 24 hours after surgery.

4.4.2 Tumor cell culture and orthotropic inoculations

Orthotopic inoculation of tumor cells was performed 2 weeks after immunologic niche implantation. 4T1-luc2-tdTomato murine triple negative breast cancer cells (PerkinElmer) were cultured in RPMI 1640 Medium (Thermo Fisher Scientific) containing 10% fetal bovine serum (FBS, INFO) for 5 days (37C, 5% CO2, #% O2) prior to inoculation. Tumor cells were enzymatically lifted from the tissue culture flask with trypsin (INFO probably Sigma) for 10 minutes at 37C and resuspended in culture medium. Cells were centrifuged at 500xg for 5 minutes and resuspended in Dulbecco′s phosphate buffered saline (DPBS) at a concentration of 40E6 cells/mL. The tumor cell line was previously confirmed to be pathogen free and authenticated by short tandem repeat DNA analysis and compared to the ATCC STR profile database (DDC Medical). Orthotopic inoculations were performed by injecting 50 uL of the cell suspension, containing 2E6 4T1 tumor cells, to the fourth right mammary fat pad of 12-week-old female Balb/c mice (Jackson Laboratory, 000651).

4.4.3 Anti-PD-1 administration

InVivoMab anti-mouse anti-PD-1 (CD279) antibody (BE0146, clone RMP1-14, BioXCell) and isotype control (BE0089, InVivoMAb rat IgG2a isotype control, BioXCell) were diluted in

DPBS to a final concentration of 1 mg/mL immediately prior to intraperitoneal (IP) injections. A volume of 100 uL of diluted aPD-1 and isotype control were administered (10 mg/kg) IP on days 9, 11, 13, and 15 post tumor-inoculation.

4.4.4 Tumor volume measurements and survival monitoring

Tumor size was recorded using standard electronic calipers (VWR) while mice were anesthetized with 2% v/v% isoflurane. Primary tumor volume was calculated (V = 0.5 x L x W2, L: length of longest dimension of the tumor, W: length perpendicular to the longest tumor dimension) as previously describe [68]. Mice were monitored for tumor size and body conditioning to determine survival. Mice were euthanized if any of the following criteria were met: tumor size of > 2cm in any dimension, ulceration of more than 50% of the visible tumor area, partial paralysis due to tumor invasion of hind limb muscle, labored breathing, ascites, lethargy, or visible weight loss.

4.4.5 Tissue isolations

Niche implants were surgically explanted at days 7, 14, and 21 (D7, D14, D21) post-tumor inoculation to study gene expression changes associated with ICB-response. Mice were anesthetized with isoflurane before an incision was made over the surface of the implant. The niche implant and any adherent encapsulating tissue were pulled through the incision and excised, and the incision closed with sutures. Immunologic niche tissues for RNA analyses were flash frozen in isopentane on dry ice and stored at -80C. For the flow cytometry analysis, mice were euthanized at study endpoint (D21) and the primary tumor, spleen, and implant isolated. Tissues were placed into PBS and stored on ice.

4.4.6 RNA isolation, purity, integrity, and bulk RNA-seq

Explanted immunologic niche tissues were immediately flash frozen in isopentane. Frozen implants were homogenized in Trizol and RNA subsequently isolated from homogenate using the Direct-zol™ RNA Kit (Zymo Research) with DNase 1 treatment. The isolated RNA was diluted to the desired concentration and submitted to the University of Michigan Advanced Genomics Core for analysis with total RNA (ribo-depletion) library preparation and bulk RNA-seq performed on the Illumina NovaSeq™ S4 at PE150 (45-60 million reads/sample). Raw counts, as prepared from demultiplexed fastq files by the Advanced Genomics Core, were converted to normalized counts using DEseq2 [209].

4.4.7 Analysis of gene expression differentially regulated pathways

Normalized RNA-seq counts were screened to identify differentially expressed genes of interest associated with response to ICB. T-tests were first performed to compare ICB-sensitive and ICB-resistant for each gene. This initial analysis identified the 100's of genes differentially expressed between sensitive and resistant. These screened genes were then probed with elastic net-based coefficient reduction, favoring group selection ($\alpha = 0.05$), with 2000 iterations of leave-one-out cross validation. Multivariate gene signatures were visualized with principal component analysis for dimensionality reduction. For pathway analysis, mouse gene symbols for RNA-seq counts were converted to human gene symbols using the biomaRt package. All computation was performed using R except for the EN-based analysis, which was performed in MATLAB. Gene Set Enrichment Analysis (GSEA) was performed on DESeq2-normalized counts and the corresponding human gene symbols. Normalized enrichment score (NES) values are visualized for the analysis of ICB-sensitive versus ICB-resistant.

4.4.8 Flow cytometry

The primary tumor, spleen, and immunologic niche tissue were mechanically and enzymatically digested as detailed previously detailed [68,207,208]. Tissues were processed through a 70 um cell strainer (Corning) to filter. Single cell suspensions of were then prepared by erythrocyte lysis in ACK buffer (Fisher, #A1049201) and washed in DPBS (2 mM EDTA, 0.5% bovine serum albumin) by centrifuging at 500xg for 5 minutes. Cells were equally split into two tubes to enable staining and analysis of innate immune cells and lymphocytes from the same tissues. Each tube was treated with anti-CD16/32 (Biolegend) to block nonspecific staining. The innate immune cell panel was stained with AF700 anti-CD45, BV510 anti-CD11b, PEcy7 anti-F4/80, PacBlue anti-Ly6G, and FITC anti-Ly6C (Biolegend) antibodies. The lymphocyte panel was stained with AF700 anti-CD45, FITC anti-CD8, V500 anti-CD4, PacBlue anti-CD19, and PECy7 anti-CD49b (Biolegend) antibodies. All samples were stained with DAPI for viability and analyzed on the BioRad flow cytometer Cytoflex Cell Analyzer. Data analysis was performed using FlowJo (BD).

4.4.9 Magnetic activated cell sorting of cell populations

Single cell suspensions were prepared from explanted immunologic niche tissues and labeled with magnetic microparticle-conjugated antibodies against CD11b (Miltenyi Biotec). Labelled cells were magnetically sorted. The positive fraction, containing enriched CD11b+ myeloid cells, and the negative fraction, representing non-myeloid cells, were washed by centrifugation at 500xg for 5 minutes. Pelleted cell populations were resuspended in Trizol and stored at -80C until RNA isolations performed.

4.4.10 Statistical Analysis

Two-tailed unpaired t-tests assuming unequal variance were performed for single comparisons between two conditions, namely ICB-sensitive and ICB-resistance. Median survival and survival curves were analyzed using a simple survival analysis (Kaplan-Meier) with log-rank (Mantel-Cox test) for statistical significance. Following the normalization of RNA-seq gene expressions with DESeq2 (citation), T-tests were performed for single gene comparisons ($p < 0.05$). Differentially expressed genes identified from the T-tests were then parsed with elastic net-based feature identification. For the GSEA analyses, pathways with $|NES| > 1$ were considered as being differentially regulated. Prism 9 (GraphPad), Excel (Microsoft), and R were used for performing statistical analyses, with $p < 0.05$ considered to be statistically significant. Error bars on plotted data are calculated as standard error mean (SEM).

4.5 Supplementary Figures

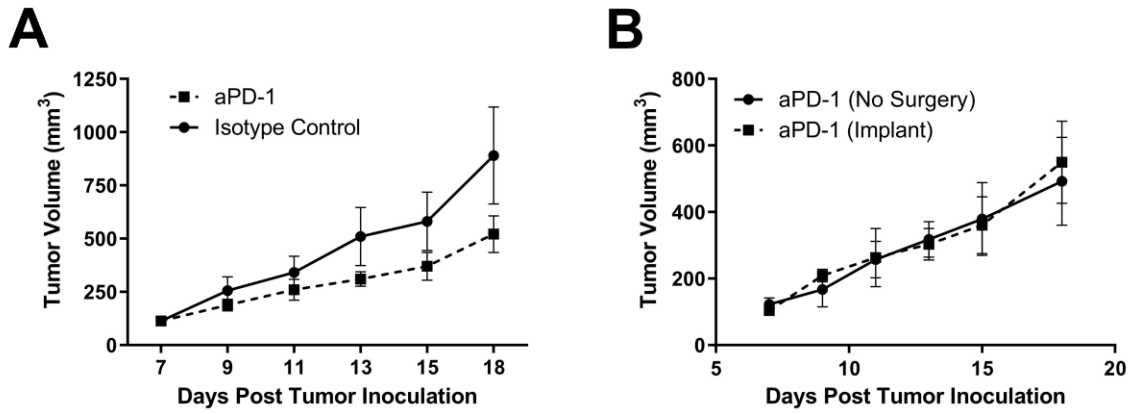

Figure 4-S1. (A) Longitudinal primary tumor volumes of all mice receiving anti-PD-1 versus isotype control. (B) Longitudinal primary tumor volumes of mice administered anti-PD-1 that either did or did not receive surgical implantation of IN. Bars show mean ± SEM.

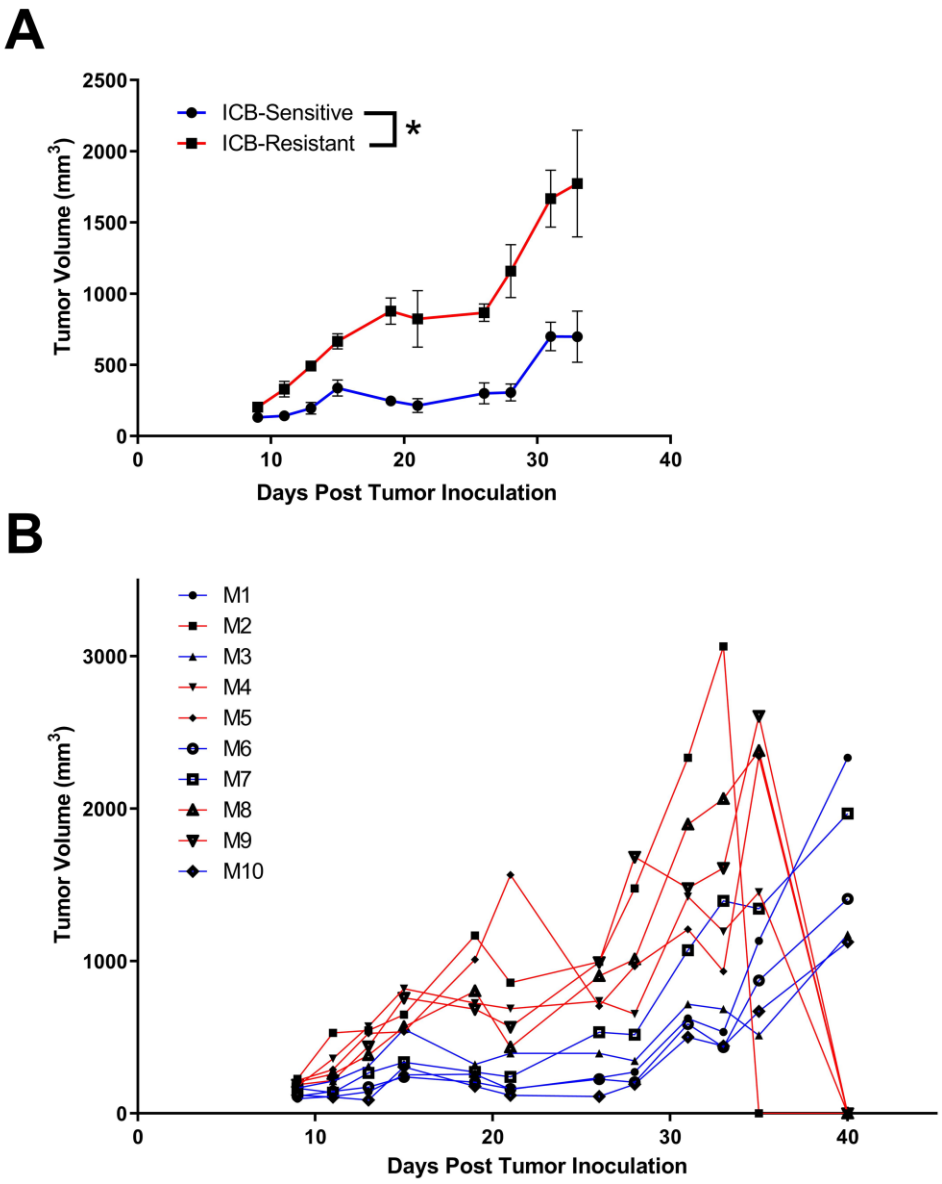

Figure 4-S2. (A) Longitudinal primary tumor volumes of ICB-sensitive and ICB-resistant cohorts in bulk RNA-seq study. (B) Longitudinal PT volumes by individual mouse from both cohorts. Bars show mean ± SEM. Two-tailed unpaired t-tests assuming unequal variance were performed for single comparisons between two conditions. * $p < 0.05$.

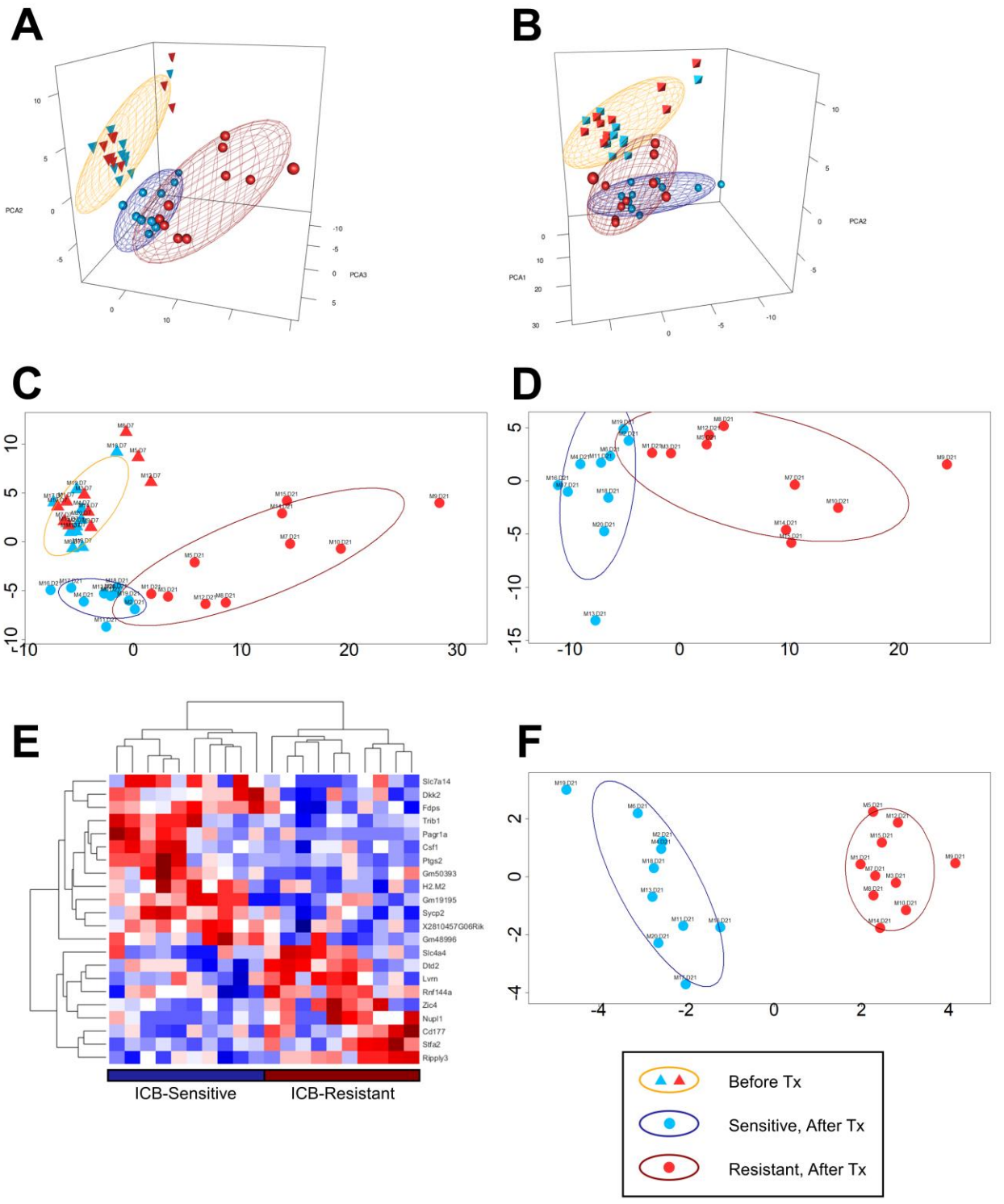

Figure 4-S3. Analysis of IN-derived gene expression after therapy. (A,B) 3D clustering of differentially expressed genes after therapy. (A) Front face – PCA 1 vs PCA2. (B) Front face – PCA 3 vs PCA2. (C,D) 2D clustering of differentially expressed genes after therapy. (C) PCA performed on all samples, whereas (D) PCA performed on just samples after therapy. Clustering (A-D) represents panel of 237 differentially expressed genes. (E) Heat map of EN-identified gene signature of 22 genes. (F) Clustering of 22-gene signature.

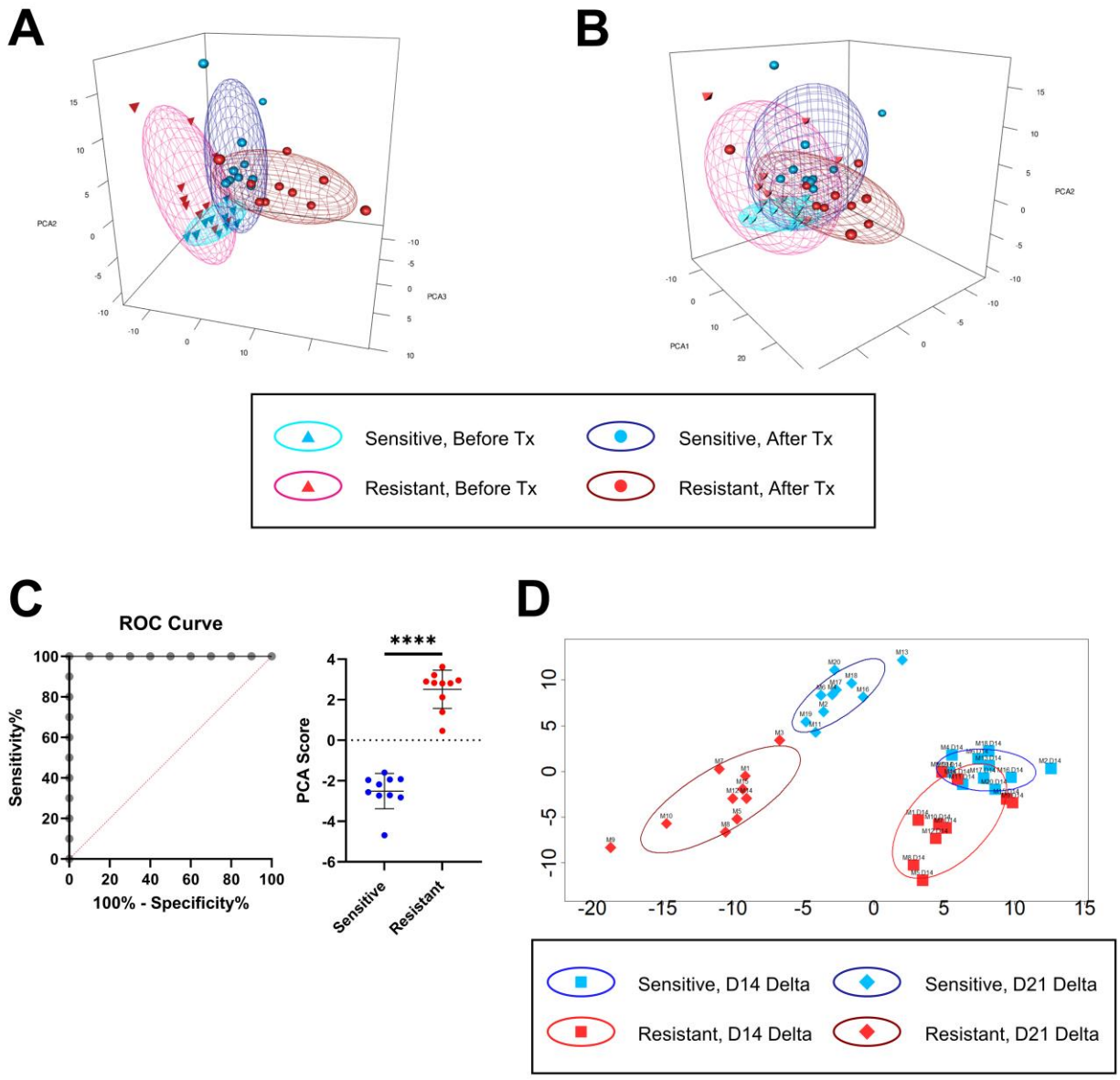

Figure 4-S4. Analysis of IN-derived gene expression with delta normalization. (A,B) 3D clustering of differentially expressed genes identified with T-tests performed on delta-normalized counts. (A) Front face – PCA 1 vs PCA2. (B) Front face – PCA 3 vs PCA2. (A,B) Clustering performed on DEseq2-normalized counts. (C) Categorization metrics for EN-identified 16-gene signature. Sensitivity, specificity, and categorization efficiency calculated with delta-normalized counts. (D) Clustering of delta-normalized counts during (D14) and after (D21) therapy. Delta normalization – gene expressions at D21 or D14 are normalized to gene expressions at D7.

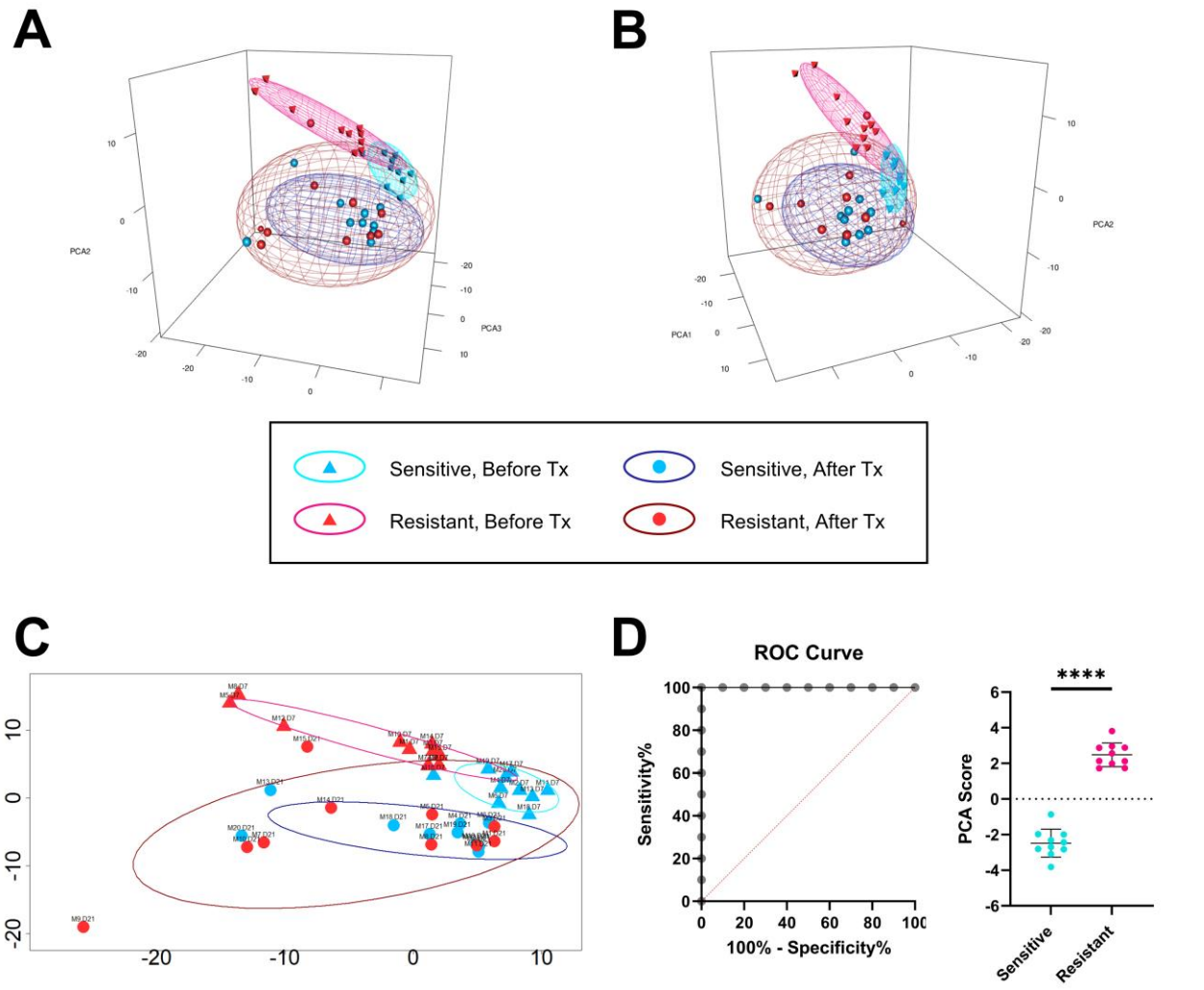

Figure 4-S5. Analysis of IN-derived gene expression before therapy. (A,B) 3D clustering of differentially expressed genes after therapy. (A) Front face – PCA 1 vs PCA2. (B) Front face – PCA 3 vs PCA2.(C) 2D clustering of differentially expressed genes before therapy. Clustering performed on DEseq2-normalized counts for 331 differentially expressed genes. (D) Categorization metrics (sensitivity, specificity, and categorization efficiency) calculated for EN-identified predictive signature of 16 genes.

Chapter 5
Conclusions and Future Directions

5.1 Summary of Findings

Taken together, the work presented in this dissertation describes the utility of engineered materials as 1) an immunomodulatory therapy for the treatment of advanced triple negative breast cancer and 2) a diagnostic for divergent responses to immune checkpoint blockade therapy. Cargo-free polymer-based nanoparticles were administered intravenously and significantly slowed primary tumor growth. We demonstrated that nanoparticles were internalized by innate immune cells and reprogrammed inflammatory responses among myeloid cells, modulating the tumor microenvironment. Excitingly, these nanoparticles were found to synergize with aPD-1, enhancing the efficacy of checkpoint blockade. We then investigated the efficacy of nanoparticles in treating metastatic disease. Nanoparticle administration reduced circulating tumor cells in the systemic vasculature and notably reduced metastatic colonization of the lungs. The immune milieu of the lungs was remodeled, such that intravenous administration of nanoparticles led to an increase in inflammatory, anti-tumor innate immune cells. Nanoparticles were delivered in the neoadjuvant and adjuvant context, in a resection model, and excitingly adjuvant nanoparticle administration led to the clearance of established pulmonary metastases. Therapeutic efficacy was completely abrogated in a T-cell deficient model, implicating the vital role of T-cells in the nanoparticle-mediated clearance of metastatic lesions at the lungs. Finally, an engineered immunologic niche was investigated as a diagnostic for monitoring response to checkpoint blockade therapy. In a model of divergent ICB-response, mice that were sensitive to therapy had reduced primary tumor

growth and enhanced survival. Gene expressions from the polymer implant were identified that showed efficacy for monitoring ICB-sensitivity and ICB-resistance, both during and after therapy. Among ICB-sensitive mice, anti-tumor innate and adaptive immune cell pathways were upregulated at the immunologic niche. Interestingly, the implant was able to capture significant differences in the ratios of myeloid cells to lymphocytes between ICB-sensitive and ICB-resistant cohorts. Immunologic niche-derived gene expressions were probed before therapy and excitingly, a predictive multivariate signature was identified for ICB-response prior to initiating ICB. The research in this dissertation continues the research efforts of others in the field and advances the translatable potential for innovative technologies to 1) treat metastatic disease by modulating inflammatory responses, 2) predict immunotherapy response prior to treatment, and 3) monitor immunotherapy response in real time.

5.2 Future Directions

The following section presents future studies that would enhance the significance and impact of the findings discussed in this dissertation.

5.2.1 Analysis of nanoparticle-mediated effects on myeloid cell trafficking and phenotype

The aim of **Chapter 2** and **Chapter 3** was to investigate the immunomodulatory properties of cargo-free PLG nanoparticles in a murine model of triple negative breast cancer. We previously demonstrated efficacy of naked nanoparticles in traumatic injury and autoimmune disease [66,67]. Nanoparticle administration was shown to mitigate pathological inflammation in these models through modulating myeloid cells. Due to the role of myeloid cells in the initiation and progression of metastatic disease, we wanted to investigate the efficacy of targeting myeloid cells with nanoparticles in a murine model of metastatic TNBC. Through *in vitro* and *in vivo* analyses, we

found that myeloid cell phenotype is altered at the blood, spleen, primary tumor, and lungs. We additionally showed that cargo-free nanoparticles are taken up by myeloid cells both in an *in vitro* assay, as well as *in vivo* with fluorescently-labelled nanoparticles. However, in the context of treating metastatic disease, it nuanced to delineate whether the clearance of pulmonary metastases is a result of 1) the uptake of nanoparticles by myeloid cells followed by a subsequent change in their phenotype prior to their trafficking to the tumor microenvironment or 2) a redirecting of their trafficking away from the tumor microenvironment following uptake. In other words, is the functional outcome of nanoparticle administration to treat metastatic disease due to 1) a change in the phenotype of nanoparticle positive cells that traffic to the metastatic niche or 2) altered trafficking of leukocyte subpopulations away from metastases toward the spleen and liver? We see that nanoparticle administration remodels the lung microenvironment, skewing myeloid cells toward inflammatory, anti-tumor phenotypes. However, it is not necessarily clear whether this is a result of modulating the phenotype of nanoparticle positive myeloid cells or trafficking myeloid cell subpopulations away from the lungs. One way to test the hypothesis that nanoparticle uptake by myeloid cells changes their phenotype toward an inflammatory, anti-tumor phenotype would be to administer fluorescently labelled particles and use flow cytometry-based cell sorting to sort nanoparticle positive myeloid cells versus nanoparticle negative ones at the primary tumor, spleen, liver, and lungs. The RNA could then be isolated from these populations and studied with RT-qPCR for the expression of genes such as Stfa2, Stfa3, Stat1, S100a8, Cxcl2, and Ccr2, motivated by the differential gene expressions found in the scRNA-seq study performed in **Chapter 3**, to investigate if the anti-tumor myeloid populations resulting from nanoparticle administration are those that have taken up particles. An alternative hypothesis is that nanoparticle administration alters the trafficking of suppressive myeloid cell populations away from the metastatic niche, and

this effect on trafficking skews the inflammatory milieu of the lungs. The proposed flow sorting study would also test this alternative hypothesis, demonstrating whether the myeloid cells at the lung, for example, that express anti-tumor-phenotype-associated genes have taken up fluorescently-labelled particles. Further investigation into this area would facilitate an improved understanding of 1) the role that suppressive myeloid cells play in the metastatic cascade and 2) how a nanoparticle intervention can disrupt the metastatic cascade through changes in phenotype and trafficking.

5.2.2 Mechanisms of action underlying the clearance of pulmonary metastases as a result of neoadjuvant and adjuvant nanoparticle administration

The work presented in this dissertation provides evidence into the nanoparticle-mediated T-cell-dependent clearance of pulmonary metastases. In **Chapter 3** we demonstrated that nanoparticle delivery, in both the neoadjuvant and adjuvant context surrounding primary tumor resection, can achieve tumor cell clearance from the lungs, and that this clearance of metastases is abrogated in a T-cell-deficient model. These findings suggest that T-cells play an integral role in the clearance of metastatic lesions, especially in the adjuvant context, where metastases are allowed to form, the primary tumor is surgically resected, and then nanoparticles are administered after resection. The neoadjuvant and adjuvant administration of immunomodulatory nanoparticles has particular clinical relevance given the great clinical interest in and recent FDA approval of checkpoint blockade as a neoadjuvant/adjuvant immunotherapy to augment surgical resection [81]. However, the direct connection between the nanoparticle-based modulation of myeloid cells and T-cell-mediated clearance of tumor cells is not well understood. We hypothesize that the nanoparticles modulate the tumor microenvironment, skewing it from an immunosuppressive to an anti-tumor milieu, and that by remodeling the microenvironment, T-cells are allowed to

infiltrate and eliminate tumor cells. One way to test this hypothesis is to perform histology on the primary tumor and lungs to look for 1) T-cell infiltration and 2) phenotypic markers of T-cell activation, anergy, or exhaustion. This could help illuminate if nanoparticle administration enables increased T-cell infiltration into the tumor microenvironment by skewing an immunosuppressive environment to mitigate factors that lead to T-cell exhaustion. Another way to test this hypothesis could be by sorting the myeloid cells from the primary tumor and lungs of mice receiving either nanoparticles or saline, and to conduct *in vitro* T-cell proliferation assays with these populations. These T-cell proliferation assays would illuminate the impact of the different cell subpopulations on suppressing or stimulating T-cell proliferation. Intracellular flow cytometry could then be performed on these T-cells for analysis of markers correlative of T-cell anergy or exhaustion to investigate the role of these myeloid cell populations on T-cell activation. Additionally, the sorted myeloid cells could be separated into nanoparticle positive versus negative fractions prior to the T-cell proliferation assays to investigate whether the impact on T-cells is due to 1) myeloid cells that have taken up nanoparticles or 2) secondary effects on remodeling of the tumor microenvironment. These approaches would help further our understanding of the connection between nanoparticle-mediated remodeling of immune cell populations and the T-cell-dependent clearance of metastases.

5.2.3 Utilizing the immunologic niche to monitor ICB-response in a resection model

In **Chapter 4** we investigated the efficacy of the implantable immunologic niche as a diagnostic for checkpoint blockade response. We excitingly found that gene expressions could be probed to predict ICB-response prior to initiating therapy, and monitored both during and after therapy to investigate immune responses to checkpoint inhibition. At the moment, the clinical utility for treating TNBC with ICB is 1) for metastatic disease or 2) as a neoadjuvant/adjuvant

therapy to augment primary tumor resection. The studies in **Chapter 4** demonstrating the efficacy of the immunologic niche as an ICB-diagnostic were performed without removing the primary tumor. Implementing a resection model could allow us to investigate the clinical utility of the implant with the current clinical context for treating TNBC with ICB. One approach to investigate this could be to first implant mice with immunologic niche scaffolds, orthotopically inoculate them with TNBC, surgically resect the primary tumor 14 days post-tumor inoculation, and then initiate aPD-1 following resection. This would more closely mimic the clinical scenario of treating a patient with aPD-1 that presents with distant recurrence [76,78]. During the post-resection administration of ICB, longitudinal biopsies of the implant could be performed for analysis of gene expressions correlative of ICB-response, as measured by survival monitoring and terminal bioluminescent imaging of the lungs for quantifying metastatic colonization. To investigate the clinical utility of implant-derived gene expressions for predicting efficacy of adjuvant aPD-1, one could set up the model as outlined and biopsy the immunologic niche between the primary tumor resection and initiating ICB. The implant-derived gene expressions could then be probed for studying analytes correlative of divergent responses to adjuvant checkpoint blockade. These investigations would be highly informative for framing the study design of a potential clinical trial with the goal of utilizing the immunologic niche to predict and monitor efficacy of ICB in treating TNBC.

5.2.4 Understanding the divergent cell populations and mechanisms underlying ICB-sensitivity and resistance

We observed divergent immune responses to checkpoint inhibition, both before and after ICB administration. At the immunologic niche, we found skewing of myeloid cell and lymphocyte phenotype by RNA-seq, as well as significant differences in the ratio of myeloid cells to

lymphocytes between ICB-sensitivity and resistance after therapy. Prior to ICB delivery, we also observed significant differences between the regulation of myeloid cell and lymphocyte pathways at the implant. We hypothesize that these initial biological findings implicate the role of thymic selection on stochastic differences that manifest in divergent responses to ICB. Specifically, it is possible that thymic selection yields different clonal populations of CD4+ T-cells that differentially recruit suppressive or inflammatory myeloid cell subpopulations. We then postulate that these stochastic differences in both the CD4+ T-cell and myeloid cell milieu impact CD8+ T-cell infiltration, proliferation, activation, and antigen recognition. It is possible that these basal differences would set up the immune system to divergently respond to an intervention with the goal of alleviating T-cell suppression by inhibiting the ligation of PD-1 with PD-L1. It is also worth noting that the PD-1/PD-L1 axis must be playing an integral role in suppressing T-cell-mediated anti-tumor responses for ICB administration to alleviate T-cell-suppression. If suppressive mechanisms aside from T-cell immune checkpoints, such as the recruitment of regulatory T-cells to the tumor microenvironment, are the predominant forces of immunosuppression, then blocking PD-1:PD-L1 ligation would not mitigate these mechanisms. Clinically, PD-1/PD-L1 has failed to perform successfully as a biomarker for predicting ICB-response, as the majority of patients with PD-L1+ tumors are resistant to ICB [84,85]. Some postulate that this could be because PD-L1 expression may not actually indicate that the PD-1/PD-L1 axis is the predominant mechanism underlying the suppression of an anti-tumor immune response. This highlights a benefit of utilizing the immunologic niche as a diagnostic for ICB-response – a multivariate signature of immune cell-derived gene expressions has the potential to illuminate a more nuanced assessment of immunosuppressive mechanisms, which could more

effectively capture if ICB is the right strategy for stimulating an anti-tumor immune response for a cancer patient.

Interestingly, in **Chapter 2** and **Chapter 3**, we found that 1) suppressive myeloid cells can be targeted to stimulate an anti-tumor immune response, 2) the efficacy of targeting myeloid cells is abrogated in a T-cell deficient model, and 3) targeting myeloid cells can be utilized to improve the efficacy of ICB. Similarly, in **Chapter 4** we observed that myeloid cells contribute to divergent ICB-responses. Collectively, this led us to hypothesize that the interaction of myeloid cells and T-cells may contribute to ICB-sensitivity versus ICB-resistance, and that a utility of the immunologic niche as an ICB-diagnostic may be in monitoring myeloid cells and myeloid-T-cell interactions. To test the hypothesis that myeloid cell phenotype and function may dictate ICB-response, one could implant an immunologic niche scaffold, orthotopically inoculate mice with TNBC, and biopsy the implant prior to initiating ICB. The gene expressions of the biopsy could be probed with the predictive ICB signature to stratify the mice that are predicted to be sensitive to ICB. Myeloid cells could be sorted from those mice predicted to be ICB-sensitive and transferred to those that are predicted to be resistant. This would allow us to investigate if adoptively transferring myeloid cells from one cohort to another prior to administering therapy changes their immune environment such that the mice predicted to be ICB-resistant are more sensitive to therapy. Another strategy could involve administering nanoparticles as an induction strategy to skew the myeloid cells toward inflammatory, anti-tumor phenotypes prior to initiating ICB. Testing this hypothesis through these studies would be instrumental in illuminating the role that myeloid cells play in the divergent responses to ICB. Clinically, these proposed studies could motivate using an implantable immunologic niche to identify patients who would be good candidates for receiving ICB monotherapy. For those that are predicted to be ICB-resistant, the immunologic niche could

be probed to glean the role myeloid cells are playing in suppressing an anti-tumor T-cell response. If it is determined that myeloid cells are responsible for underlying resistance to ICB, cargo-free nanoparticles could be administered to modulate the inflammatory milieu and stimulate a cytotoxic T-cell response, as a combination, multimodal therapy.

5.2.5 Identifying critical design aspects of engineered materials

In **Chapter 1**, the role of the material characteristics of NPs on particle-mediated immunomodulation was briefly overviewed. Our lab has previously investigated the impact of surfactant type and polymer molecular weight on innate immune responses both in murine models of TLR activation and breast cancer [61,68]. In this first study of tunable, cargo-free polymer NPs, the authors found that intravenous PLA-PEMA administration prolonged the survival of mice challenged with lipopolysaccharide. In vitro internalization studies were performed in both manuscripts and showed that the surfactant type used, which alters the NP surface charge, impacts NP internalization by innate immune cells [61,68]. Notably, whereas the first manuscript tested different NP formulations in vivo, the second manuscript (**Chapter 2**) focusing on NPs in breast cancer only validated NP formulations in vitro. In light of the evidence that the physiochemical properties of NPs impact their internalization by innate immune cells and the scRNA-seq data from **Chapter 3** showing that modulating innate immune cell phenotype disrupts the metastatic cascade, it would be valuable to study the role of NP formulation on metastatic colonization. To this end, one could prepare a library of polymer nanoparticles by altering the polymer molecular weight and surfactant. The NP material properties could then be characterized by dynamic light scattering to quantify the size and zeta potential of the different formulations. Finally, two in vivo studies could be pursued to probe the impact that NP physiochemical properties play on their functional utility. Conjugating the library of NP formulations with a fluorescent molecule, such as Cy5.5, and

intravenously administering the fluorescent NPs would allow us to study their biodistribution. Single cell suspensions could be isolated from the lungs, primary tumor, and spleen, and analyzed with flow cytometry to investigate how particle properties impact uptake by myeloid cell populations at different tissues. Additionally, the disparate NP formulations could be administered to separate cohorts of tumor bearing mice and lung BLI performed to quantify pulmonary metastases to illuminate the role of NP properties on metastatic colonization.

The engineered immunologic niche, discussed in **Chapter 4**, is a PCL scaffold with interconnected pores that integrates with the host upon surgical implantation. Our lab's original publication of the immunologic niche implant, for monitoring breast cancer spread, utilized a porogen-leached PLG scaffold with 250 - 425 μm pores [205]. Due to the degradable nature of PLG over short time scales, our lab employed PCL for the subsequent studies of the immunologic niche, utilizing a polymer with greater in vivo stability to bolster the implant's clinical utility [206]. The microporous PCL implants were engineered with the same dimensions and porosity as the PLG scaffolds, and both polymer scaffolds showed early recruitment of metastatic tumor cells and dynamic changes in leukocyte recruitment with disease progression. As such, I hypothesize that the architecture of the implant, as opposed to the polymer composition, governs its method of action. However, while I postulate that the polymer type does not impact the function of these immunologic niche scaffolds (e.g. PLG versus PCL), I hypothesize that an implant fabricated out of a more immunogenic material (e.g. fibrin) would significantly disrupt the utility of these implants. To test these hypotheses, one could fabricate a diversity of scaffolds composed of materials with varying degradability and immunogenicity, including PLG, PCL, fibrin, alginate, and poly(ethylene glycol). For each of these materials, the density of porogen in the implant could be altered, while maintaining the same pore size (250 - 425 μm), so that there are scaffold

conditions 1) with interconnected pores that allow infiltration of tissue throughout and 2) without interconnected pores. This library of scaffolds could then be implanted in the subcutaneous space of tumor-bearing mice and analyzed for both the arrival of metastatic tumor cells as well as their immune cell milieu. This would allow us to investigate the role of biodegradability, immunogenicity, and architecture in the functional utility of the engineered immunologic niche. The insights from these proposed studies, focusing on the impact of tunable material characteristics on the technology's functional utility, would be highly valuable for the clinical translation of both the nanoparticle and immunologic niche platforms.

5.3 Concluding Remarks

In conclusion, the preclinical findings reported in this dissertation provide the framework for the immunotherapeutic and diagnostic potential of engineered materials. Both of these approaches present novel opportunities for treating metastatic disease and gleaning biomarkers indicative of therapy response. Interestingly, the nanoparticles and immunologic niche implant have shown exciting efficacy in multiple different indications. Our lab has investigated the utility of immunomodulatory, cargo-free NPs in murine models of TLR activation, spinal cord injury, and metastatic breast cancer [61,66,68]. All three of these indications share a commonality of aberrant inflammation, and in each of these studies, we found functional utility as a result of reprogramming myeloid cells. As such, I hypothesize that cargo-free polymer NPs could also show exciting activity in other pathologies of aberrant inflammation that are driven by myeloid cell dysregulation. Similarly, our lab has studied the utility of the immunologic niche implant for monitoring the progression of diseases of aberrant inflammation, including breast cancer, multiple sclerosis, and pancreatic cancer [205,208,218]. In all three indications, it was found that the gene expressions of myeloid cells at the immunologic niche could be monitored to glean insight into

disease progression. Because of the enrichment of myeloid cells at the immunologic niche and the ability to longitudinally monitor dynamics among these leukocytes, I hypothesize that the immunologic niche could be highly useful for gleaning insight into the progression of other pathologies of aberrant inflammation. In fact, researchers in our lab are currently investigating the utility of the immunologic niche implant in type 1 diabetes, organ transplant, and preeclampsia, with encouraging initial results. Due to the exciting pre-clinical studies we've published in our lab, the translatable nature of our study design, and the pressing clinical need of the medical problems we're addressing, both the cargo-free nanoparticle platform and immunologic niche are moving toward clinical translation. COUR Pharmaceutical has submitted an Investigational New Drug (IND) application to the FDA based on the data we presented in **Chapter 3**, which has been approved toward the first-in-human clinical trial of cargo-free nanoparticles in cancer. Additionally, our lab has been diligently working with the University of Michigan Innovation Partnerships, National Science Foundation Innovation Corps, FDA, and Institutional Review Boards with the goal of investigating the efficacy of the immunologic niche implant in a first-in-human clinical trial. Collectively, one could imagine the application of these technologies such that a patient receives an immunologic niche implant, the implant is biopsied to probe for immunotherapy-associated biomarkers, an immune-based resistance mechanism is identified, and the mechanism is targeted with immunomodulatory nanoparticles. The findings in this dissertation provide the foundation for studies and trials to follow that have the potential to shift the paradigm for immunotherapies and companion diagnostics in the treatment of metastatic disease.

Bibliography

[1] R.L. Siegel, K.D. Miller, H.E. Fuchs, A. Jemal, Cancer statistics, 2022, CA: A Cancer Journal for Clinicians. 72 (2022) 7–33. https://doi.org/10.3322/caac.21708.

[2] H. Sung, J. Ferlay, R.L. Siegel, M. Laversanne, I. Soerjomataram, A. Jemal, F. Bray, Global Cancer Statistics 2020: GLOBOCAN Estimates of Incidence and Mortality Worldwide for 36 Cancers in 185 Countries, CA: A Cancer Journal for Clinicians. 71 (2021) 209–249. https://doi.org/10.3322/caac.21660.

[3] P. Zhang, Y. Zhai, Y. Cai, Y. Zhao, Y. Li, Nanomedicine-Based Immunotherapy for the Treatment of Cancer Metastasis, Adv Mater. 31 (2019) e1904156. https://doi.org/10.1002/adma.201904156.

[4] K. Ganesh, J. Massagué, Targeting metastatic cancer, Nat Med. 27 (2021) 34–44. https://doi.org/10.1038/s41591-020-01195-4.

[5] S. Kruger, M. Ilmer, S. Kobold, B.L. Cadilha, S. Endres, S. Ormanns, G. Schuebbe, B.W. Renz, J.G. D'Haese, H. Schloesser, V. Heinemann, M. Subklewe, S. Boeck, J. Werner, M. von Bergwelt-Baildon, Advances in cancer immunotherapy 2019 – latest trends, J Exp Clin Cancer Res. 38 (2019) 268. https://doi.org/10.1186/s13046-019-1266-0.

[6] S. Upadhaya, V.M. Hubbard-Lucey, J.X. Yu, Immuno-oncology drug development forges on despite COVID-19, Nature Reviews Drug Discovery. 19 (2020) 751–752. https://doi.org/10.1038/d41573-020-00166-1.

[7] D. Hanahan, R.A. Weinberg, Hallmarks of cancer: the next generation, Cell. 144 (2011) 646–674. https://doi.org/10.1016/j.cell.2011.02.013.

[8] R.D. Schreiber, L.J. Old, M.J. Smyth, Cancer immunoediting: integrating immunity's roles in cancer suppression and promotion, Science. 331 (2011) 1565–1570. https://doi.org/10.1126/science.1203486.

[9] R. Greil, G. Anether, K. Johrer, I. Tinhofer, Tuning the rheostat of the myelopoietic system via Fas and TRAIL, Crit Rev Immunol. 23 (2003) 301–322. https://doi.org/10.1615/critrevimmunol.v23.i4.30.

[10] E.J. Wherry, M. Kurachi, Molecular and cellular insights into T cell exhaustion, Nat Rev Immunol. 15 (2015) 486–499. https://doi.org/10.1038/nri3862.

[11] Z.G. Fridlender, J. Sun, S. Kim, V. Kapoor, G. Cheng, L. Ling, G.S. Worthen, S.M. Albelda, Polarization of Tumor-Associated Neutrophil (TAN) Phenotype by TGF-β: "N1" versus "N2" TAN, Cancer Cell. 16 (2009) 183–194. https://doi.org/10.1016/j.ccr.2009.06.017.

[12] M. Kiss, A.A. Caro, G. Raes, D. Laoui, Systemic Reprogramming of Monocytes in Cancer, Frontiers in Oncology. 10 (2020). https://www.frontiersin.org/article/10.3389/fonc.2020.01399 (accessed March 14, 2022).

[13] Y. Pan, Y. Yu, X. Wang, T. Zhang, Tumor-Associated Macrophages in Tumor Immunity, Frontiers in Immunology. 11 (2020). https://www.frontiersin.org/article/10.3389/fimmu.2020.583084 (accessed March 14, 2022).

[14] R. Rotondo, G. Barisione, L. Mastracci, F. Grossi, A.M. Orengo, R. Costa, M. Truini, M. Fabbi, S. Ferrini, O. Barbieri, IL-8 induces exocytosis of arginase 1 by neutrophil

polymorphonuclears in nonsmall cell lung cancer, International Journal of Cancer. 125 (2009) 887–893. https://doi.org/10.1002/ijc.24448.
[15] C.A. Corzo, M.J. Cotter, P. Cheng, F. Cheng, S. Kusmartsev, E. Sotomayor, T. Padhya, T.V. McCaffrey, J.C. McCaffrey, D.I. Gabrilovich, Mechanism regulating reactive oxygen species in tumor-induced myeloid-derived suppressor cells, J Immunol. 182 (2009) 5693–5701. https://doi.org/10.4049/jimmunol.0900092.
[16] H. Zhang, Z.-L. Li, S.-B. Ye, L.-Y. Ouyang, Y.-S. Chen, J. He, H.-Q. Huang, Y.-X. Zeng, X.-S. Zhang, J. Li, Myeloid-derived suppressor cells inhibit T cell proliferation in human extranodal NK/T cell lymphoma: a novel prognostic indicator, Cancer Immunol Immunother. 64 (2015) 1587–1599. https://doi.org/10.1007/s00262-015-1765-6.
[17] P. Li, M. Lu, J. Shi, L. Hua, Z. Gong, Q. Li, L.D. Shultz, G. Ren, Dual roles of neutrophils in metastatic colonization are governed by the host NK cell status, Nat Commun. 11 (2020) 4387. https://doi.org/10.1038/s41467-020-18125-0.
[18] K. Movahedi, D. Laoui, C. Gysemans, M. Baeten, G. Stangé, J. Van den Bossche, M. Mack, D. Pipeleers, P. In't Veld, P. De Baetselier, J.A. Van Ginderachter, Different tumor microenvironments contain functionally distinct subsets of macrophages derived from Ly6C(high) monocytes, Cancer Res. 70 (2010) 5728–5739. https://doi.org/10.1158/0008-5472.CAN-09-4672.
[19] A.L. Doedens, C. Stockmann, M.P. Rubinstein, D. Liao, N. Zhang, D.G. DeNardo, L.M. Coussens, M. Karin, A.W. Goldrath, R.S. Johnson, Macrophage expression of hypoxia-inducible factor-1 alpha suppresses T-cell function and promotes tumor progression, Cancer Res. 70 (2010) 7465–7475. https://doi.org/10.1158/0008-5472.CAN-10-1439.
[20] T.J. Curiel, G. Coukos, L. Zou, X. Alvarez, P. Cheng, P. Mottram, M. Evdemon-Hogan, J.R. Conejo-Garcia, L. Zhang, M. Burow, Y. Zhu, S. Wei, I. Kryczek, B. Daniel, A. Gordon, L. Myers, A. Lackner, M.L. Disis, K.L. Knutson, L. Chen, W. Zou, Specific recruitment of regulatory T cells in ovarian carcinoma fosters immune privilege and predicts reduced survival, Nat Med. 10 (2004) 942–949. https://doi.org/10.1038/nm1093.
[21] I. Kryczek, L. Zou, P. Rodriguez, G. Zhu, S. Wei, P. Mottram, M. Brumlik, P. Cheng, T. Curiel, L. Myers, A. Lackner, X. Alvarez, A. Ochoa, L. Chen, W. Zou, B7-H4 expression identifies a novel suppressive macrophage population in human ovarian carcinoma, J Exp Med. 203 (2006) 871–881. https://doi.org/10.1084/jem.20050930.
[22] K. Wu, I. Kryczek, L. Chen, W. Zou, T.H. Welling, Kupffer cell suppression of CD8+ T cells in human hepatocellular carcinoma is mediated by B7-H1/programmed death-1 interactions, Cancer Res. 69 (2009) 8067–8075. https://doi.org/10.1158/0008-5472.CAN-09-0901.
[23] S. Brandau, K. Moses, S. Lang, The kinship of neutrophils and granulocytic myeloid-derived suppressor cells in cancer: cousins, siblings or twins?, Semin Cancer Biol. 23 (2013) 171–182. https://doi.org/10.1016/j.semcancer.2013.02.007.
[24] J.D. Spicer, B. McDonald, J.J. Cools-Lartigue, S.C. Chow, B. Giannias, P. Kubes, L.E. Ferri, Neutrophils promote liver metastasis via Mac-1-mediated interactions with circulating tumor cells, Cancer Res. 72 (2012) 3919–3927. https://doi.org/10.1158/0008-5472.CAN-11-2393.
[25] B.-Z. Qian, J. Li, H. Zhang, T. Kitamura, J. Zhang, L.R. Campion, E.A. Kaiser, L.A. Snyder, J.W. Pollard, CCL2 recruits inflammatory monocytes to facilitate breast-tumour metastasis, Nature. 475 (2011) 222–225. https://doi.org/10.1038/nature10138.

[26] B.A. Aguado, G.G. Bushnell, S.S. Rao, J.S. Jeruss, L.D. Shea, Engineering the pre-metastatic niche, Nat Biomed Eng. 1 (2017) 0077. https://doi.org/10.1038/s41551-017-0077.
[27] A.D. Waldman, J.M. Fritz, M.J. Lenardo, A guide to cancer immunotherapy: from T cell basic science to clinical practice, Nat Rev Immunol. 20 (2020) 651–668. https://doi.org/10.1038/s41577-020-0306-5.
[28] M.W. Nachman, S.L. Crowell, Estimate of the mutation rate per nucleotide in humans., Genetics. 156 (2000) 297–304.
[29] S.R.M. Bennett, F.R. Carbone, F. Karamalis, J.F.A.P. Miller, W.R. Heath, Induction of a CD8+ Cytotoxic T Lymphocyte Response by Cross-priming Requires Cognate CD4+ T Cell Help, J Exp Med. 186 (1997) 65–70.
[30] S. Shalapour, M. Karin, Immunity, inflammation, and cancer: an eternal fight between good and evil, J Clin Invest. 125 (2015) 3347–3355. https://doi.org/10.1172/JCI80007.
[31] D.R. Leach, M.F. Krummel, J.P. Allison, Enhancement of Antitumor Immunity by CTLA-4 Blockade, Science. 271 (1996) 1734–1736. https://doi.org/10.1126/science.271.5256.1734.
[32] Y. Iwai, M. Ishida, Y. Tanaka, T. Okazaki, T. Honjo, N. Minato, Involvement of PD-L1 on tumor cells in the escape from host immune system and tumor immunotherapy by PD-L1 blockade, Proceedings of the National Academy of Sciences. 99 (2002) 12293–12297. https://doi.org/10.1073/pnas.192461099.
[33] V.L. Perez, L. Van Parijs, A. Biuckians, X.X. Zheng, T.B. Strom, A.K. Abbas, Induction of Peripheral T Cell Tolerance In Vivo Requires CTLA-4 Engagement, Immunity. 6 (1997) 411–417. https://doi.org/10.1016/S1074-7613(00)80284-8.
[34] E.I. Buchbinder, A. Desai, CTLA-4 and PD-1 Pathways, Am J Clin Oncol. 39 (2016) 98–106. https://doi.org/10.1097/COC.0000000000000239.
[35] S. Chikuma, S. Terawaki, T. Hayashi, R. Nabeshima, T. Yoshida, S. Shibayama, T. Okazaki, T. Honjo, PD-1-Mediated Suppression of IL-2 Production Induces CD8+ T Cell Anergy In Vivo, The Journal of Immunology. 182 (2009) 6682–6689. https://doi.org/10.4049/jimmunol.0900080.
[36] A.H. Sharpe, E.J. Wherry, R. Ahmed, G.J. Freeman, The function of programmed cell death 1 and its ligands in regulating autoimmunity and infection, Nat Immunol. 8 (2007) 239–245. https://doi.org/10.1038/ni1443.
[37] A.H. Sharpe, K.E. Pauken, The diverse functions of the PD1 inhibitory pathway, Nat Rev Immunol. 18 (2018) 153–167. https://doi.org/10.1038/nri.2017.108.
[38] T. Yokosuka, M. Takamatsu, W. Kobayashi-Imanishi, A. Hashimoto-Tane, M. Azuma, T. Saito, Programmed cell death 1 forms negative costimulatory microclusters that directly inhibit T cell receptor signaling by recruiting phosphatase SHP2, J Exp Med. 209 (2012) 1201–1217. https://doi.org/10.1084/jem.20112741.
[39] J.M. Taube, R.A. Anders, G.D. Young, H. Xu, R. Sharma, T.L. McMiller, S. Chen, A.P. Klein, D.M. Pardoll, S.L. Topalian, L. Chen, Colocalization of Inflammatory Response with B7-H1 Expression in Human Melanocytic Lesions Supports an Adaptive Resistance Mechanism of Immune Escape, Sci Transl Med. 4 (2012) 127ra37. https://doi.org/10.1126/scitranslmed.3003689.
[40] R. Barth, J. Mule, P. Spiess, S. Rosenberg, Interferon gamma and tumor necrosis factor have a role in tumor regressions mediated by murine CD8+ tumor-infiltrating lymphocytes, J Exp Med. 173 (1991) 647–658.

[41] M. Santoni, E. Romagnoli, T. Saladino, L. Foghini, S. Guarino, M. Capponi, M. Giannini, P.D. Cognigni, G. Ferrara, N. Battelli, Triple negative breast cancer: Key role of Tumor-Associated Macrophages in regulating the activity of anti-PD-1/PD-L1 agents, Biochimica et Biophysica Acta (BBA) - Reviews on Cancer. 1869 (2018) 78–84. https://doi.org/10.1016/j.bbcan.2017.10.007.
[42] S.R. Gordon, R.L. Maute, B.W. Dulken, G. Hutter, B.M. George, M.N. McCracken, R. Gupta, J.M. Tsai, R. Sinha, D. Corey, A.M. Ring, A.J. Connolly, I.L. Weissman, PD-1 expression by tumour-associated macrophages inhibits phagocytosis and tumour immunity, Nature. 545 (2017) 495–499. https://doi.org/10.1038/nature22396.
[43] W. Zou, J.D. Wolchok, L. Chen, PD-L1 (B7-H1) and PD-1 Pathway Blockade for Cancer Therapy: Mechanisms, Response Biomarkers and Combinations, Sci Transl Med. 8 (2016) 328rv4. https://doi.org/10.1126/scitranslmed.aad7118.
[44] J.-I. Youn, S. Nagaraj, M. Collazo, D.I. Gabrilovich, Subsets of Myeloid-Derived Suppressor Cells in Tumor Bearing Mice, J Immunol. 181 (2008) 5791–5802.
[45] L. Cortesi, H.S. Rugo, C. Jackisch, An Overview of PARP Inhibitors for the Treatment of Breast Cancer, Target Oncol. 16 (2021) 255–282. https://doi.org/10.1007/s11523-021-00796-4.
[46] S.C. Edwards, W.H.M. Hoevenaar, S.B. Coffelt, Emerging immunotherapies for metastasis, Br J Cancer. 124 (2021) 37–48. https://doi.org/10.1038/s41416-020-01160-5.
[47] C. Meyer, L. Cagnon, C.M. Costa-Nunes, P. Baumgaertner, N. Montandon, L. Leyvraz, O. Michielin, E. Romano, D.E. Speiser, Frequencies of circulating MDSC correlate with clinical outcome of melanoma patients treated with ipilimumab, Cancer Immunol Immunother. 63 (2014) 247–257. https://doi.org/10.1007/s00262-013-1508-5.
[48] R.D. Dolan, B.J.A. Laird, P.G. Horgan, D.C. McMillan, The prognostic value of the systemic inflammatory response in randomised clinical trials in cancer: A systematic review, Crit Rev Oncol Hematol. 132 (2018) 130–137. https://doi.org/10.1016/j.critrevonc.2018.09.016.
[49] A. Swierczak, J.W. Pollard, Myeloid Cells in Metastasis, Cold Spring Harb Perspect Med. 10 (2020) a038026. https://doi.org/10.1101/cshperspect.a038026.
[50] M.K. Srivastava, L. Zhu, M. Harris-White, U.K. Kar, U. Kar, M. Huang, M.F. Johnson, J.M. Lee, D. Elashoff, R. Strieter, S. Dubinett, S. Sharma, Myeloid suppressor cell depletion augments antitumor activity in lung cancer, PLoS One. 7 (2012) e40677. https://doi.org/10.1371/journal.pone.0040677.
[51] H. Griesmann, C. Drexel, N. Milosevic, B. Sipos, J. Rosendahl, T.M. Gress, P. Michl, Pharmacological macrophage inhibition decreases metastasis formation in a genetic model of pancreatic cancer, Gut. 66 (2017) 1278–1285. https://doi.org/10.1136/gutjnl-2015-310049.
[52] S.K. Wculek, I. Malanchi, Neutrophils support lung colonization of metastasis-initiating breast cancer cells, Nature. 528 (2015) 413–417. https://doi.org/10.1038/nature16140.
[53] F. Veglia, E. Sanseviero, D.I. Gabrilovich, Myeloid-derived suppressor cells in the era of increasing myeloid cell diversity, Nat Rev Immunol. 21 (2021) 485–498. https://doi.org/10.1038/s41577-020-00490-y.
[54] Z. Granot, E. Henke, E. Comen, T. King, L. Norton, R. Benezra, Tumor entrained neutrophils inhibit seeding in the premetastatic lung, Cancer Cell. 20 (2011) 300–314. https://doi.org/10.1016/j.ccr.2011.08.012.
[55] E. Uribe-Querol, C. Rosales, Neutrophils in Cancer: Two Sides of the Same Coin, J Immunol Res. 2015 (2015) 983698. https://doi.org/10.1155/2015/983698.

[56] J.L. Guerriero, Macrophages: The Road Less Traveled, Changing Anticancer Therapy, Trends Mol Med. 24 (2018) 472–489. https://doi.org/10.1016/j.molmed.2018.03.006.
[57] M. Yang, D. McKay, J.W. Pollard, C.E. Lewis, Diverse Functions of Macrophages in Different Tumor Microenvironments, Cancer Res. 78 (2018) 5492–5503. https://doi.org/10.1158/0008-5472.CAN-18-1367.
[58] H.Y. Yoon, S.T. Selvan, Y. Yang, M.J. Kim, D.K. Yi, I.C. Kwon, K. Kim, Engineering nanoparticle strategies for effective cancer immunotherapy, Biomaterials. 178 (2018) 597–607. https://doi.org/10.1016/j.biomaterials.2018.03.036.
[59] Y. Yao, Y. Zhou, L. Liu, Y. Xu, Q. Chen, Y. Wang, S. Wu, Y. Deng, J. Zhang, A. Shao, Nanoparticle-Based Drug Delivery in Cancer Therapy and Its Role in Overcoming Drug Resistance, Front Mol Biosci. 7 (2020) 193. https://doi.org/10.3389/fmolb.2020.00193.
[60] A.C. Anselmo, S. Mitragotri, Nanoparticles in the clinic: An update, Bioeng Transl Med. 4 (2019) e10143. https://doi.org/10.1002/btm2.10143.
[61] L.M. Casey, S. Kakade, J.T. Decker, J.A. Rose, K. Deans, L.D. Shea, R.M. Pearson, Cargo-less nanoparticles program innate immune cell responses to toll-like receptor activation, Biomaterials. 218 (2019) 119333. https://doi.org/10.1016/j.biomaterials.2019.119333.
[62] R.P. Allen, A. Bolandparvaz, J.A. Ma, V.A. Manickam, J.S. Lewis, Latent, Immunosuppressive Nature of Poly(lactic-co-glycolic acid) Microparticles, ACS Biomater Sci Eng. 4 (2018) 900–918. https://doi.org/10.1021/acsbiomaterials.7b00831.
[63] E. Saito, R. Kuo, R.M. Pearson, N. Gohel, B. Cheung, N.J.C. King, S.D. Miller, L.D. Shea, Designing drug-free biodegradable nanoparticles to modulate inflammatory monocytes and neutrophils for ameliorating inflammation, J Control Release. 300 (2019) 185–196. https://doi.org/10.1016/j.jconrel.2019.02.025.
[64] H.H. Gustafson, D. Holt-Casper, D.W. Grainger, H. Ghandehari, Nanoparticle Uptake: The Phagocyte Problem, Nano Today. 10 (2015) 487–510. https://doi.org/10.1016/j.nantod.2015.06.006.
[65] D.R. Getts, R.L. Terry, M.T. Getts, C. Deffrasnes, M. Müller, C. van Vreden, T.M. Ashhurst, B. Chami, D. McCarthy, H. Wu, J. Ma, A. Martin, L.D. Shae, P. Witting, G.S. Kansas, J. Kühn, W. Hafezi, I.L. Campbell, D. Reilly, J. Say, L. Brown, M.Y. White, S.J. Cordwell, S.J. Chadban, E.B. Thorp, S. Bao, S.D. Miller, N.J.C. King, Therapeutic Inflammatory Monocyte Modulation Using Immune-Modifying Microparticles, Sci Transl Med. 6 (2014) 219ra7. https://doi.org/10.1126/scitranslmed.3007563.
[66] J. Park, Y. Zhang, E. Saito, S.J. Gurczynski, B.B. Moore, B.J. Cummings, A.J. Anderson, L.D. Shea, Intravascular innate immune cells reprogrammed via intravenous nanoparticles to promote functional recovery after spinal cord injury, Proc Natl Acad Sci U S A. 116 (2019) 14947–14954. https://doi.org/10.1073/pnas.1820276116.
[67] R.M. Pearson, L.M. Casey, K.R. Hughes, L.Z. Wang, M.G. North, D.R. Getts, S.D. Miller, L.D. Shea, Controlled Delivery of Single or Multiple Antigens in Tolerogenic Nanoparticles Using Peptide-Polymer Bioconjugates, Mol Ther. 25 (2017) 1655–1664. https://doi.org/10.1016/j.ymthe.2017.04.015.
[68] Y. Zhang, K.R. Hughes, R.M. Raghani, J. Ma, S. Orbach, J.S. Jeruss, L.D. Shea, Cargo-free immunomodulatory nanoparticles combined with anti-PD-1 antibody for treating metastatic breast cancer, Biomaterials. 269 (2021) 120666. https://doi.org/10.1016/j.biomaterials.2021.120666.

[69] C.P. Kelly, J.A. Murray, D.A. Leffler, D.R. Getts, A.C. Bledsoe, G. Smithson, M.R. First, A. Morris, M. Boyne, A. Elhofy, T.-T. Wu, J.R. Podojil, S.D. Miller, TAK-101 Study Group, TAK-101 Nanoparticles Induce Gluten-Specific Tolerance in Celiac Disease: A Randomized, Double-Blind, Placebo-Controlled Study, Gastroenterology. 161 (2021) 66-80.e8. https://doi.org/10.1053/j.gastro.2021.03.014.

[70] A.H. Morris, K.R. Hughes, L.D. Shea, 3 - Nanotechnology and biomaterials for immune modulation and monitoring, in: S.F. Badylak, J.H. Elisseeff (Eds.), Immunomodulatory Biomaterials, Woodhead Publishing, 2021: pp. 41–65. https://doi.org/10.1016/B978-0-12-821440-4.00001-3.

[71] A.-S. Heimes, M. Schmidt, Atezolizumab for the treatment of triple-negative breast cancer, Expert Opinion on Investigational Drugs. 28 (2019) 1–5. https://doi.org/10.1080/13543784.2019.1552255.

[72] H.R. Ali, L. Chlon, P.D.P. Pharoah, F. Markowetz, C. Caldas, Patterns of Immune Infiltration in Breast Cancer and Their Clinical Implications: A Gene-Expression-Based Retrospective Study, PLoS Med. 13 (2016) e1002194. https://doi.org/10.1371/journal.pmed.1002194.

[73] R.D. Bense, C. Sotiriou, M.J. Piccart-Gebhart, J.B.A.G. Haanen, M.A.T.M. van Vugt, E.G.E. de Vries, C.P. Schröder, R.S.N. Fehrmann, Relevance of Tumor-Infiltrating Immune Cell Composition and Functionality for Disease Outcome in Breast Cancer, J Natl Cancer Inst. 109 (2016) djw192. https://doi.org/10.1093/jnci/djw192.

[74] R. Thomas, G. Al-Khadairi, J. Decock, Immune Checkpoint Inhibitors in Triple Negative Breast Cancer Treatment: Promising Future Prospects, Frontiers in Oncology. 10 (2021). https://www.frontiersin.org/article/10.3389/fonc.2020.600573 (accessed March 9, 2022).

[75] R. Nanda, L.Q.M. Chow, E.C. Dees, R. Berger, S. Gupta, R. Geva, L. Pusztai, K. Pathiraja, G. Aktan, J.D. Cheng, V. Karantza, L. Buisseret, Pembrolizumab in Patients With Advanced Triple-Negative Breast Cancer: Phase Ib KEYNOTE-012 Study, J Clin Oncol. 34 (2016) 2460–2467. https://doi.org/10.1200/JCO.2015.64.8931.

[76] S. Adams, S. Loi, D. Toppmeyer, D.W. Cescon, M. De Laurentiis, R. Nanda, E.P. Winer, H. Mukai, K. Tamura, A. Armstrong, M.C. Liu, H. Iwata, L. Ryvo, P. Wimberger, H.S. Rugo, A.R. Tan, L. Jia, Y. Ding, V. Karantza, P. Schmid, Pembrolizumab monotherapy for previously untreated, PD-L1-positive, metastatic triple-negative breast cancer: cohort B of the phase II KEYNOTE-086 study, Annals of Oncology. 30 (2019) 405–411. https://doi.org/10.1093/annonc/mdy518.

[77] S. Adams, P. Schmid, H.S. Rugo, E.P. Winer, D. Loirat, A. Awada, D.W. Cescon, H. Iwata, M. Campone, R. Nanda, R. Hui, G. Curigliano, D. Toppmeyer, J. O'Shaughnessy, S. Loi, S. Paluch-Shimon, A.R. Tan, D. Card, J. Zhao, V. Karantza, J. Cortés, Pembrolizumab monotherapy for previously treated metastatic triple-negative breast cancer: cohort A of the phase II KEYNOTE-086 study, Annals of Oncology. 30 (2019) 397–404. https://doi.org/10.1093/annonc/mdy517.

[78] E.P. Winer, O. Lipatov, S.-A. Im, A. Goncalves, E. Muñoz-Couselo, K.S. Lee, P. Schmid, K. Tamura, L. Testa, I. Witzel, S. Ohtani, N. Turner, S. Zambelli, N. Harbeck, F. Andre, R. Dent, X. Zhou, V. Karantza, J. Mejia, J. Cortes, Pembrolizumab versus investigator-choice chemotherapy for metastatic triple-negative breast cancer (KEYNOTE-119): a randomised, open-label, phase 3 trial, The Lancet Oncology. 22 (2021) 499–511. https://doi.org/10.1016/S1470-2045(20)30754-3.

[79] L.A. Emens, C. Cruz, J.P. Eder, F. Braiteh, C. Chung, S.M. Tolaney, I. Kuter, R. Nanda, P.A. Cassier, J.-P. Delord, M.S. Gordon, E. ElGabry, C.-W. Chang, I. Sarkar, W. Grossman, C. O'Hear, M. Fassò, L. Molinero, P. Schmid, Long-term Clinical Outcomes and Biomarker Analyses of Atezolizumab Therapy for Patients With Metastatic Triple-Negative Breast Cancer, JAMA Oncol. 5 (2019) 74–82. https://doi.org/10.1001/jamaoncol.2018.4224.

[80] L.Y. Dirix, I. Takacs, G. Jerusalem, P. Nikolinakos, H.-T. Arkenau, A. Forero-Torres, R. Boccia, M.E. Lippman, R. Somer, M. Smakal, L.A. Emens, B. Hrinczenko, W. Edenfield, J. Gurtler, A. von Heydebreck, H.J. Grote, K. Chin, E.P. Hamilton, Avelumab, an anti-PD-L1 antibody, in patients with locally advanced or metastatic breast cancer: a phase 1b JAVELIN Solid Tumor study, Breast Cancer Res Treat. 167 (2018) 671–686. https://doi.org/10.1007/s10549-017-4537-5.

[81] P. Schmid, J. Cortes, L. Pusztai, H. McArthur, S. Kümmel, J. Bergh, C. Denkert, Y.H. Park, R. Hui, N. Harbeck, M. Takahashi, T. Foukakis, P.A. Fasching, F. Cardoso, M. Untch, L. Jia, V. Karantza, J. Zhao, G. Aktan, R. Dent, J. O'Shaughnessy, Pembrolizumab for Early Triple-Negative Breast Cancer, New England Journal of Medicine. 382 (2020) 810–821. https://doi.org/10.1056/NEJMoa1910549.

[82] B. Pellegrino, C. Tommasi, O.E. Cursio, A. Musolino, E. Migliori, P. De Silva, T.H. Senevirathne, M. Schena, M. Scartozzi, D. Farci, K. Willard-Gallo, C. Solinas, A review of immune checkpoint blockade in breast cancer, Semin Oncol. 48 (2021) 208–225. https://doi.org/10.1053/j.seminoncol.2021.09.002.

[83] G. Planes-Laine, P. Rochigneux, F. Bertucci, A.-S. Chrétien, P. Viens, R. Sabatier, A. Gonçalves, PD-1/PD-L1 Targeting in Breast Cancer: The First Clinical Evidences are Emerging—A Literature Review, Cancers (Basel). 11 (2019) 1033. https://doi.org/10.3390/cancers11071033.

[84] L. Gandhi, D. Rodríguez-Abreu, S. Gadgeel, E. Esteban, E. Felip, F. De Angelis, M. Domine, P. Clingan, M.J. Hochmair, S.F. Powell, S.Y.-S. Cheng, H.G. Bischoff, N. Peled, F. Grossi, R.R. Jennens, M. Reck, R. Hui, E.B. Garon, M. Boyer, B. Rubio-Viqueira, S. Novello, T. Kurata, J.E. Gray, J. Vida, Z. Wei, J. Yang, H. Raftopoulos, M.C. Pietanza, M.C. Garassino, Pembrolizumab plus Chemotherapy in Metastatic Non–Small-Cell Lung Cancer, New England Journal of Medicine. 378 (2018) 2078–2092. https://doi.org/10.1056/NEJMoa1801005.

[85] P. Schmid, S. Adams, H.S. Rugo, A. Schneeweiss, C.H. Barrios, H. Iwata, V. Diéras, R. Hegg, S.-A. Im, G. Shaw Wright, V. Henschel, L. Molinero, S.Y. Chui, R. Funke, A. Husain, E.P. Winer, S. Loi, L.A. Emens, Atezolizumab and Nab-Paclitaxel in Advanced Triple-Negative Breast Cancer, New England Journal of Medicine. 379 (2018) 2108–2121. https://doi.org/10.1056/NEJMoa1809615.

[86] A. Marabelle, D.T. Le, P.A. Ascierto, A.M. Di Giacomo, A. De Jesus-Acosta, J.-P. Delord, R. Geva, M. Gottfried, N. Penel, A.R. Hansen, S.A. Piha-Paul, T. Doi, B. Gao, H.C. Chung, J. Lopez-Martin, Y.-J. Bang, R.S. Frommer, M. Shah, R. Ghori, A.K. Joe, S.K. Pruitt, L.A. Diaz Jr, Efficacy of Pembrolizumab in Patients With Noncolorectal High Microsatellite Instability/Mismatch Repair–Deficient Cancer: Results From the Phase II KEYNOTE-158 Study, J Clin Oncol. 38 (2020) 1–10. https://doi.org/10.1200/JCO.19.02105.

[87] Y. Lei, X. Li, Q. Huang, X. Zheng, M. Liu, Progress and Challenges of Predictive Biomarkers for Immune Checkpoint Blockade, Front Oncol. 11 (2021) 617335. https://doi.org/10.3389/fonc.2021.617335.

[88] R. Barroso-Sousa, E. Jain, O. Cohen, D. Kim, J. Buendia-Buendia, E. Winer, N. Lin, S.M. Tolaney, N. Wagle, Prevalence and mutational determinants of high tumor mutation burden in breast cancer, Annals of Oncology. 31 (2020) 387–394. https://doi.org/10.1016/j.annonc.2019.11.010.
[89] T.P. McVeigh, M.J. Kerin, Clinical use of the Oncotype DX genomic test to guide treatment decisions for patients with invasive breast cancer, Breast Cancer (Dove Med Press). 9 (2017) 393–400. https://doi.org/10.2147/BCTT.S109847.
[90] S.L. Davis, S.G. Eckhardt, J.J. Tentler, J.R. Diamond, Triple-negative breast cancer: bridging the gap from cancer genomics to predictive biomarkers, Ther Adv Med Oncol. 6 (2014) 88–100. https://doi.org/10.1177/1758834013519843.
[91] D.J. McGrail, P.G. Pilié, N.U. Rashid, L. Voorwerk, M. Slagter, M. Kok, E. Jonasch, M. Khasraw, A.B. Heimberger, B. Lim, N.T. Ueno, J.K. Litton, R. Ferrarotto, J.T. Chang, S.L. Moulder, S.-Y. Lin, High tumor mutation burden fails to predict immune checkpoint blockade response across all cancer types, Ann Oncol. (2021) S0923-7534(21)00123-X. https://doi.org/10.1016/j.annonc.2021.02.006.
[92] P. Hofman, S. Heeke, C. Alix-Panabières, K. Pantel, Liquid biopsy in the era of immuno-oncology: is it ready for prime-time use for cancer patients?, Annals of Oncology. 30 (2019) 1448–1459. https://doi.org/10.1093/annonc/mdz196.
[93] D.G. Rothwell, M. Ayub, N. Cook, F. Thistlethwaite, L. Carter, E. Dean, N. Smith, S. Villa, J. Dransfield, A. Clipson, D. White, K. Nessa, S. Ferdous, M. Howell, A. Gupta, B. Kilerci, S. Mohan, K. Frese, S. Gulati, C. Miller, A. Jordan, H. Eaton, N. Hickson, C. O'Brien, D. Graham, C. Kelly, S. Aruketty, R. Metcalf, J. Chiramel, N. Tinsley, A.J. Vickers, R. Kurup, H. Frost, J. Stevenson, S. Southam, D. Landers, A. Wallace, R. Marais, A.M. Hughes, G. Brady, C. Dive, M.G. Krebs, Utility of ctDNA to support patient selection for early phase clinical trials: the TARGET study, Nat Med. 25 (2019) 738–743. https://doi.org/10.1038/s41591-019-0380-z.
[94] B.T. Li, F. Janku, B. Jung, C. Hou, K. Madwani, R. Alden, P. Razavi, J.S. Reis-Filho, R. Shen, J.M. Isbell, A.W. Blocker, N. Eattock, S. Gnerre, R.V. Satya, H. Xu, C. Zhao, M.P. Hall, Y. Hu, A.J. Sehnert, D. Brown, M. Ladanyi, C.M. Rudin, N. Hunkapiller, N. Feeney, G.B. Mills, C.P. Paweletz, P.A. Janne, D.B. Solit, G.J. Riely, A. Aravanis, G.R. Oxnard, Ultra-deep next-generation sequencing of plasma cell-free DNA in patients with advanced lung cancers: results from the Actionable Genome Consortium, Ann Oncol. 30 (2019) 597–603. https://doi.org/10.1093/annonc/mdz046.
[95] J.C.M. Wan, C. Massie, J. Garcia-Corbacho, F. Mouliere, J.D. Brenton, C. Caldas, S. Pacey, R. Baird, N. Rosenfeld, Liquid biopsies come of age: towards implementation of circulating tumour DNA, Nat Rev Cancer. 17 (2017) 223–238. https://doi.org/10.1038/nrc.2017.7.
[96] Y. Yan, Q. Guo, F. Wang, R. Adhikari, Z. Zhu, H. Zhang, W. Zhou, H. Yu, J. Li, J. Zhang, Cell-Free DNA: Hope and Potential Application in Cancer, Frontiers in Cell and Developmental Biology. 9 (2021). https://www.frontiersin.org/article/10.3389/fcell.2021.639233 (accessed March 9, 2022).
[97] X. Yang, Y. Hu, K. Yang, D. Wang, J. Lin, J. Long, F. Xie, J. Mao, J. Bian, M. Guan, J. Pan, L. Huo, K. Hu, X. Yang, Y. Mao, X. Sang, J. Zhang, X. Wang, H. Zhang, H. Zhao, Cell-free DNA copy number variations predict efficacy of immune checkpoint inhibitor-based therapy in hepatobiliary cancers, J Immunother Cancer. 9 (2021) e001942. https://doi.org/10.1136/jitc-2020-001942.

[98] T.J. Jensen, A.M. Goodman, S. Kato, C.K. Ellison, G.A. Daniels, L. Kim, P. Nakashe, E. McCarthy, A.R. Mazloom, G. McLennan, D.S. Grosu, M. Ehrich, R. Kurzrock, Genome-Wide Sequencing of Cell-Free DNA Identifies Copy-Number Alterations That Can Be Used for Monitoring Response to Immunotherapy in Cancer Patients, Molecular Cancer Therapeutics. 18 (2019) 448–458. https://doi.org/10.1158/1535-7163.MCT-18-0535.
[99] Y.R. Murciano-Goroff, A.B. Warner, J.D. Wolchok, The future of cancer immunotherapy: microenvironment-targeting combinations, Cell Res. 30 (2020) 507–519. https://doi.org/10.1038/s41422-020-0337-2.
[100] M. Dhar, J. Wong, J. Che, M. Matsumoto, T. Grogan, D. Elashoff, E.B. Garon, J.W. Goldman, E. Sollier Christen, D. Di Carlo, R.P. Kulkarni, Evaluation of PD-L1 expression on vortex-isolated circulating tumor cells in metastatic lung cancer, Sci Rep. 8 (2018) 2592. https://doi.org/10.1038/s41598-018-19245-w.
[101] D.L. Adams, D.K. Adams, J. He, N. Kalhor, M. Zhang, T. Xu, H. Gao, J.M. Reuben, Y. Qiao, R. Komaki, Z. Liao, M.J. Edelman, C.-M. Tang, S.H. Lin, Sequential Tracking of PD-L1 Expression and RAD50 Induction in Circulating Tumor and Stromal Cells of Lung Cancer Patients Undergoing Radiotherapy, Clinical Cancer Research. 23 (2017) 5948–5958. https://doi.org/10.1158/1078-0432.CCR-17-0802.
[102] N. Guibert, M. Delaunay, A. Lusque, N. Boubekeur, I. Rouquette, E. Clermont, J. Mourlanette, S. Gouin, I. Dormoy, G. Favre, J. Mazieres, A. Pradines, PD-L1 expression in circulating tumor cells of advanced non-small cell lung cancer patients treated with nivolumab, Lung Cancer. 120 (2018) 108–112. https://doi.org/10.1016/j.lungcan.2018.04.001.
[103] C. Nicolazzo, C. Raimondi, M. Mancini, S. Caponnetto, A. Gradilone, O. Gandini, M. Mastromartino, G. del Bene, A. Prete, F. Longo, E. Cortesi, P. Gazzaniga, Monitoring PD-L1 positive circulating tumor cells in non-small cell lung cancer patients treated with the PD-1 inhibitor Nivolumab, Sci Rep. 6 (2016) 31726. https://doi.org/10.1038/srep31726.
[104] Q. Wang, L. Zhao, L. Han, X. Tuo, S. Ma, Y. Wang, X. Feng, D. Liang, C. Sun, Q. Wang, Q. Song, Q. Li, The Discordance of Gene Mutations between Circulating Tumor Cells and Primary/Metastatic Tumor, Molecular Therapy - Oncolytics. 15 (2019) 21–29. https://doi.org/10.1016/j.omto.2019.08.006.
[105] T. Kitamura, B.-Z. Qian, J.W. Pollard, Immune cell promotion of metastasis, Nature Reviews Immunology. 15 (2015) 73–86. https://doi.org/10.1038/nri3789.
[106] B. Qian, Y. Deng, J.H. Im, R.J. Muschel, Y. Zou, J. Li, R.A. Lang, J.W. Pollard, A distinct macrophage population mediates metastatic breast cancer cell extravasation, establishment and growth, PLoS ONE. 4 (2009). https://doi.org/10.1371/journal.pone.0006562.
[107] S. Singhal, J. Stadanlick, M.J. Annunziata, A.S. Rao, P.S. Bhojnagarwala, S. O'Brien, E.K. Moon, E. Cantu, G. Danet-Desnoyers, H.J. Ra, L. Litzky, T. Akimova, U.H. Beier, W.W. Hancock, S.M. Albelda, E.B. Eruslanov, Human tumor-associated monocytes/macrophages and their regulation of T cell responses in early-stage lung cancer, Science Translational Medicine. 11 (2019). https://doi.org/10.1126/scitranslmed.aat1500.
[108] B. Psaila, D. Lyden, The metastatic niche: adapting the foreign soil, Nature Reviews Cancer. 9 (2009) 285–293. https://doi.org/10.1038/nrc2621.
[109] D.I. Gabrilovich, S. Nagaraj, Myeloid-derived-supressor cells as regulators of th eimmune system, Nature Reviews Immunology. 9 (2009) 162–174. https://doi.org/10.1038/nri2506.Myeloid-derived-suppressor.

[110] S.K. Wculek, I. Malanchi, Neutrophils support lung colonization of metastasis-initiating breast cancer cells., Nature. advance on (2015) 1–21. https://doi.org/10.1038/nature16140.
[111] J. Sceneay, M.T. Chow, A. Chen, H.M. Halse, C.S.F. Wong, D.M. Andrews, E.K. Sloan, B.S. Parker, D.D. Bowtell, M.J. Smyth, A. Möller, Primary tumor hypoxia recruits CD11b+/Ly6Cmed/ Ly6G+ immune suppressor cells and compromises NK cell cytotoxicity in the premetastatic niche, Cancer Research. 72 (2012) 3906–3911. https://doi.org/10.1158/0008-5472.CAN-11-3873.
[112] L. Sun, P.E. Clavijo, Y. Robbins, P. Patel, J. Friedman, S. Greene, R. Das, C. Silvin, C. Van Waes, L.A. Horn, J. Schlom, C. Palena, D. Maeda, J. Zebala, C.T. Allen, Inhibiting myeloid-derived suppressor cell trafficking enhances T cell immunotherapy, JCI Insight. 4 (2019). https://doi.org/10.1172/jci.insight.126853.
[113] S. Gazzaniga, A.I. Bravo, A. Guglielmotti, N. Van Rooijen, F. Maschi, A. Vecchi, A. Mantovani, J. Mordoh, R. Wainstok, Targeting tumor-associated macrophages and inhibition of MCP-1 reduce angiogenesis and tumor growth in a human melanoma xenograft, Journal of Investigative Dermatology. 127 (2007) 2031–2041. https://doi.org/10.1038/sj.jid.5700827.
[114] A.M. Gil-Bernabé, S. Ferjancic, M. Tlalka, L. Zhao, P.D. Allen, J.H. Im, K. Watson, S.A. Hill, A. Amirkhosravi, J.L. Francis, J.W. Pollard, W. Ruf, R.J. Muschel, Recruitment of monocytes/macrophages by tissue factor-mediated coagulation is essential for metastatic cell survival and premetastatic niche establishment in mice, Blood. 119 (2012) 3164–3175. https://doi.org/10.1182/blood-2011-08-376426.The.
[115] S.H. Colligan, S.L. Tzetzo, S.I. Abrams, Myeloid-driven mechanisms as barriers to antitumor CD8+ T cell activity, Molecular Immunology. 118 (2020) 165–173. https://doi.org/10.1016/j.molimm.2019.12.012.
[116] W. He, N. Kapate, C.W. Shields, S. Mitragotri, Drug delivery to macrophages: A review of targeting drugs and drug carriers to macrophages for inflammatory diseases, Advanced Drug Delivery Reviews. (2019). https://doi.org/10.1016/j.addr.2019.12.001.
[117] K. Kim, A.D. Skora, Z. Li, Q. Liu, A.J. Tam, R.L. Blosser, L.A. Diaz, N. Papadopoulos, K.W. Kinzler, B. Vogelstein, S. Zhou, Eradication of metastatic mouse cancers resistant to immune checkpoint blockade by suppression of myeloid-derived cells., Proceedings of the National Academy of Sciences of the United States of America. 111 (2014) 11774–9. https://doi.org/10.1073/pnas.1410626111.
[118] D.C. Strachan, B. Ruffell, Y. Oei, M.J. Bissell, L.M. Coussens, N. Pryer, D. Daniel, CSF1R inhibition delays cervical and mammary tumor growth in murine models by attenuating the turnover of tumor-associated macrophages and enhancing infiltration by CD8+ T cells, OncoImmunology. 2 (2013). https://doi.org/10.4161/onci.26968.
[119] K. Nakamura, M.J. Smyth, Myeloid immunosuppression and immune checkpoints in the tumor microenvironment, Cellular and Molecular Immunology. (2019) 1–12. https://doi.org/10.1038/s41423-019-0306-1.
[120] M. Rashidian, M.W. LaFleur, V.L. Verschoor, A. Dongre, Y. Zhang, T.H. Nguyen, S. Kolifrath, A.R. Aref, C.J. Lau, C.P. Paweletz, X. Bu, G.J. Freeman, M. Inmaculada Barrasa, R.A. Weinberg, A.H. Sharpe, H.L. Ploegh, Immuno-PET identifies the myeloid compartment as a key contributor to the outcome of the antitumor response under PD-1 blockade, Proceedings of the National Academy of Sciences of the United States of America. 116 (2019) 16971–16980. https://doi.org/10.1073/pnas.1905005116.
[121] M.G. Lechner, S.S. Karimi, K. Barry-Holson, T.E. Angell, K.A. Murphy, C.H. Church, J.R. Ohlfest, P. Hu, A.L. Epstein, Immunogenicity of Murine Solid Tumor Models as a

Defining Feature of In Vivo Behavior and Response to Immunotherapy, Journal of Immunotherapy. 36 (2013) 477–489. https://doi.org/10.1097/01.cji.0000436722.46675.4a.
[122] K. Movahedi, D. Laoui, C. Gysemans, M. Baeten, G. Stangé, J. Den Van Bossche, M. Mack, D. Pipeleers, P. In't Veld, P. De Baetselier, J.A. Van Ginderachter, Different tumor microenvironments contain functionally distinct subsets of macrophages derived from Ly6C(high) monocytes, Cancer Research. 70 (2010) 5728–5739. https://doi.org/10.1158/0008-5472.CAN-09-4672.
[123] D.R. Getts, R.L. Terry, M.T. Getts, C. Deffrasnes, M. Muller, C. van Vreden, T.M. Ashhurst, B. Chami, D. McCarthy, H. Wu, J. Ma, A. Martin, L.D. Shae, P. Witting, G.S. Kansas, J. Kuhn, W. Hafezi, I.L. Campbell, D. Reilly, J. Say, L. Brown, M.Y. White, S.J. Cordwell, S.J. Chadban, E.B. Thorp, S. Bao, S.D. Miller, N.J.C. King, Therapeutic Inflammatory Monocyte Modulation Using Immune-Modifying Microparticles, Science Translational Medicine. 6 (2014) 219ra7. https://doi.org/10.1126/scitranslmed.3007563.
[124] Q.V. Le, G. Yang, Y. Wu, H.W. Jang, M. Shokouhimehr, Y.K. Oh, Nanomaterials for modulating innate immune cells in cancer immunotherapy, Asian Journal of Pharmaceutical Sciences. 14 (2019) 16–29. https://doi.org/10.1016/j.ajps.2018.07.003.
[125] S. Sharma, I. Ifergan, J.E. Kurz, R.A. Linsenmeier, D. Xu, J.G. Cooper, S.D. Miller, J.A. Kessler, Intravenous Immunomodulatory Nanoparticle Treatment for Traumatic Brain Injury, Annals of Neurology. 87 (2020) 442–455. https://doi.org/10.1002/ana.25675.
[126] J. Park, Y. Zhang, E. Saito, S.J. Gurczynski, B.B. Moore, B.J. Cummings, A.J. Anderson, L.D. Shea, Intravascular innate immune cells reprogrammed via intravenous nanoparticles to promote functional recovery after spinal cord injury, Proceedings of the National Academy of Sciences of the United States of America. 116 (2019) 14947–14954. https://doi.org/10.1073/pnas.1820276116.
[127] A.R. Pyzer, L. Cole, J. Rosenblatt, D.E. Avigan, Myeloid-derived suppressor cells as effectors of immune suppression in cancer, International Journal of Cancer. (2016). https://doi.org/10.1002/ijc.30232.
[128] S.S. Rao, G.G. Bushnell, S.M. Azarin, G. Spicer, B.A. Aguado, J.R. Stoehr, E.J. Jiang, V. Backman, L.D. Shea, J.S. Jeruss, Enhanced survival with implantable scaffolds that capture metastatic breast cancer cells in vivo, Cancer Research. 76 (2016) 5209–5218. https://doi.org/10.1158/0008-5472.CAN-15-2106.
[129] T.E. Angell, M.G. Lechner, A.M. Smith, S.E. Martin, S.G. Groshen, D.R. Maceri, P.A. Singer, A.L. Epstein, Circulating myeloid-derived suppressor cells predict differentiated thyroid cancer diagnosis and extent, Thyroid. (2016). https://doi.org/10.1089/thy.2015.0289.
[130] A.L. Feng, J.K. Zhu, J.T. Sun, M.X. Yang, M.R. Neckenig, X.W. Wang, Q.Q. Shao, B.F. Song, Q.F. Yang, B.H. Kong, X. Qu, CD16+ monocytes in breast cancer patients: Expanded by monocyte chemoattractant protein-1 and may be useful for early diagnosis, Clinical and Experimental Immunology. 164 (2011) 57–65. https://doi.org/10.1111/j.1365-2249.2011.04321.x.
[131] R.A. Mukhtar, O. Nseyo, M.J. Campbell, L.J. Esserman, Tumor-associated macrophages in breast cancer as potential biomarkers for new treatments and diagnostics, Expert Review of Molecular Diagnostics. 11 (2011) 91–100. https://doi.org/10.1586/erm.10.97.
[132] A. Hamm, H. Prenen, W. Van Delm, M. Di Matteo, M. Wenes, E. Delamarre, T. Schmidt, J. Weitz, R. Sarmiento, A. Dezi, G. Gasparini, F. Rothé, R. Schmitz, A. D'Hoore, H. Iserentant, A. Hendlisz, M. Mazzone, Tumour-educated circulating monocytes are

powerful candidate biomarkers for diagnosis and disease follow-up of colorectal cancer, Gut. 65 (2016) 990–1000. https://doi.org/10.1136/gutjnl-2014-308988.
[133] D. Schauer, P. Starlinger, C. Reiter, N. Jahn, P. Zajc, E. Buchberger, T. Bachleitner-Hofmann, M. Bergmann, A. Stift, T. Gruenberger, C. Brostjan, Intermediate Monocytes but Not TIE2-Expressing Monocytes Are a Sensitive Diagnostic Indicator for Colorectal Cancer, PLoS ONE. 7 (2012) 1–10. https://doi.org/10.1371/journal.pone.0044450.
[134] J.M. Daley, A.A. Thomay, M.D. Connolly, J.S. Reichner, J.E. Albina, Use of Ly6G-specific monoclonal antibody to deplete neutrophils in mice, Journal of Leukocyte Biology. 83 (2008) 64–70. https://doi.org/10.1189/jlb.0407247.
[135] M.K. Srivastava, L. Zhu, M. Harris-White, U. Kar, M. Huang, M.F. Johnson, J.M. Lee, D. Elashoff, R. Strieter, S. Dubinett, S. Sharma, Myeloid suppressor cell depletion augments antitumor activity in lung cancer, PLoS ONE. 7 (2012). https://doi.org/10.1371/journal.pone.0040677.
[136] M. Bosiljcic, R.A. Cederberg, M.J. Hamilton, N.E. Lepard, B.T. Harbourne, J.L. Collier, E.C. Halvorsen, R. Shi, S.E. Franks, A.Y. Kim, J.P. Banáth, M. Hamer, F.M. Rossi, K.L. Bennewith, Targeting myeloid-derived suppressor cells in combination with primary mammary tumor resection reduces metastatic growth in the lungs, Breast Cancer Research. 21 (2019) 1–16. https://doi.org/10.1186/s13058-019-1189-x.
[137] L. Bonapace, M.M. Coissieux, J. Wyckoff, K.D. Mertz, Z. Varga, T. Junt, M. Bentires-Alj, Cessation of CCL2 inhibition accelerates breast cancer metastasis by promoting angiogenesis, Nature. 515 (2014) 130–133. https://doi.org/10.1038/nature13862.
[138] M. Beffinger, P.T. de Lara, S. Tugues, M. Vermeer, Y. Montagnolo, I. Ohs, V. Cecconi, G. Lucchiari, A. Gagliardi, N. Misljencevic, J. Sutton, R. Spörri, B. Becher, A. Gupta, M. van den Broek, CSF1R-dependent myeloid cells are required for NK-mediated control of metastasis, JCI Insight. 3 (2018). https://doi.org/10.1172/jci.insight.97792.
[139] M.G. Lechner, D.J. Liebertz, A.L. Epstein, Characterization of Cytokine-Induced Myeloid-Derived Suppressor Cells from Normal Human Peripheral Blood Mononuclear Cells, The Journal of Immunology. 185 (2010) 2273–2284. https://doi.org/10.4049/jimmunol.1000901.
[140] C. Perez, C. Botta, A. Zabaleta, N. Puig, M.-T. Cedena, I. Goicoechea, D. Alameda, E. San-José Enériz, J. Merino, P. Rodriguez-Otero, C.A.D.S. Maia, D. Alignani, P. Maiso, I. Manrique, D. Lara-Astiaso, A. Vilas-Zornoza, S. Sarvide, C. Riillo, M. Rossi, L. Rosiñol, A. Oriol, M.-J. Blanchard, R. Rios, A. Sureda, J. Martín Sánchez, R. Martinez, J. Bargay, J. de la Rubia, M.T. Hernandez Garcia, J. Martínez-López, A. Orfao, X. Agirre, F. Prosper, M.-V. Mateos, J.-J. Lahuerta, J. Bladé, J. San Miguel, B. Paiva, Immunogenomic identification and characterization of granulocytic myeloid derived suppressor cells in multiple myeloma., Blood. (2020). https://doi.org/10.1182/blood.2019004537.
[141] E. Saito, R. Kuo, R.M. Pearson, N. Gohel, B. Cheung, N.J.C. King, S.D. Miller, L.D. Shea, Designing drug-free biodegradable nanoparticles to modulate inflammatory monocytes and neutrophils for ameliorating inflammation, Journal of Controlled Release. 300 (2019) 185–196. https://doi.org/10.1016/j.jconrel.2019.02.025.
[142] J. Park, Y. Zhang, E. Saito, S.J. Gurczynski, B.B. Moore, B.J. Cummings, A.J. Anderson, L.D. Shea, Intravascular innate immune cells reprogrammed via intravenous nanoparticles to promote functional recovery after spinal cord injury, Proceedings of the National Academy of Sciences of the United States of America. 116 (2019) 14947–14954. https://doi.org/10.1073/pnas.1820276116.

[143] C.A. Fromen, W.J. Kelley, M.B. Fish, R. Adili, J. Noble, M.J. Hoenerhoff, M. Holinstat, O. Eniola-Adefeso, Neutrophil-Particle Interactions in Blood Circulation Drive Particle Clearance and Alter Neutrophil Responses in Acute Inflammation, ACS Nano. 11 (2017) 10797–10807. https://doi.org/10.1021/acsnano.7b03190.
[144] Y. Sawanobori, S. Ueha, M. Kurachi, T. Shimaoka, J.E. Talmadge, J. Abe, Y. Shono, M. Kitabatake, K. Kakimi, N. Mukaida, K. Matsushima, Chemokine-mediated rapid turnover of myeloid-derived suppressor cells in tumor-bearing mice, Blood. (2008). https://doi.org/10.1182/blood-2008-01-136895.
[145] B.-Z. Qian, J. Li, H. Zhang, T. Kitamura, J. Zhang, L.R. Campion, E.A. Kaiser, L.A. Snyder, J.W. Pollard, CCL2 recruits inflammatory monocytes to facilitate breast-tumour metastasis., Nature. 475 (2011) 222–5. https://doi.org/10.1038/nature10138.
[146] V. Bronte, S. Brandau, S.-H. Chen, M.P. Colombo, A.B. Frey, T.F. Greten, S. Mandruzzato, P.J. Murray, A. Ochoa, S. Ostrand-Rosenberg, P.C. Rodriguez, A. Sica, V. Umansky, R.H. Vonderheide, D.I. Gabrilovich, Recommendations for myeloid-derived suppressor cell nomenclature and characterization standards, Nature Communications. 7 (2016) 12150. https://doi.org/10.1038/ncomms12150.
[147] C. Wu, M.E. Muroski, J. Miska, C. Lee-Chang, Y. Shen, A. Rashidi, P. Zhang, T. Xiao, Y. Han, A. Lopez-Rosas, Y. Cheng, M.S. Lesniak, Repolarization of myeloid derived suppressor cells via magnetic nanoparticles to promote radiotherapy for glioma treatment, Nanomedicine: Nanotechnology, Biology, and Medicine. 16 (2019) 126–137. https://doi.org/10.1016/j.nano.2018.11.015.
[148] L.M. Casey, S. Kakade, J.T. Decker, J.A. Rose, K. Deans, L.D. Shea, R.M. Pearson, Cargo-less nanoparticles program innate immune cell responses to toll-like receptor activation, Biomaterials. 218 (2019) 119333. https://doi.org/10.1016/j.biomaterials.2019.119333.
[149] S. Jeon, J. Clavadetscher, D.K. Lee, S. V. Chankeshwara, M. Bradley, W.S. Cho, Surface charge-dependent cellular uptake of polystyrene nanoparticles, Nanomaterials. 8 (2018) 1–11. https://doi.org/10.3390/NANO8121028.
[150] L. Pinton, S. Magri, E. Masetto, M. Vettore, I. Schibuola, V. Ingangi, I. Marigo, K. Matha, J.P. Benoit, A. Della Puppa, V. Bronte, G. Lollo, S. Mandruzzato, Targeting of immunosuppressive myeloid cells from glioblastoma patients by modulation of size and surface charge of lipid nanocapsules, Journal of Nanobiotechnology. 18 (2020) 1–12. https://doi.org/10.1186/s12951-020-00589-3.
[151] B.R. Smith, E.E.B. Ghosn, H. Rallapalli, J.A. Prescher, T. Larson, L.A. Herzenberg, S.S. Gambhir, Selective uptake of single-walled carbon nanotubes by circulating monocytes for enhanced tumour delivery, Nature Nanotechnology. 9 (2014) 481–487. https://doi.org/10.1038/nnano.2014.62.
[152] S. Li, Q. Wang, Y. Shen, M. Hassan, J. Shen, W. Jiang, Y. Su, J. Chen, L. Bai, W. Zhou, Y. Wang, Pseudoneutrophil Cytokine Sponges Disrupt Myeloid Expansion and Tumor Trafficking to Improve Cancer Immunotherapy., Nano Letters. (2019) 2–11. https://doi.org/10.1021/acs.nanolett.9b03753.
[153] R.S. Oakes, G.G. Bushnell, S.M. Orbach, P. Kandagatla, Y. Zhang, A.H. Morris, M.S. Hall, P. LaFaire, J.T. Decker, R.M. Hartfield, M.D. Brooks, M.S. Wicha, J.S. Jeruss, L.D. Shea, Metastatic Conditioning of Myeloid Cells at a Subcutaneous Synthetic Niche Reflects Disease Progression and Predicts Therapeutic Outcomes, Cancer Research. 80 (2020) 602–612. https://doi.org/10.1158/0008-5472.CAN-19-1932.

[154] P. Xiao, X. Wan, B. Cui, Y. Liu, C. Qiu, J. Rong, M. Zheng, Y. Song, L. Chen, J. He, Q. Tan, X. Wang, X. Shao, Y. Liu, X. Cao, Q. Wang, Interleukin 33 in tumor microenvironment is crucial for the accumulation and function of myeloid-derived suppressor cells, OncoImmunology. (2016). https://doi.org/10.1080/2162402X.2015.1063772.
[155] S. Ostrand-Rosenberg, D.W. Beury, K.H. Parker, L.A. Horn, Survival of the fittest: how myeloid-derived suppressor cells survive in the inhospitable tumor microenvironment, Cancer Immunology, Immunotherapy. (2019). https://doi.org/10.1007/s00262-019-02388-8.
[156] V. Umansky, C. Blattner, C. Gebhardt, J. Utikal, The role of myeloid-derived suppressor cells (MDSC) in cancer progression, Vaccines. (2016). https://doi.org/10.3390/vaccines4040036.
[157] K.S.N. Atretkhany, M.S. Drutskaya, Myeloid-derived suppressor cells and proinflammatory cytokines as targets for cancer therapy, Biochemistry (Moscow). (2016). https://doi.org/10.1134/S0006297916110055.
[158] Y. Liu, X. Cao, Characteristics and Significance of the Pre-metastatic Niche, Cancer Cell. 30 (2016) 668–681. https://doi.org/10.1016/j.ccell.2016.09.011.
[159] A. Montfort, C. Colacios, T. Levade, N. Andrieu-Abadie, N. Meyer, B. Ségui, The TNF paradox in cancer progression and immunotherapy, Frontiers in Immunology. (2019). https://doi.org/10.3389/fimmu.2019.01818.
[160] A.D. Smith, C. Lu, D. Payne, A. V. Paschall, J.D. Klement, P.S. Redd, M.L. Ibrahim, D. Yang, Q. Han, Z. Liu, H. Shi, T.J. Hartney, A. Nayak-Kapoor, K. Liu, Autocrine IL6-Mediated Activation of the STAT3-DNMT Axis Silences the TNFα-RIP1 Necroptosis Pathway to Sustain Survival and Accumulation of Myeloid-Derived Suppressor Cells, Cancer Research. (2020). https://doi.org/10.1158/0008-5472.CAN-19-3670.
[161] K. Moriwaki, J. Bertin, P.J. Gough, G.M. Orlowski, F.K.M. Chan, Differential roles of RIPK1 and RIPK3 in TNF-induced necroptosis and chemotherapeutic agent-induced cell death, Cell Death and Disease. (2015). https://doi.org/10.1038/cddis.2015.16.
[162] A. Wilkerson, J. Kim, A.Y. Huang, M. Zhang, Nanoparticle Systems Modulating Myeloid-Derived Suppressor Cells for Cancer Immunotherapy, Current Topics in Medicinal Chemistry. (2017). https://doi.org/10.2174/1568026617666161122121412.
[163] M.S. Sasso, G. Lollo, M. Pitorre, S. Solito, L. Pinton, S. Valpione, G. Bastiat, S. Mandruzzato, V. Bronte, I. Marigo, J.P. Benoit, Low dose gemcitabine-loaded lipid nanocapsules target monocytic myeloid-derived suppressor cells and potentiate cancer immunotherapy, Biomaterials. (2016). https://doi.org/10.1016/j.biomaterials.2016.04.010.
[164] G.T. Yu, L. Rao, H. Wu, L.L. Yang, L.L. Bu, W.W. Deng, L. Wu, X. Nan, W.F. Zhang, X.Z. Zhao, W. Liu, Z.J. Sun, Myeloid-Derived Suppressor Cell Membrane-Coated Magnetic Nanoparticles for Cancer Theranostics by Inducing Macrophage Polarization and Synergizing Immunogenic Cell Death, Advanced Functional Materials. (2018). https://doi.org/10.1002/adfm.201801389.
[165] S. Sau, H.O. Alsaab, K. Bhise, R. Alzhrani, G. Nabil, A.K. Iyer, Multifunctional nanoparticles for cancer immunotherapy: A groundbreaking approach for reprogramming malfunctioned tumor environment, Journal of Controlled Release. (2018). https://doi.org/10.1016/j.jconrel.2018.01.028.
[166] J. Zhou, Y. Nefedova, A. Lei, D. Gabrilovich, Neutrophils and PMN-MDSC: Their biological role and interaction with stromal cells, Seminars in Immunology. (2018). https://doi.org/10.1016/j.smim.2017.12.004.

[167] D.I. Gabrilovich, Myeloid-derived suppressor cells, Cancer Immunology Research. (2017). https://doi.org/10.1158/2326-6066.CIR-16-0297.
[168] O. Veiseh, J.C. Doloff, M. Ma, A.J. Vegas, H.H. Tam, A.R. Bader, J. Li, E. Langan, J. Wyckoff, W.S. Loo, S. Jhunjhunwala, A. Chiu, S. Siebert, K. Tang, J. Hollister-Lock, S. Aresta-Dasilva, M. Bochenek, J. Mendoza-Elias, Y. Wang, M. Qi, D.M. Lavin, M. Chen, N. Dholakia, R. Thakrar, I. Lacík, G.C. Weir, J. Oberholzer, D.L. Greiner, R. Langer, D.G. Anderson, Size- and shape-dependent foreign body immune response to materials implanted in rodents and non-human primates, Nature Materials. (2015). https://doi.org/10.1038/nmat4290.
[169] Z. Zhao, A. Ukidve, J. Kim, S. Mitragotri, Targeting Strategies for Tissue-Specific Drug Delivery, Cell. (2020). https://doi.org/10.1016/j.cell.2020.02.001.
[170] D.M. Goncalves, R. de Liz, D. Girard, Activation of neutrophils by nanoparticles., TheScientificWorldJournal. (2011). https://doi.org/10.1100/2011/768350.
[171] M.A. Dobrovolskaia, M. Shurin, A.A. Shvedova, Current understanding of interactions between nanoparticles and the immune system, Toxicology and Applied Pharmacology. (2016). https://doi.org/10.1016/j.taap.2015.12.022.
[172] N. Patsoukis, J. Brown, V. Petkova, F. Liu, L. Li, V.A. Boussiotis, Selective Effects of PD-1 on Akt and Ras Pathways Regulate Molecular Components of the Cell Cycle and Inhibit T Cell Proliferation, Science Signaling. 5 (2012) ra46–ra46. https://doi.org/10.1126/scisignal.2002796.
[173] Z. Hunter, D.P. McCarthy, W.T. Yap, C.T. Harp, D.R. Getts, L.D. Shea, S.D. Miller, A biodegradable nanoparticle platform for the induction of antigen-specific immune tolerance for treatment of autoimmune disease, ACS Nano. (2014). https://doi.org/10.1021/nn405033r.
[174] C.B. Smarr, W.T. Yap, T.P. Neef, R.M. Pearson, Z.N. Hunter, I. Ifergan, D.R. Getts, P.J. Bryce, L.D. Shea, S.D. Miller, Biodegradable antigen-associated PLG nanoparticles tolerize Th2-mediated allergic airway inflammation pre- and postsensitization, Proceedings of the National Academy of Sciences of the United States of America. (2016). https://doi.org/10.1073/pnas.1505782113.
[175] M.I. Love, W. Huber, S. Anders, Moderated estimation of fold change and dispersion for RNA-seq data with DESeq2, Genome Biology. 15 (2014) 1–21. https://doi.org/10.1186/s13059-014-0550-8.
[176] A. Zhu, J.G. Ibrahim, M.I. Love, Heavy-Tailed prior distributions for sequence count data: Removing the noise and preserving large differences, Bioinformatics. 35 (2019) 2084–2092. https://doi.org/10.1093/bioinformatics/bty895.
[177] S.S. Rao, G.G. Bushnell, S.M. Azarin, G. Spicer, B.A. Aguado, J.R. Stoehr, E.J. Jiang, V. Backman, L.D. Shea, J.S. Jeruss, Enhanced survival with implantable scaffolds that capture metastatic breast cancer cells in vivo, Cancer Res. 76 (2016) 5209–5218. https://doi.org/10.1158/0008-5472.CAN-15-2106.
[178] H. Gonzalez, C. Hagerling, Z. Werb, Roles of the immune system in cancer: from tumor initiation to metastatic progression, Genes Dev. 32 (2018) 1267–1284. https://doi.org/10.1101/gad.314617.118.
[179] T. Kitamura, B.-Z. Qian, J.W. Pollard, Immune cell promotion of metastasis, Nat Rev Immunol. 15 (2015) 73–86. https://doi.org/10.1038/nri3789.
[180] S. Kruger, M. Ilmer, S. Kobold, B.L. Cadilha, S. Endres, S. Ormanns, G. Schuebbe, B.W. Renz, J.G. D'Haese, H. Schloesser, V. Heinemann, M. Subklewe, S. Boeck, J. Werner, M.

von Bergwelt-Baildon, Advances in cancer immunotherapy 2019 - latest trends, J Exp Clin Cancer Res. 38 (2019) 268. https://doi.org/10.1186/s13046-019-1266-0.
[181] S. Upadhaya, V.M. Hubbard-Lucey, J.X. Yu, Immuno-oncology drug development forges on despite COVID-19, Nat Rev Drug Discov. 19 (2020) 751–752. https://doi.org/10.1038/d41573-020-00166-1.
[182] L. Barrueto, F. Caminero, L. Cash, C. Makris, P. Lamichhane, R.R. Deshmukh, Resistance to Checkpoint Inhibition in Cancer Immunotherapy, Transl Oncol. 13 (2020) 100738. https://doi.org/10.1016/j.tranon.2019.12.010.
[183] A. Marra, G. Curigliano, Adjuvant and Neoadjuvant Treatment of Triple-Negative Breast Cancer With Chemotherapy, Cancer J. 27 (2021) 41–49. https://doi.org/10.1097/PPO.0000000000000498.
[184] A. Makkouk, V.B. Joshi, A. Wongrakpanich, C.D. Lemke, B.P. Gross, A.K. Salem, G.J. Weiner, Biodegradable microparticles loaded with doxorubicin and CpG ODN for in situ immunization against cancer, AAPS J. 17 (2015) 184–193. https://doi.org/10.1208/s12248-014-9676-6.
[185] D. Schmid, C.G. Park, C.A. Hartl, N. Subedi, A.N. Cartwright, R.B. Puerto, Y. Zheng, J. Maiarana, G.J. Freeman, K.W. Wucherpfennig, D.J. Irvine, M.S. Goldberg, T cell-targeting nanoparticles focus delivery of immunotherapy to improve antitumor immunity, Nat Commun. 8 (2017) 1747. https://doi.org/10.1038/s41467-017-01830-8.
[186] C. Groth, X. Hu, R. Weber, V. Fleming, P. Altevogt, J. Utikal, V. Umansky, Immunosuppression mediated by myeloid-derived suppressor cells (MDSCs) during tumour progression, Br J Cancer. 120 (2019) 16–25. https://doi.org/10.1038/s41416-018-0333-1.
[187] K. Alicea-Torres, E. Sanseviero, J. Gui, J. Chen, F. Veglia, Q. Yu, L. Donthireddy, A. Kossenkov, C. Lin, S. Fu, C. Mulligan, B. Nam, G. Masters, F. Denstman, J. Bennett, N. Hockstein, A. Rynda-Apple, Y. Nefedova, S.Y. Fuchs, D.I. Gabrilovich, Immune suppressive activity of myeloid-derived suppressor cells in cancer requires inactivation of the type I interferon pathway, Nat Commun. 12 (2021) 1717. https://doi.org/10.1038/s41467-021-22033-2.
[188] T. Kitamura, B.-Z. Qian, D. Soong, L. Cassetta, R. Noy, G. Sugano, Y. Kato, J. Li, J.W. Pollard, CCL2-induced chemokine cascade promotes breast cancer metastasis by enhancing retention of metastasis-associated macrophages, J Exp Med. 212 (2015) 1043–1059. https://doi.org/10.1084/jem.20141836.
[189] Y. Wu, Y.-Y. Li, K. Matsushima, T. Baba, N. Mukaida, CCL3-CCR5 axis regulates intratumoral accumulation of leukocytes and fibroblasts and promotes angiogenesis in murine lung metastasis process, J Immunol. 181 (2008) 6384–6393. https://doi.org/10.4049/jimmunol.181.9.6384.
[190] B. Seubert, B. Grünwald, J. Kobuch, H. Cui, F. Schelter, S. Schaten, J.T. Siveke, N.H. Lim, H. Nagase, N. Simonavicius, M. Heikenwalder, T. Reinheckel, J.P. Sleeman, K.-P. Janssen, P.A. Knolle, A. Krüger, Tissue inhibitor of metalloproteinases (TIMP)-1 creates a premetastatic niche in the liver through SDF-1/CXCR4-dependent neutrophil recruitment in mice, Hepatology. 61 (2015) 238–248. https://doi.org/10.1002/hep.27378.
[191] A. Müller, B. Homey, H. Soto, N. Ge, D. Catron, M.E. Buchanan, T. McClanahan, E. Murphy, W. Yuan, S.N. Wagner, J.L. Barrera, A. Mohar, E. Verástegui, A. Zlotnik, Involvement of chemokine receptors in breast cancer metastasis, Nature. 410 (2001) 50–56. https://doi.org/10.1038/35065016.

[192] I. Corbeau, W. Jacot, S. Guiu, Neutrophil to Lymphocyte Ratio as Prognostic and Predictive Factor in Breast Cancer Patients: A Systematic Review, Cancers (Basel). 12 (2020) E958. https://doi.org/10.3390/cancers12040958.
[193] C. Hagerling, H. Gonzalez, K. Salari, C.-Y. Wang, C. Lin, I. Robles, M. van Gogh, A. Dejmek, K. Jirström, Z. Werb, Immune effector monocyte-neutrophil cooperation induced by the primary tumor prevents metastatic progression of breast cancer, Proc Natl Acad Sci U S A. 116 (2019) 21704–21714. https://doi.org/10.1073/pnas.1907660116.
[194] E. Pylaeva, S. Lang, J. Jablonska, The Essential Role of Type I Interferons in Differentiation and Activation of Tumor-Associated Neutrophils, Frontiers in Immunology. 7 (2016). https://www.frontiersin.org/article/10.3389/fimmu.2016.00629 (accessed March 14, 2022).
[195] R. Wang, W. Bao, M. Pal, Y. Liu, K. Yazdanbakhsh, H. Zhong, Intermediate monocytes induced by IFN-γ inhibit cancer metastasis by promoting NK cell activation through FOXO1 and interleukin-27, J Immunother Cancer. 10 (2022) e003539. https://doi.org/10.1136/jitc-2021-003539.
[196] D. Jorgovanovic, M. Song, L. Wang, Y. Zhang, Roles of IFN-γ in tumor progression and regression: a review, Biomark Res. 8 (2020) 49. https://doi.org/10.1186/s40364-020-00228-x.
[197] E. Comen, P. Wojnarowicz, V.E. Seshan, R. Shah, C. Coker, L. Norton, R. Benezra, TNF is a key cytokine mediating neutrophil cytotoxic activity in breast cancer patients, Npj Breast Cancer. 2 (2016) 1–8. https://doi.org/10.1038/npjbcancer.2016.9.
[198] C.B. Williams, E.S. Yeh, A.C. Soloff, Tumor-associated macrophages: unwitting accomplices in breast cancer malignancy, NPJ Breast Cancer. 2 (2016) 15025. https://doi.org/10.1038/npjbcancer.2015.25.
[199] A. Xia, Y. Zhang, J. Xu, T. Yin, X.-J. Lu, T Cell Dysfunction in Cancer Immunity and Immunotherapy, Front Immunol. 10 (2019) 1719. https://doi.org/10.3389/fimmu.2019.01719.
[200] D.I. Gabrilovich, S. Nagaraj, Myeloid-derived-suppressor cells as regulators of the immune system, Nat Rev Immunol. 9 (2009) 162–174. https://doi.org/10.1038/nri2506.
[201] L. Fultang, S. Panetti, M. Ng, P. Collins, S. Graef, N. Rizkalla, S. Booth, R. Lenton, B. Noyvert, C. Shannon-Lowe, G. Middleton, F. Mussai, C.D. Santo, MDSC targeting with Gemtuzumab ozogamicin restores T cell immunity and immunotherapy against cancers, EBioMedicine. 47 (2019) 235–246. https://doi.org/10.1016/j.ebiom.2019.08.025.
[202] R.V. Sionov, T. Fainsod-Levi, T. Zelter, L. Polyansky, C.T. Pham, Z. Granot, Neutrophil Cathepsin G and Tumor Cell RAGE Facilitate Neutrophil Anti-Tumor Cytotoxicity, Oncoimmunology. 8 (2019) e1624129. https://doi.org/10.1080/2162402X.2019.1624129.
[203] E. Lin, L. Rivera-Báez, S. Fouladdel, H.J. Yoon, S. Guthrie, J. Wieger, Y. Deol, E. Keller, V. Sahai, D.M. Simeone, M.L. Burness, E. Azizi, M.S. Wicha, S. Nagrath, High-Throughput Microfluidic Labyrinth for the Label-free Isolation of Circulating Tumor Cells, Cell Systems. 5 (2017) 295-304.e4. https://doi.org/10.1016/j.cels.2017.08.012.
[204] A. Butler, P. Hoffman, P. Smibert, E. Papalexi, R. Satija, Integrating single-cell transcriptomic data across different conditions, technologies, and species, Nat Biotechnol. 36 (2018) 411–420. https://doi.org/10.1038/nbt.4096.
[205] S.M. Azarin, J. Yi, R.M. Gower, B.A. Aguado, M.E. Sullivan, A.G. Goodman, E.J. Jiang, S.S. Rao, Y. Ren, S.L. Tucker, V. Backman, J.S. Jeruss, L.D. Shea, In vivo capture and

label-free detection of early metastatic cells, Nat Commun. 6 (2015) 8094. https://doi.org/10.1038/ncomms9094.
[206] S.S. Rao, G.G. Bushnell, S.M. Azarin, G. Spicer, B.A. Aguado, J.R. Stoehr, E.J. Jiang, V. Backman, L.D. Shea, J.S. Jeruss, Enhanced survival with implantable scaffolds that capture metastatic breast cancer cells in vivo, Cancer Res. 76 (2016) 5209–5218. https://doi.org/10.1158/0008-5472.CAN-15-2106.
[207] R.S. Oakes, G.G. Bushnell, S.M. Orbach, P. Kandagatla, Y. Zhang, A.H. Morris, M.S. Hall, P. LaFaire, J.T. Decker, R.M. Hartfield, M.D. Brooks, M.S. Wicha, J.S. Jeruss, L.D. Shea, Metastatic conditioning of myeloid cells at a subcutaneous synthetic niche reflects disease progression and predicts therapeutic outcomes, Cancer Res. 80 (2020) 602–612. https://doi.org/10.1158/0008-5472.CAN-19-1932.
[208] A.H. Morris, K.R. Hughes, R.S. Oakes, M.M. Cai, S.D. Miller, D.N. Irani, L.D. Shea, Engineered immunological niches to monitor disease activity and treatment efficacy in relapsing multiple sclerosis, Nat Commun. 11 (2020) 3871. https://doi.org/10.1038/s41467-020-17629-z.
[209] M.I. Love, W. Huber, S. Anders, Moderated estimation of fold change and dispersion for RNA-seq data with DESeq2, Genome Biology. 15 (2014) 550. https://doi.org/10.1186/s13059-014-0550-8.
[210] A. Subramanian, P. Tamayo, V.K. Mootha, S. Mukherjee, B.L. Ebert, M.A. Gillette, A. Paulovich, S.L. Pomeroy, T.R. Golub, E.S. Lander, J.P. Mesirov, Gene set enrichment analysis: A knowledge-based approach for interpreting genome-wide expression profiles, Proceedings of the National Academy of Sciences. 102 (2005) 15545–15550. https://doi.org/10.1073/pnas.0506580102.
[211] M. Li, D. Spakowicz, J. Burkart, S. Patel, M. Husain, K. He, E.M. Bertino, P.G. Shields, D.P. Carbone, C.F. Verschraegen, C.J. Presley, G.A. Otterson, K. Kendra, D.H. Owen, Change in neutrophil to lymphocyte ratio during immunotherapy treatment is a non-linear predictor of patient outcomes in advanced cancers, J Cancer Res Clin Oncol. 145 (2019) 2541–2546. https://doi.org/10.1007/s00432-019-02982-4.
[212] A. Gogia, S.V.S. Deo, D. Sharma, R.K. Phulia, S. Thulkar, P.S. Malik, S. Mathur, Discordance in Biomarker Expression in Breast Cancer After Metastasis: Single Center Experience in India, J Glob Oncol. 5 (2019) 1–8. https://doi.org/10.1200/JGO.18.00184.
[213] Q. Wang, J. Gao, X. Wu, Pseudoprogression and hyperprogression after checkpoint blockade, International Immunopharmacology. 58 (2018) 125–135. https://doi.org/10.1016/j.intimp.2018.03.018.
[214] L. Voorwerk, M. Slagter, H.M. Horlings, K. Sikorska, K.K. van de Vijver, M. de Maaker, I. Nederlof, R.J.C. Kluin, S. Warren, S. Ong, T.G. Wiersma, N.S. Russell, F. Lalezari, P.C. Schouten, N.A.M. Bakker, S.L.C. Ketelaars, D. Peters, C.A.H. Lange, E. van Werkhoven, H. van Tinteren, I.A.M. Mandjes, I. Kemper, S. Onderwater, M. Chalabi, S. Wilgenhof, J.B.A.G. Haanen, R. Salgado, K.E. de Visser, G.S. Sonke, L.F.A. Wessels, S.C. Linn, T.N. Schumacher, C.U. Blank, M. Kok, Immune induction strategies in metastatic triple-negative breast cancer to enhance the sensitivity to PD-1 blockade: the TONIC trial, Nat Med. 25 (2019) 920–928. https://doi.org/10.1038/s41591-019-0432-4.
[215] D. Alizadeh, M. Trad, N.T. Hanke, C.B. Larmonier, N. Janikashvili, B. Bonnotte, E. Katsanis, N. Larmonier, Doxorubicin Eliminates Myeloid-Derived Suppressor Cells and Enhances the Efficacy of Adoptive T Cell Transfer in Breast Cancer, Cancer Res. 74 (2014) 104–118. https://doi.org/10.1158/0008-5472.CAN-13-1545.

[216] A.R. de Biasi, J. Villena-Vargas, P.S. Adusumilli, Cisplatin-Induced Antitumor Immunomodulation: A Review of Preclinical and Clinical Evidence, Clin Cancer Res. 20 (2014) 5384–5391. https://doi.org/10.1158/1078-0432.CCR-14-1298.

[217] C. Nangia, P. Soon-Shiong, S. Rabizadeh, J.H. Lee, L. Sender, F. Jones, M. Kistler, K. Niazi, T. Seery, A. Rock, O. Jafari, Complete responses in patients with second-line or greater metastatic triple negative breast cancer (TNBC) following first-in-human immunotherapy combining NK and T cell activation with off-the-shelf high-affinity CD16 NK cell line (haNK), Annals of Oncology. 30 (2019) v130. https://doi.org/10.1093/annonc/mdz242.053.

[218] S.B. Kemp, N.G. Steele, E.S. Carpenter, K.L. Donahue, G.G. Bushnell, A.H. Morris, S. The, S.M. Orbach, V.R. Sirihorachai, Z.C. Nwosu, C. Espinoza, F. Lima, K. Brown, A.A. Girgis, V. Gunchick, Y. Zhang, C.A. Lyssiotis, T.L. Frankel, F. Bednar, A. Rao, V. Sahai, L.D. Shea, H.C. Crawford, M.P. di Magliano, Pancreatic cancer is marked by complement-high blood monocytes and tumor-associated macrophages, Life Science Alliance. 4 (2021). https://doi.org/10.26508/lsa.202000935.